Tunneling Spectroscopy with Two-Dimensional Electron Gases

Diplomarbeit

von

Julia S. Meyer

UNIVERSITÄT ZU KÖLN
INSTITUT FÜR THEORETISCHE PHYSIK

FEBRUAR 1999

Zusammenfassung

Im Rahmen der Festkörperphysik wurde der Tunneleffekt erstmals 1958 beobachtet, als Esaki [1] Strommessungen an durch eine Potentialbarriere getrennten Halbleitern durchführte. Es folgten zahlreiche Untersuchungen, bis Anfang der 90er Jahre Tunnelexperimente zwischen zweidimensionalen Elektronengasen (2DEGs) in Halbleiterheterostrukturen möglich wurden [5]. Da diese Systeme eine reichhaltige Phänomenologie aufweisen, experimentell gut handhabbar sind und sich eine technologische Nutzung abzeichnet, nehmen sie einen wichtigen Platz in der aktuellen Forschung ein [4].

In der vorliegenden Arbeit wird das Tunneln zwischen 2DEGs im parallelen Magnetfeld und dabei insbesondere die Magnetfeldabhängigkeit der durch Unordnung verursachten Stromfluktuationen theoretisch untersucht. Ganz allgemein ist der Tunnelstrom durch ein Überlappintegral der Spektralfunktionen, welche die Physik der beteiligten Systeme in weiten Teilen charakterisieren, bestimmt. Die Besonderheit der betrachteten Anordnung ist nun, daß sich dieser Überlapp durch Variation externer Parameter (wie z.B. Magnetfelder) leicht kontrollieren läßt. Dies ermöglicht es, die Spektralfunktionen „abzutasten“, und dadurch weitreichende Informationen über die mikroskopische Struktur der einzelnen 2DEGs zu gewinnen. Die Charakteristika des *unordnungsgemittelten* Tunnelstroms wurden bereits eingehend von Eisenstein *et al.* [22] (experimentell) und Zheng und MacDonald [23] (theoretisch) behandelt. Die gemittelten Größen beinhalten jedoch nur einen kleinen Teil der Informationen, die eine detaillierte Analyse des Tunnelstroms liefert, was in dieser Arbeit anhand der Magnetfeldabhängigkeit der Stromfluktuationen gezeigt wird.

Der Zusammenhang zwischen Tunnelstrom und Unordnung erklärt sich dadurch, daß der Tunnelstrom durch Prozesse dominiert wird, bei denen ein Elektron von einem 2DEG zum anderen tunnelt, dann innerhalb dieses 2DEGs propagiert und schließlich an einer beliebigen Stelle zurücktunnelt, um mit dem zurückgelassenen Loch zu rekombinieren. Da so magnetischer Fluß eingeschlossen wird, läßt sich mittels des magnetischen Feldes die typische Reichweite der zum Strom beitragenden Prozesse ermitteln. Diese sind durch die Ein-Teilchen Green'schen Funktionen, welche die Propagation von Elektron und Loch in den 2DEGs beschreiben, bestimmt. Der mittlere Strom zeigt Struktur auf einer charakteri-

stischen Feldskala $B_c[\langle I\rangle] \sim l^{-1}$, was der Tatsache entspricht, daß die „Reichweite“ der unordnungsgemittelten Green'schen Funktion durch die mittlere freie Weglänge l gegeben ist. Hier wird nun gezeigt, daß dahingegen die Stromfluktuationen bzw. der *typische* Strom (einer Probe *vor* Unordnungsmittelung) aufgrund der Langreichweitigkeit der ungemittelten Green'schen Funktion wesentlich empfindlicher auf das Magnetfeld reagieren. Die charakteristische Feldskala hierfür ist durch $B_c[(\Delta I)^2] \sim (\sqrt{D/eV})^{-1}$ gegeben, wobei $\sqrt{D/eV} \gg l$ einer Diffusionslänge bei vorgegebener Zeit $(eV)^{-1}$ entspricht (D Diffusionskonstante, eV Potentialdifferenz zwischen den 2DEGs). Das bedeutet, daß sich die Magnetfeldabhängigkeit der Fluktuationen in einem Bereich messen läßt, über den der mittlere Strom noch weitgehend konstant ist.

Zu den Fluktuationen gibt es zwei verschiedene dominante Beiträge, wovon jedoch nur einer magnetfeldabhängig ist. Es wurde zudem gezeigt, daß sich dieser magnetfeldabhängige Beitrag gerade als Fouriertransformierte (bezüglich des Magnetfelds bzw. des zugehörigen Vektorpotentials) des Produkts der Korrelationsfunktionen beider 2DEGs auffassen läßt. Dadurch bietet sich die Möglichkeit, über die Magnetfeldabhängigkeit des typischen Stromes räumliche Korrelationen abzutasten. Setzt man also die Eigenschaften des einen 2DEGs als bekannt voraus, kann man somit das andere spektroskopieren.

In dieser Arbeit wurde eine störungstheoretische Analyse des Tunnelstroms durchgeführt. Eine darüber hinausgehende Untersuchung des Problems erfordert nichtstörungstheoretische wie z.B. feldtheoretische Methoden, da Divergenzen, die bei sehr niedrigen Energien in endlichen Systemen auftreten, darauf hindeuten, daß das Problem nicht-perturbativ ist. Eine weitere mögliche Verallgemeinerung stellt die Berücksichtigung von Coulomb-Wechselwirkung zwischen den 2DEGs sowie die Behandlung nicht-konstanter Tunnelmatrixelemente dar.

Die Arbeit ist folgendermaßen aufgebaut: Nach einer allgemeinen Einleitung wird in Kapitel 2 die experimentelle Realisierung von 2DEGs kurz umrissen sowie ein Überblick über Forschungsergebnisse gegeben, die im Zusammenhang mit Tunneln zwischen parallelen 2DEGs stehen. Kapitel 3 dient der Einführung der verwendeten Methoden zur theoretischen Beschreibung des Tunnelstroms. Den Hauptteil der Arbeit bildet schließlich Kapitel 4, in dem sowohl der mittlere Tunnelstrom als auch die Fluktuationen detailliert untersucht werden. Dabei werden zwei interessante Fälle unterschieden: zum einen Tunneln zwischen einem „sauberen“ und einem ungeordneten 2DEG in Kapitel 4.2 und zum anderen Tunneln zwischen zwei ungeordneten 2DEGs in Kapitel 4.3. Abschließend werden die Ergebnisse zusammengefaßt.

Contents

List of Symbols

$\mathbf{A} \quad (A)$	vector potential
$A(\mathbf{k}, \mathbf{k}'; \epsilon)$	spectral function
$A^{\mathrm{o}}(\mathbf{k}, \epsilon)$	unperturbed spectral function
$a(\mathbf{k}, \epsilon; \tau)$	impurity averaged spectral function
$\mathbf{B} \quad (B)$	magnetic field
$B_{\mathrm{c}}[\langle I \rangle] = B_{\mathrm{c}}^{(l)}$	characteristic field for the average current
$B_{\mathrm{c}}[(\Delta I)^2] = B_{\mathrm{c}}^{(L_{\mathrm{d}})}$	characteristic field for the current fluctuations
$\mathrm{C}(\mathbf{Q}, \omega)$	Cooperon
$c_k^\dagger$, c_k	Fermi creation and annihilation operators
$D = v_{\mathrm{F}} l/2$	diffusion constant
d	distance of the 2DEGs
$\mathrm{D}(\mathbf{q}, \omega)$	diffuson
$\Delta = 1/(\nu L^2)$	level spacing
$-e$	electron charge
$E_{\mathrm{Th}} = D/L^2$	Thouless energy
ϵ_{F}	Fermi energy
ϕ	magnetic flux
$\mathrm{G}(V)$	differential conductance
$\bar{\mathrm{g}} = \mathrm{G}(0)\epsilon_{\mathrm{F}}(eI_{\mathrm{o}})^{-1}$	dimensionless zero-bias conductance
$G^{\pm}(\mathbf{k}, \mathbf{k}'; \epsilon)$	Green's function
$G_{\mathrm{o}}^{\pm}(\mathbf{k}, \epsilon)$	unperturbed Green's function
$g^{\pm}(\mathbf{k}, \epsilon; \tau)$	impurity averaged Green's function
$\Gamma(\mathbf{k_1}, \mathbf{k_2}, \mathbf{k}'_{\mathbf{1}}, \mathbf{k}'_{\mathbf{2}}; \epsilon_1, \epsilon_2)$	reducible vertex function
$I_{\mathrm{o}} = e\,\lvert T \rvert^2 L^2 \nu$	reference current
$k_{\mathrm{F}} = m v_{\mathrm{F}}$	Fermi wave vector
L	system size

$l = v_{\mathrm{F}}\tau$	mean free path
$L_{\mathrm{b}} = v_{\mathrm{F}}/\omega$	ballistic length for a given time ω^{-1}
$L_{\mathrm{d}} = \sqrt{D/\omega}$	diffusion length for a given time ω^{-1}
L_ϕ	phase coherence length
$l_{\mathrm{m}} = \sqrt{2}(eBd)^{-1}$	magnetic length
$\lambda_{\mathrm{F}} = 2\pi/k_{\mathrm{F}}$	Fermi wave length
m	effective mass
μ	chemical potential
$n_{\mathrm{F}}(\epsilon)$	Fermi distribution function
ν	density of states at the Fermi energy
$\Pi(\mathbf{q}, \omega)$	irreducible vertex function
Σ	self-energy
T_τ	τ-ordering operator
$T_{\mathbf{xx'}}$, $T_{\mathbf{kp}}$	tunneling matrix element
τ	scattering time or mean free time
V	applied voltage
v_{F}	Fermi velocity

Chapter 1

Introduction

Historically, tunneling as a quantum phenomenon which reflects the wave-particle dualism has been known in the context of nuclear α-decay soon after the establishment of quantum theory. First measurements of electron tunneling between solids separated by a potential barrier can be found in the work of Esaki [1] on p-n junctions in 1958. In the following years, the activities concentrated on tunneling between metals and superconductors as well as between superconductors themselves. In this context the approach of the *tunneling Hamiltonian* [2] as a perturbative many-body theory has been developed. Starting from the 70s a new class of experiments became accessible due to advances in semiconductor device technologies. After the pioneering work of Chang *et al.* [3], extensive studies on double-barrier structures have been performed; for a list of references cf. [4]. Tunneling experiments between two-dimensional systems are realizable only since the late 80s [5].

The smallness of the structures needed for the observation of electron tunneling leads us to the subject of *mesoscopic physics*. The expression 'mesoscopic' has been coined by van Kampen in 1981 [6] in the context of statistical physics and it has become common use after a work of Imry [7]. The fascinating feature of this subject is the possibility of observing quantum effects on macroscopic objects. Mesoscopic physics studies systems that are too large and complex to find an exact description on a microscopic level since they have too many degrees of freedom, but, on the other hand, are too small to be fully described in the thermodynamic limit since quantum interference effects are still important. To understand what large or small means in this context we have to identify the relevant length scales of the system. The smallest length scale is the wave length of the particles, *i.e.* at low temperatures the Fermi wave length λ_{F}. Quantum interference is observable as long as phase coherence is not destroyed by inelastic processes. Coherent transport through the entire system is possible, if the phase coherence length L_ϕ becomes larger than the system size L. Then quantum interference effects play an essential role and one can measure *finger prints* of

the microscopic details of the sample. The mean free path l is the relevant scale to measure the strength of disorder. One can distinguish between *ballistic* and *diffusive* transport. If impurity scattering is negligible, *i.e.* the system is 'clean', the particle motion is ballistic, and therefore the transport properties are governed by the boundaries or, in other words, the geometry of the sample. This can be studied in so-called 'quantum billiards' which are the model systems for research on *quantum chaos* [8]. In diffusive systems a variety of interesting phenomena like weak localization [9], universal conductance fluctuations (UCF) [10], and the electronic Aharonov-Bohm effect [10, 11] have been observed.

Over the last decades technical progress has made it possible to tailor make more and more sophisticated structures. A specific class of these mesoscopic systems are two-dimensional electron gases (2DEGs) which can be realized in semiconductor heterostructures [12]. To date, these 2DEGs are the systems of choice for studying transport because they show a rich phenomenology, the most prominent example being the quantum Hall effect discovered by von Klitzing *et al.* in 1980 [13], and are easily manageable experimentally. A wide class of experiments is based on 2DEGs coupled via quantum mechanical tunneling since it has become possible to build up layered structures of 2DEGs. The simplest extension of the standard two-dimensional (2D) system is the so-called double quantum well (DQW), consisting of two parallel 2DEGs separated by a potential barrier. The first experimental realizations of DQWs only allowed simultaneous contact to both layers. With this setup one can study the influence of tunneling on the in-plane transport [14–17]. New techniques for creating independent contacts [18–21] opened the possibilities for novel experiments, *i.e.* direct observation of the tunneling current between 2DEGs has become accessible. The first measurements have been reported by Smoliner *et al.* [5].

Measurements of the tunneling current provide information about the intralayer transport complementary to what can be found from in-plane measurements, *i.e.* the tunneling current is a function of the one-particle Green's functions while in-plane transport depends on the two-particle Green's functions. This concept has been discussed in various works, *e.g.* [22–25] (furthermore cf. [26] for 1D-2D tunneling). The dependence of the tunneling current on macroscopic system parameters can be used to reconstruct the microscopic details encoded in the Green's function. Thus, it allows the local transport properties of the system to be studied without the crude intervention of plugging contacts on the layers.

This work studies the dependence of the tunneling current between two parallel 2DEGs on a weak in-plane magnetic field. Theoretical [23] as well as experimental [22] investigations of this setup are well established. But while previous investigations concentrated on the average current, the aim of this work is to show that the study of the current fluctuations yields additional information which is not contained in the impurity averaged quantities. The determination of the current fluctuations allows one to describe the field dependence of the

typical tunneling current within a particular system. The tunneling current is dominated by processes where an electron tunnels, propagates within the layer, then tunnels back, and recombines with the hole left behind. Since this 'loop' encloses magnetic flux, the field dependence measures the typical 'range' of the dominant processes. In contrast to the averaged Green's function, the Green's function of a specific sample is long-ranged. This results in a drastic enhancement of the sensitivity to an external magnetic field as will be shown. One can distinguish the characteristic field scales $B_{\rm c}[\langle I\rangle]$ and $B_{\rm c}[\overline{(\Delta I)^2}]$ and relate them to the mean free path l and the diffusion length $L_{\rm d} = \sqrt{D/eV}$ (for a given time interval $(eV)^{-1}$), respectively. In fact, there are two dominant contributions to the current fluctuations, only one of them being field dependent. We have shown that this so-called 'Cooperon' contribution can be seen as the Fourier transform (with respect to the magnetic field, *i.e.* the vector potential) of the product of the correlation functions of the 2DEGs. Thus, the field dependence of the tunneling current is a means to probe spatial correlations.

The present work is organized as follows: In chapter 2 the experimental realization of 2DEGs in semiconductor heterostructures is presented. The specific properties of the tunneling setup are briefly discussed. Furthermore, related theoretical and experimental results are reviewed, concentrating mainly on two aspects, namely the influence of magnetic fields and electron-electron interactions, where a keyword is the 'Coulomb drag' effect. In chapter 3 the model used in this work is introduced and the techniques needed in the evaluation of the tunneling current are given. In addition, the effects of an in-plane magnetic field are discussed. In chapter 4 the setup is specified, before coming to the calculations. A setup with two clean 2DEGs serves as a starting point for the evaluation of the tunneling current between a clean and a disordered 2DEG in section 4.2 and between two disordered 2DEGs in section 4.3. As mentioned above, we concentrate on the current fluctuations, but, for completeness, the average current (cf. Eisenstein *et al.* [22], Zheng and MacDonald [23]) is reviewed, too. The main results are summarized in chapter 5. Furthermore, the prospects for future investigations in the subject are discussed there. In order to preserve a more transparent structure in the main text, some technical tools as well as details of the calculations can be found in the appendices.

Chapter 2

Experimental situation and related works

Since tunneling experiments between two-dimensional electron gases have first been reported in 1988 by Smoliner *et al.* [5], many investigations followed in this research area. In order to embed the present work in this context, a selection of theoretical and experimental results related to tunneling between two-dimensional electron gases is reviewed in section 2.2. As an introduction before discussing the more complex system of two coupled two-dimensional electron gases, in section 2.1 the basic properties of a single two-dimensional electron gas are presented.

2.1 Two-dimensional electron gases

In order to illustrate what is meant by 'two-dimensional' (2D), consider a system as a box of volume $L_x \times L_y \times L_z$. If one of these lengths, *e.g.* L_z, is of the order of magnitude of the wave length of the particles (while the other two lengths are still much larger), momentum quantization becomes important in that direction, *i.e.* $k_z = n \cdot 2\pi/L_z$ ($n \in \mathbb{Z}$). Thus, the system is quasi-2D since the motion in x- and y-direction is free whereas with respect to k_z different 'modes' exist. At low temperatures, the particle energies are limited by the Fermi energy. Thus, for $L_z < \lambda_\mathrm{F} \ll L_x, L_y$, only $k_z = 0$ is allowed and therefore the particle motion is confined to the x-y-plane. Then the system is effectively two-dimensional.

Technically, these so-called two-dimensional electron gases (2DEGs) can be realized in MOSFETs (metal-oxide-semiconductor field-effect transistors) and semiconductor heterostructures [27]. In semiconductor heterostructures high mobilities are achieved due to the spatial separation of the carriers from their donors. The properties of heterojunctions between dissimilar semiconductors are governed

by the lineup of the valence and conduction bands at the interface. One needs modern growth techniques like molecular beam epitaxy (MBE) [28] to produce abrupt interfaces with the band structure changing within a few atomic layers. Furthermore, in order to reduce interface defects, the two materials have to be 'lattice matched', *i.e.* they have to share a similar lattice structure, a prerequisite which is almost ideally fulfilled by the system AlGaAs/GaAs.

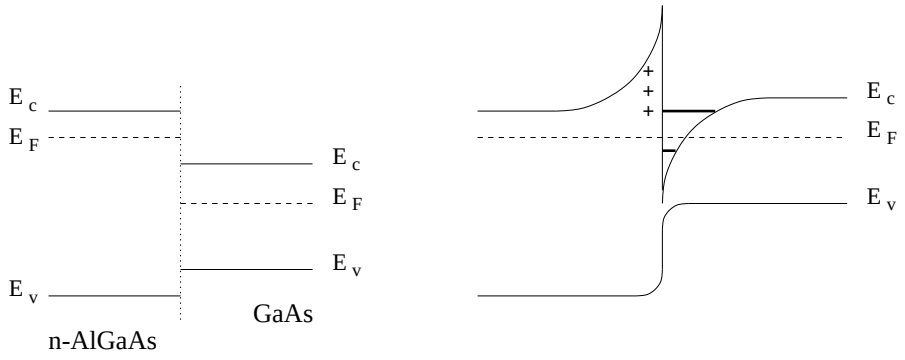

Figure 2.1: Band diagram of a 2DEG in an AlGaAs-GaAs heterostructure. (E_v: energy of the valence band, E_c: energy of the conduction band)

AlGaAS has a wide band-gap while GaAs is a narrow gap material (see Fig. 2.1). Furthermore, AlGaAs has the smaller electron affinity. So-called modulation doping (MD), *i.e.* selective doping of the wide gap material (usually with Si), leads to the diffusion of free carriers from the n-AlGaAs into the GaAs, leaving positively charged donors behind. This charge separation leads to an electrostatic potential which causes band bending as shown in Fig. 2.1. An almost triangular potential well is formed, trapping the electrons within a short distance of a few nanometers from the interface. Due to this confinement, momentum quantization occurs in the perpendicular direction whereas free motion within the interface is possible. However, the particles are scattered by the remote donors, thus limiting the mobility. This effect can be reduced by placing an additional undoped AlGaAs spacer between the doped n-AlGaAs and the GaAs layer. Today it is possible to achieve mean free paths up to about 10μm. The typical parameters of a 2DEG in AlGaAs-GaAs heterostructures are shown in table 2.1. Since the phase coherence length is strongly temperature dependent[1], experiments have to be performed at very low temperatures.

[1]The $\mathrm{T}^{-1/2}$ temperature dependence given in table 2.1 is only meant as an indication. In general, a simple power law cannot be found.

Effective mass m	$0.067 \cdot m_e$
Fermi wave vector k_F	$1.58 \cdot 10^6\,\mathrm{cm}^{-1}$
Fermi energy $\epsilon_F = (\hbar k_F)^2/(2m)$	$14\,\mathrm{meV}$
Fermi wave length $\lambda_F = 2\pi/k_F$	$40\,\mathrm{nm}$
Fermi velocity $v_F = \hbar k_F/m$	$2.7\,\mathrm{cm/s}$
Scattering time τ	$0.38 - 38\,\mathrm{ps}$
Electron mobility $\mu = \tau \cdot e/m$	$10^4 - 10^6\,\mathrm{cm}^2/(\mathrm{Vs})$
Mean free path $l = v_F\tau$	$10^2 - 10^4\,\mathrm{nm}$
Diffusion constant $D = v_F l/2$	$140 - 14000\,\mathrm{cm}^2/\mathrm{s}$
Phase coherence length L_ϕ	$> 200(\mathrm{T/K})^{-1/2}\,\mathrm{nm}$

Table 2.1: Electronic properties of 2DEGs in AlGaAs-GaAs heterostructures (taken from [4]).

2.2 Overview on the state of research on tunneling between 2DEGs

The system studied in this work is not a single 2DEG, but a structure with two closely spaced, parallel 2DEGs, *i.e.* a so-called double quantum well (DQW). The typical distance between the two layers ranges from a few ångstrøms to some tens of nanometers, depending on the effects one wants to observe. A schematic picture is shown in Fig. 2.2. Only a selection of the results related to tunneling between 2DEGs can be presented here. We will restrict ourselves to an overview on tunneling in a magnetic field (2.2.1) followed by a short discussion of the impact of tunneling coupling on the in-plane transport (2.2.2) and of the so-called Coulomb drag effect (2.2.3).

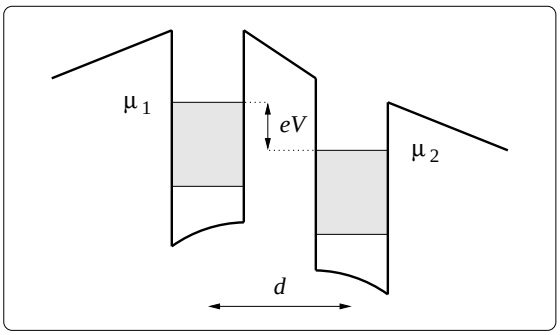

Figure 2.2: Schematic potential profile of the DQW structure.

2.2.1 Tunneling in a magnetic field

Tunneling between two-dimensional systems (2D-2D) is characterized by momentum and energy conservation [29] which is in sharp contrast to 2D-3D or 3D-3D junctions where tunneling occurs over a wide range of energies ($\sim \epsilon_{\mathrm{F}}$). Thus, the current-voltage characteristics shows pronounced resonant features since tunneling is only possible if the energy levels of the 2DEGs are aligned. This unique property of 2D-2D tunneling allows to extract far reaching information about the underlying spectral functions of the 2DEGs.

The I-B-characteristics for tunneling between 2DEGs in an in-plane magnetic field have been investigated first by Eisenstein *et al.* [22]. The results can be explained by the displacement of the Fermi surfaces of the two layers (as depicted in Fig. 2.3) caused by the magnetic field. Due to momentum and energy conservation, tunneling only takes place at the overlap of the two Fermi circles. This 'geometrical' explanation (originally introduced by Zavlavsky *et al.* [30] for 2D-3D tunneling) will be discussed explicitly in section 4.1. Similar arguments apply also for the dependence of the tunneling conductance on the ratio of the densities at fixed magnetic field. The influence of disorder on these characteristics, leading to a broadening of the resonant features, has been studied by Zheng and MacDonald [23]. Since these results are essential for the present work, they will be discussed in detail in chapter 4.

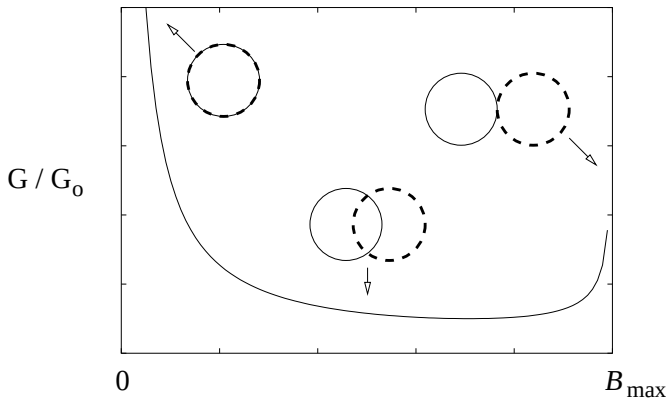

Figure 2.3: Tunneling conductance versus in-plane magnetic field, explained by the relative shift of the Fermi circles. For $B > B_{\mathrm{max}}$ tunneling is completely suppressed.

Other broadening mechanism could be spatial variations of the barrier width which result in non-uniformities of the tunneling probability [31] or electron-electron interactions [24, 32]. The importance of the former contribution is not very well known, yet, since no non-destructive methods of measuring the barrier width are available so far [33]. Electron-electron interactions are negligible at

low temperatures due to phase space restrictions. In fact, their contribution to the linewidth can be distinguished from the other effects by the temperature dependence [24]. In [23] also the effects of interlayer correlations of the disorder potential have been studied. It has been shown that only strong correlations lead to a significant change of the current characteristics at low magnetic fields. Then disorder no longer suppresses the divergence of the tunneling conductance at $B = 0$. However, strong correlations are only expected if the disorder potential is caused by impurities between the layers. In the usual case of remote impurities only the layer nearby is influenced while the other 2DEG is screened.

The rich facilities of tunneling spectroscopy have also been demonstrated in the work of Altland *et al.* [26] where the idea of using magnetotunneling as a spectrometer has been applied to 1D-2D tunneling, *i.e.* tunneling between a quantum wire (defined by gates) running in parallel with a 2DEG. The quantum wire being a one-dimensional electron system (1DES) cannot be described by the usual Fermi liquid picture as already very weak interactions make it unstable towards a highly correlated state, the so-called Luttinger liquid (LL). A main characteristic of the LL phase is spin-charge separation. Although experiments are consistent with many features of LL behavior, there is no clear evidence for this phenomenon so far. Altland *et al.* propose an experiment probing spin-charge separation by measuring the dependence of the tunneling conductance on the applied voltage V and an in-plane magnetic field B. Tuning these parameters, four different regimes with distinct current characteristics should be found if the 1DES can be described as a LL. The boundaries of these regimes are determined by the velocities of spin and charge density waves. Thus, the experiment provides a way to measure the ratio of spin and charge velocity, *i.e.* the parameter characterizing the LL phase.

2.2.2 In-plane transport in DQWs

The tunneling resonance described above can also be observed by studying the in-plane resistance of a DQW at small layer separation when the tunneling coupling is large. For that purpose the 2DEGs are contacted in parallel. Off resonance, *i.e.* when the energy levels of the 2DEGs are not matched, tunneling is suppressed and, thus, the 2DEGs are decoupled. Then the combined resistance of the parallel configuration is simply given as $R_{\mathrm{off}} \sim (\tau_1 + \tau_2)^{-1}$. At resonance, however, the particles are not localized within one 2DEG, but rather described by symmetric and antisymmetric states separated by an energy gap Δ_{SAS}. In this case the resistance is given as $R_{\mathrm{res}} \sim \tau_1^{-1} + \tau_2^{-1}$ [14, 34], assuming that the scattering rates of the two layers are additive. If the mobilities of the 2DEGs are different, the off-resonance resistance is governed by the higher mobility layer while at resonance the lower mobility layer is dominant which leads to a resistance resonance.

The influence of an in-plane magnetic field has been investigated in [15, 16, 35]. Again the results can be described by the relative shift of the Fermi circles. Since

the field decouples the layers, the resonance is suppressed, *i.e.* the resistance approaches its off-resonance value. The effect is anisotropic with respect to the orientation of the current and the in-plane magnetic field. This can be attributed to the fact that for $\mathbf{B} \parallel \mathbf{j}$ the current carrying states have momenta in the vicinity of the (quasi-)intersection points of the Fermi circles and thus still participate in tunneling. Therefore the suppression of the resistance resonance is not complete in this case.

A different setup has been chosen in [36] where tunneling coupled mesoscopic wires have been studied. Under application of an in-plane magnetic field, fluctuations of the in-plane conductance have been observed. With increasing distance between the layers (corresponding to decreasing tunneling probabilities) the fluctuations become less pronounced. As the electrons stay longer within one well before tunneling, the probability of inelastic scattering increases, *i.e.* quantum interference effects are destroyed. Furthermore, for $B > B_{\max}$ (cf. Fig. 2.3) the fluctuations vanish because the two wells decouple.

2.2.3 The Coulomb drag

In section 2.2.1 *intra*layer electron-electron interactions have already been addressed. Now we come to the other aspect of the problem, namely the *inter*layer electron-electron interactions which are responsible for the so-called *Coulomb drag* effect. The first theoretical discussions of the Coulomb drag between spatially separated electron layers date back to Pogrebinskii [37] and Price [38], while the earliest direct experimental observation in DQWs has been reported by Gramila *et al.* [39].

Drag experiments are usually performed in a regime where tunneling is suppressed, either due to a mismatch of the energy levels, cf. section 2.2.1, or at large layer separation $d > \lambda_{\mathrm{F}}$. A current applied to the so-called active layer causes a current in the other (passive) layer due to the mutual friction. If no current is allowed to flow there, a voltage is induced, compensating the effect of the interlayer force. The ratio of the induced voltage V_{passive} and the applied current I_{active} is called the transresistance or drag coefficient ρ_{D} which measures the momentum transfer rate between the layers. The dependence of ρ_{D} on the layer separation as well as on temperature is given as $\rho_{\mathrm{D}} \sim d^{-4}T^2$ (see *e.g.* [39, 40]). Alternatively to the drag coefficient, a corresponding interlayer scattering rate τ_{D}^{-1} can be defined. The measured values for typical samples do not exceed about 1% of the mobility scattering rate τ^{-1}, *i.e.* the effect is negligibly small. However, strong disorder ($l < d$) [41, 42] or interlayer correlations of the impurity potential [43] lead to an enhancement.

Chapter 3

The current formula

Chapter 2 giving an overview of the research on tunneling between 2DEGs, this chapter is dedicated to the introduction of the model as well as the techniques used in the present work. Some technical tools are presented in more detail in appendix A.

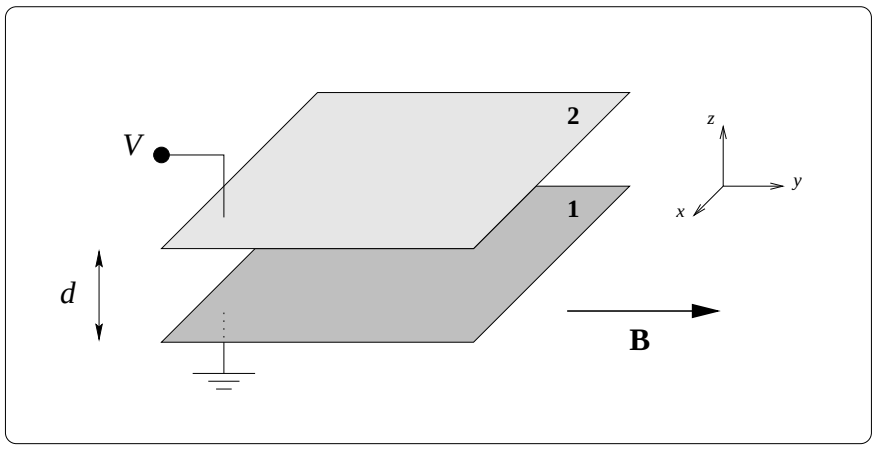

Figure 3.1: Schematic setup.

The experimental setup under consideration is shown schematically in Fig. 3.1: Two parallel 2DEGs are separated by a tunneling barrier of thickness d. A tunneling current between the layers is driven by the external voltage V. In addition, a homogeneous, in-plane magnetic field $\mathbf{B}$ may be applied.

In order to find a full description of the tunneling current between the 2DEGs, three main aspects will be addressed in this chapter: a general approach to tunneling between two reservoirs, the impact of a magnetic field, and finally the transport properties within the layers themselves, *i.e.* the influence of disorder. This suggests to divide the chapter into three parts:

- In section 3.1 the tunneling Hamiltonian formalism is presented and a current formula is derived. The formula is kept as general as possible; the specific features of the setup under investigation will be introduced later.
- The modifications of the formula caused by a weak, in-plane magnetic field are shown in section 3.2.
- Section 3.3 is concerned with the transport within the layers. The influence of disorder is reviewed using a diagrammatic approach to calculate impurity averages. This is necessary to calculate the average current as well as its fluctuations.

3.1 The tunneling Hamiltonian

The tunneling Hamiltonian was introduced in 1962 by Cohen *et al.* [2] to explain experimental results on tunneling between normal metals and superconductors. Since then it has been widely used to describe tunneling in superconductors, but the underlying concept is more general. In the following, we will derive a formula for the tunneling current starting from this concept and also discuss its limitations. The outline of the section is based on Mahan's book [44]. For an alternative discussion see *e.g.* [45].

Consider two conducting layers, labeled 1 and 2, separated by an insulating barrier. The basic idea is to decompose the Hamiltonian of the total system into three terms:

$$H = H_1 + H_2 + H_\mathrm{T}\,, \tag{3.1}$$

where H_1 (H_2) is the Hamiltonian for layer 1 (2) while H_T describes tunneling through the barrier.

Thus, the tunneling can be separated from the physics within the layers. The H_i ($i \in \{1,2\}$) may contain impurity scattering, electron-electron interactions, ... , *i.e.* all the many-body interactions on either side of the tunneling junction. So far nothing has to be known about their properties. The only assumption is that the two sides are independent, and therefore

$$[H_1, H_2] = 0\,.$$

In fact we even need the stronger condition that the Hamiltonians commute term by term. If H_1 can be expressed in terms of a set of Fermi creation and annihilation operators $c_k^\dagger, c_k$ while H_2 is expressed in terms of a different set of operators $c_p^\dagger, c_p$ (where k, p are the quantum numbers appropriate for the problem of interest), we have to claim that these operators anticommute. That is

$$\{c_k, c_p^\dagger\} = 0\,, \quad \{c_p, c_k^\dagger\} = 0\,.$$

The coupling between the two layers is contained in H_T which has the following form:

$$H_\mathrm{T} = \sum_{k,p} (T_{kp} c_k^\dagger c_p + T_{kp}^* c_p^\dagger c_k) \,, \tag{3.2}$$

where T_{kp} are the tunneling matrix elements. $T_{kp}^* = T_{pk}$ is the complex conjugate of T_{kp}. The first term describes tunneling from layer 2 to layer 1, *i.e.* an electron with quantum number p is annihilated in layer 2 and an electron with quantum number k is created in layer 1, the amplitude for this being T_{kp}, while the second term describes the inverse process.

The tunneling current is now defined as the expectation value of the rate of change of the number of particles N_i in one layer, say layer 2, multiplied by their charge $-e$:

$$I(t) = -e\langle \dot{N}_2 \rangle \,, \tag{3.3}$$

where $\langle ... \rangle$ denotes the expectation value and $\dot{N}_2 = \frac{\mathrm{d}}{\mathrm{d}t} N_2$.

Since the H_i conserve the particle number, *i.e.* $[H_i, N_j] = 0$, the equation of motion for $N_2 = \sum_p c_p^\dagger c_p$ reduces to[1]

$$\dot{N}_2 = \mathrm{i}[H_\mathrm{T}, N_2] = \mathrm{i} \sum_{k,p} (T_{kp} c_k^\dagger c_p - T_{kp}^* c_p^\dagger c_k) \,. \tag{3.4}$$

In the following we choose the interaction representation with H_T as perturbation: $O(t) = \mathrm{e}^{\mathrm{i}\tilde{H}t} O \mathrm{e}^{-\mathrm{i}\tilde{H}t}$ for any operator O, with $\tilde{H}$ being the unperturbed part of the Hamiltonian, *i.e.* $\tilde{H} = H_1 + H_2$. Then linear response theory[2] gives the expression for the current in leading order in T_{kp}:

$$I(t) = -\mathrm{i}e \int_{-\infty}^{t} \mathrm{d}t' \, \langle [\dot{N}_2(t), H_\mathrm{T}(t')] \rangle \,. \tag{3.5}$$

Multiple tunneling contributions are neglected. This is reasonable as long as the tunneling probability is sufficiently low.

The next step in the derivation is to introduce the applied voltage V into the formula. This can be done by insertion of the chemical potentials of the layers. For the Hamiltonian with respect to the chemical potential the symbol K_i is used ($K_i = H_i - \mu_i N_i$). Since the number operators N_i commute with $\tilde{H} = \tilde{K} + \mu_1 N_1 + \mu_2 N_2$, it is possible to separate the exponentials in the time evolution of the operators: $\mathrm{e}^{\pm \mathrm{i}\tilde{H}t} = \mathrm{e}^{\pm \mathrm{i}\tilde{K}t} \mathrm{e}^{\pm \mathrm{i}(\mu_1 N_1 + \mu_2 N_2)t}$. The commutator of H_T with the number operators then produces a factor $\mathrm{e}^{\pm \mathrm{i}(\mu_2 - \mu_1)t}$. The difference of

[1] For convenience, natural units where $\hbar = 1$ are used throughout this work.

[2] The steps leading to Eq. 3.5 are very similar to the derivation of the Kubo formula.

the chemical potentials can be identified as the applied voltage: $\mu_2 - \mu_1 = eV$. We assume that both sides of the tunneling junction are in separate thermodynamic equilibrium.

Introducing the shorthand notation $\mathcal{A}(t) = \sum_{k,p} T_{kp} c_k^\dagger(t) c_p(t)$, where now the time dependence is governed by K_1 and K_2, respectively, the equation takes the form

$$I(t) = e \int_{-\infty}^{t} \mathrm{d}t' \, \langle [\mathrm{e}^{-\mathrm{i}eVt}\mathcal{A}(t) - \mathrm{e}^{\mathrm{i}eVt}\mathcal{A}^\dagger(t), \mathrm{e}^{-\mathrm{i}eVt'}\mathcal{A}(t') + \mathrm{e}^{\mathrm{i}eVt'}\mathcal{A}^\dagger(t')] \rangle \, . \tag{3.6}$$

There are four different terms: the contributions containing $\mathcal{A}\mathcal{A}^\dagger$ or $\mathcal{A}^\dagger\mathcal{A}$ describe the single-particle tunneling while the others are responsible for pair tunneling, known as the Josephson effect in superconductors [46]. Here, we will only be concerned with normal conducting materials. Thus, writing

$$I = I_\mathrm{S} + I_\mathrm{J} \tag{3.7}$$

for the single-particle and the Josephson contribution, we only need to consider

$$I_\mathrm{S} = e \int_{-\infty}^{\infty} \mathrm{d}t' \, \theta(t-t') \big\{ \mathrm{e}^{\mathrm{i}eV(t'-t)} \langle [\mathcal{A}(t), \mathcal{A}^\dagger(t')] \rangle - \mathrm{e}^{-\mathrm{i}eV(t'-t)} \langle [\mathcal{A}^\dagger(t), \mathcal{A}(t')] \rangle \big\} \, . \tag{3.8}$$

Since the expression in the integral can be shown to depend on the time difference $\Delta t = t - t'$ only, I_S is time-independent. (In the following the index S will be dropped again.)

The first term has the form of a retarded correlation function while the second term is just its Hermitian conjugate. Defining

$$\tilde{X}_\mathrm{ret}(t) = -\mathrm{i}\theta(t) \langle [\mathcal{A}(t), \mathcal{A}^\dagger(0)] \rangle \, , \tag{3.9}$$

the single-particle tunneling current takes the simple form

$$I(eV) = -2e \, \mathrm{Im} \, [X_\mathrm{ret}(-eV)] \, , \tag{3.10}$$

where $X_\mathrm{ret}(-eV)$ is the Fourier transform of $\tilde{X}_\mathrm{ret}(t)$. For further evaluation it is convenient to use the Matsubara formalism (see appendix A), *i.e.*

$$\begin{aligned} \mathcal{X}(\mathrm{i}\omega) &= -\int_0^\beta \mathrm{d}\tau \langle \mathrm{T}_\tau \, \mathcal{A}(\tau) \mathcal{A}^\dagger(0) \rangle \, \mathrm{e}^{\mathrm{i}\omega\tau} \\ &= -\sum_{k,p;k',p'} T_{kp} T^*_{k'p'} \int_0^\beta \mathrm{d}\tau \langle \mathrm{T}_\tau \, c_k^\dagger(\tau) c_p(\tau) c_{p'}^\dagger(0) c_{k'}(0) \rangle \, \mathrm{e}^{\mathrm{i}\omega\tau} \, , \end{aligned}$$

where T_τ is the τ-ordering operator (see appendix A). The correlation function $\mathcal{X}(\mathrm{i}\omega)$ can be shown to be related to $X_{\mathrm{ret}}(-eV)$ by analytic continuation.

Specifying that the quantum numbers k, p are momenta (in the following denoted by bold letters $\mathbf{k}, \mathbf{p}$), $\mathcal{X}(\mathrm{i}\omega)$ can be expressed as the product of two Green's functions. The expectation values are to be taken separately for the different layers, *i.e.* $\langle \mathrm{T}_\tau\, c^\dagger_{\mathbf{k}}(\tau) c_{\mathbf{p}}(\tau) c^\dagger_{\mathbf{p}'}(0) c_{\mathbf{k}'}(0)\rangle = \langle \mathrm{T}_\tau\, c^\dagger_{\mathbf{k}}(\tau) c_{\mathbf{k}'}(0)\rangle \langle \mathrm{T}_\tau\, c_{\mathbf{p}}(\tau) c^\dagger_{\mathbf{p}'}(0)\rangle$, because the layers are independent. Hence,

$$\mathcal{X}(\mathrm{i}\omega) = \sum_{\mathbf{k},\mathbf{p};\mathbf{k}',\mathbf{p}'} T_{\mathbf{k}\mathbf{p}} T^*_{\mathbf{k}'\mathbf{p}'} \int_0^\beta \mathrm{d}\tau\, \mathcal{G}_1(\mathbf{k},\mathbf{k}';-\tau)\mathcal{G}_2(\mathbf{p}',\mathbf{p};\tau)\, \mathrm{e}^{\mathrm{i}\omega\tau}\,. \tag{3.11}$$

Here we assume that the tunneling matrix elements depend only on momentum. This is not true in general, but it is a good approximation if the energy range of the particles involved is narrow enough. The tunneling particles do have energies near the Fermi energy ϵ_{F} within an interval determined by the temperature T and the voltage V. If these energy scales are small ($\Delta E \ll \epsilon_{\mathrm{F}}$), the tunneling matrix elements can be approximated by their value at the Fermi energy.

After frequency summation (see *e.g.* [44]) this finally leads to the formula [47]

$$\boxed{I = 2e \sum_{\mathbf{k},\mathbf{p};\mathbf{k}',\mathbf{p}'} T_{\mathbf{k}\mathbf{p}} T^*_{\mathbf{k}'\mathbf{p}'} \int_{-\infty}^{\infty} \tfrac{\mathrm{d}\epsilon}{2\pi} [n_{\mathrm{F}}(\epsilon) - n_{\mathrm{F}}(\epsilon + eV)] A_1(\mathbf{k},\mathbf{k}';\epsilon) A_2(\mathbf{p}',\mathbf{p};\epsilon + eV)}\,, \tag{3.12}$$

where n_{F} Fermi distribution function: $n_{\mathrm{F}}(\epsilon) = (\mathrm{e}^{\beta\epsilon}+1)^{-1} \xrightarrow[\beta\to\infty]{} \theta(\epsilon)$,

A_i spectral function for layer i:
$A_i = \mathrm{i}(G_i^+ - G_i^-)$ (for the definition of $G_i^\pm$ see appendix A).

There is one more simplification that can be done. As the tunneling probability decays exponentially with the barrier thickness, we assume that tunneling only occurs perpendicular to the planes because this involves the smallest distance. Then the tunneling matrix elements are diagonal in coordinate representation.[3] In momentum representation they only depend on the difference of momenta: $T_{\mathbf{k}\mathbf{p}} = T(\mathbf{p}-\mathbf{k})$. By Fourier transforming Eq. 3.12 we get

$$I = \frac{2e}{L^4} \int \mathrm{d}^2x \mathrm{d}^2x'\, T_{\mathbf{x}} T^*_{\mathbf{x}'} \int (\mathrm{d}\epsilon^{[eV]})\, A_1(\mathbf{x},\mathbf{x}';\epsilon) A_2(\mathbf{x}',\mathbf{x};\epsilon + eV)\,, \tag{3.13}$$

where the shorthand notation $\int(\mathrm{d}\epsilon^{[eV]}) = \int_{-\infty}^{\infty} \frac{\mathrm{d}\epsilon}{2\pi}[n_{\mathrm{F}}(\epsilon) - n_{\mathrm{F}}(\epsilon+eV)]$ has been introduced.

This describes a particle tunneling at point $\mathbf{x}$ from layer 2 to layer 1, propagating within this layer to $\mathbf{x}'$, tunneling back to layer 2 and finally returning there to its starting point $\mathbf{x}$, thus describing a closed loop (as depicted in Fig. 3.2).

[3] Here it becomes important that the systems are two-dimensional. Therefore the spatial as well as the momentum coordinates are two-component vectors in the x-y-plane. Note that the third dimension will be needed in the implementation of the magnetic field.

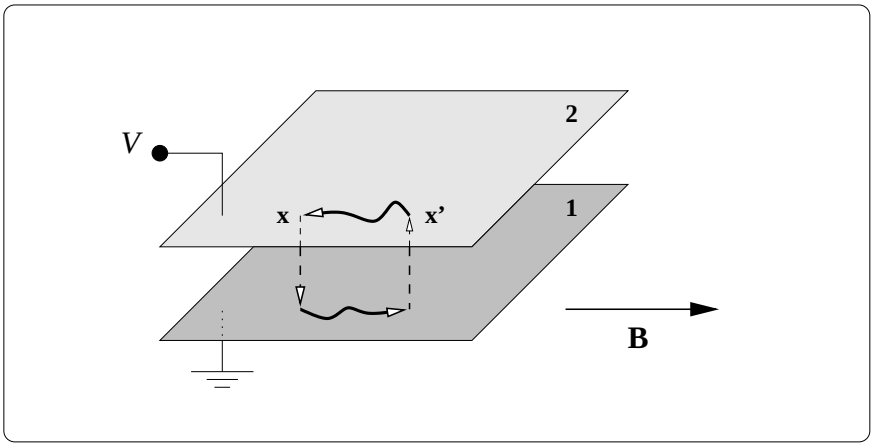

Figure 3.2: Schematic setup with current loop.

Let us summarize. In this section an expression for the tunneling current based on the tunneling Hamiltonian model has been derived. Linear response theory in H_{T} has led to a formula which is quadratic in the tunneling matrix elements and has the form of a spectral function. In the derivation the following assumptions have been made:

- The two sides of the tunneling junction are independent systems which only interact via the tunneling matrix elements. Without tunneling they are in separate thermodynamic equilibrium.
- The tunneling probability is small enough to be considered as a perturbation. Therefore multiple tunneling events can be neglected and linear response theory applies. Furthermore, the tunneling matrix elements do not depend on energy.
- Tunneling occurs only perpendicular to the barrier. Other processes are negligible since the tunneling probability decays exponentially with distance.

For these assumptions to be adequate, the experimental setup has to satisfy some requirements. However, these conditions can be fulfilled in a typical setup. Therefore they are not too restrictive.

- The barrier has to be rather thick. A typical value would be in the order of a few tens of nanometers.
- The applied voltage has to be small compared to the Fermi energy. We will see later that the interesting range of voltages for the problem to study is even much smaller.

Having derived the general tunneling formula, the next step will be to implement the modifications caused by a magnetic field.

3.2 The effects of an in-plane magnetic field

The particular situation to be studied in this work is the application of a weak, homogeneous, in-plane magnetic field $\mathbf{B}$. In contrast to the application of a perpendicular magnetic field, this does not give rise to energy quantization in Landau levels.

Defining a coordinate system as shown in Fig. 3.1 with the z-axis perpendicular to the planes and the origin situated in layer 2, we can choose a gauge where the corresponding vector potential $\mathbf{A}$ lies in the x-y-plane as well as $\mathbf{B}$ itself. Then its value depends only on z: $\mathbf{A} = z\,\mathbf{B} \times \mathbf{e_z}$, where $\mathbf{e_z}$ is the unit vector in z-direction.[4] Within the layers this has the constant values

$$\mathbf{A}(1) = d\,\mathbf{B} \times \mathbf{e_z} \qquad \text{and} \qquad \mathbf{A}(2) = 0\,,$$

where d is the distance of the 2DEGs.

The tunneling formula in momentum representation

The vector potential $\mathbf{A}$ is implemented into the Hamiltonian by minimal coupling, thus shifting the momentum $\mathbf{k}$ to $\mathbf{K} = \mathbf{k} - e\mathbf{A}$.

This implies that the magnetic field dependence can be incorporated in the spectral functions (or Green's functions) for layer 1 while not affecting the other layer. Due to the fact that $\mathbf{A}$ is constant within the planes, the effect in layer 1 amounts to a shift of the origin of momentum by $ed\,\mathbf{B} \times \mathbf{e_z}$.

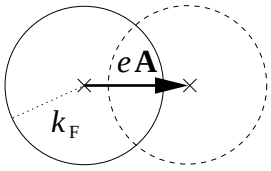

Then the Green's function with magnetic field $A_1(\mathbf{k}, \mathbf{k}', \epsilon; \mathbf{B})$ is just the zero-field Green's function where $\mathbf{k}^{(\prime)}$ is replaced by $\mathbf{K}^{(\prime)}$, *i.e.*

$$A_1(\mathbf{k}, \mathbf{k}', \epsilon; \mathbf{B}) = A_1(\mathbf{K}, \mathbf{K}', \epsilon; \mathbf{B} = 0)\,. \tag{3.14}$$

[4] Only in this section three-component vectors are used. After having fixed the values of the vector potential within the different layers, the additional z-component of the spatial coordinates can be chosen to be an arbitrary constant.

This leads to the following expression for the tunneling current:

$$I = 2e \sum_{\mathbf{k},\mathbf{p};\mathbf{k}',\mathbf{p}'} T_{\mathbf{kp}} T^*_{\mathbf{k}'\mathbf{p}'} \int (\mathrm{d}\epsilon^{[eV]}) A_1(\mathbf{K},\mathbf{K}';\epsilon) A_2(\mathbf{p}',\mathbf{p};\epsilon+eV)\,. \tag{3.15}$$

The tunneling formula in coordinate representation

Here it is most convenient to attribute the entire magnetic field dependence to the tunneling matrix elements, giving them a phase factor:

$$T_{\mathbf{x}} \longrightarrow T_{\mathbf{x}} \mathrm{e}^{-\mathrm{i}e\int_{\mathbf{x_o}}^{\mathbf{x}} \mathbf{A}(\mathbf{x}')\mathrm{d}\mathbf{x}'} = T_{\mathbf{x}} \mathrm{e}^{-\mathrm{i}ed(\mathbf{B}\times\mathbf{e_z})(\mathbf{x}-\mathbf{x_o})}\,, \tag{3.16}$$

where $\mathbf{x_o}$ is an arbitrary starting point. The choice of $\mathbf{x_o}$ does not affect the result because in the current formula only the product $T_{\mathbf{x}} T^*_{\mathbf{x}'}$ appears, so that $\mathbf{x_o}$ cancels. Then the tunneling current is given as

$$I = \frac{2e}{L^4} \int \mathrm{d}^2x \mathrm{d}^2x'\, T_{\mathbf{x}} T^*_{\mathbf{x}'} \int (\mathrm{d}\epsilon^{[eV]})\, \mathrm{e}^{-\mathrm{i}ed(\mathbf{B}\times\mathbf{e_z})(\mathbf{x}-\mathbf{x}')} A_1(\mathbf{x},\mathbf{x}';\epsilon) A_2(\mathbf{x}',\mathbf{x};\epsilon+eV)\,. \tag{3.17}$$

Thus, the magnetic field enters the equation as the flux ϕ enclosed by the current loop:

$$\mathrm{e}^{-\mathrm{i}ed(\mathbf{B}\times\mathbf{e_z})(\mathbf{x}-\mathbf{x}')} = \mathrm{e}^{2\pi\mathrm{i}\phi/\phi_\mathrm{o}}\,,$$

where $\phi = d\mathbf{B}(\Delta\mathbf{x})_\perp$ with $(\Delta\mathbf{x})_\perp = (\mathbf{x}-\mathbf{x}')\times\mathbf{e_z}$ and $\phi_\mathrm{o} = h/e$.

The particular paths within the layers do not play a role as only the distance, perpendicular to the magnetic field, of the tunneling sites determines the effect.

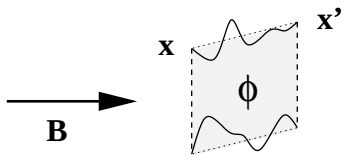

We now can define a magnetic length

$$l_\mathrm{m} \equiv \sqrt{2}(eBd)^{-1}\,, \tag{3.18}$$

given by the relation $\Delta\varphi(l_\mathrm{m}) = 2\pi\phi(l_\mathrm{m})/\phi_\mathrm{o} \doteq 1$. Our definition differs from the usual magnetic length $\tilde{l}_\mathrm{m} = (eB)^{-1/2}$ because of the specific geometry. In a magnetic field perpendicular to the plane, the magnetic length $\tilde{l}_\mathrm{m}$ is defined in such a way that the area $F = 2\pi\tilde{l}^2_\mathrm{m}$ encloses one flux quantum. Since in our case the relevant area does not lie within the plane but between the two layers, and the distance between them is fixed, only one side of the enclosed area, *i.e.* the distance within the x-y-plane, may be varied. Furthermore, only the area perpendicular to the magnetic field is relevant because $\phi = BF_\perp$. In order to account for this, the definition of l_m has to be chosen in the following way:

1. The two sides of the relevant area are treated differently, *i.e.* $\phi(l_\mathrm{m}) \sim B l_\mathrm{m} d$ (in contrast to $\phi(\tilde{l}_\mathrm{m}) = B\tilde{l}_\mathrm{m}^2$). Therefore the magnetic length is proportional to $(eBd)^{-1}$.

2. The orientation of the magnetic field and the current loop has to be considered: $F_\perp = F\,|\sin\alpha|$. Since no particular direction is preferred, we average over all angles. Thus, the average area perpendicular to the field is $\langle F_\perp \rangle = F/\sqrt{2}$, which leads to the factor $\sqrt{2}$ in (3.18).

Defining the magnetic length l_m in that way, the area $F = 2\pi l_\mathrm{m} d$ encloses one flux quantum on average.

We will see that both pictures, the coordinate as well as the momentum representation, are very useful in explaining the current characteristics. The relative shift of the two Fermi circles gives us a qualitative understanding of the overall shape of the I-B-curve. This will be explained in section 4.1 when discussing the tunneling current between 'clean' 2DEGs. The enclosed flux sets the magnetic length in relation with typical length scales of the system. That is why the field dependence of the tunneling current allows one to study transport properties of the 2DEGs. This is an important point to be discussed in much more detail in chapter 4 under different aspects.

3.3 Green's functions and impurity averages

In the current formula (3.12) two spectral functions appear. As they are combinations of Green's functions, we now will discuss the properties of those.

The simplest case is that of a 'clean' system without disorder, *i.e.* a pure metal. Neglecting electron-electron interactions, the electrons can be described as free particles in a Fermi sea. Their propagation is characterized by the unperturbed Green's function $G_\mathrm{o}^\pm$. In general, the situation is more complicated because a realistic system always contains some impurities. Thus, a particle moving through the system is scattered. In the discussed heterostructures *e.g.*, the electrons are scattered from the remote donors. Then it is not possible to calculate the exact Green's function for the problem. Assuming weak disorder, the Green's function for the disordered system can be obtained using perturbation theory.

The unperturbed Green's function $G_\mathrm{o}^\pm$

The Green's function $G_\mathrm{o}^\pm$ describing the propagation of a free particle is well known. The problem is invariant under translation, and the Green's function

$G_{\mathrm{o}}^{\pm}(\mathbf{r}-\mathbf{r}';E)$ is determined by the differential equation

$$(E \pm \mathrm{i}\eta - H_{\mathrm{o}}(\mathbf{r}))\, G_{\mathrm{o}}^{\pm}(\mathbf{r}-\mathbf{r}';E) = \delta(\mathbf{r}-\mathbf{r}')\,, \tag{3.19}$$

where $\eta \in \mathbb{R}_+$ is an infinitesimal quantity necessary to shift the poles away from the real axis (see appendix A) and $H_{\mathrm{o}}(\mathbf{r}) = -\nabla^2/(2m)$.

After Fourier transformation we find

$$G_{\mathrm{o}}^{\pm}(\mathbf{k};E) = \frac{1}{E - \epsilon_{\mathbf{k}} \pm \mathrm{i}\eta}\,,$$

where $\epsilon_{\mathbf{k}} = \mathbf{k}^2/(2m)$.

Or, measuring the energy with respect to the chemical potential ($\epsilon = E - \mu$),

$$G_{\mathrm{o}}^{\pm}(\mathbf{k};\epsilon) = \frac{1}{\epsilon - \xi_{\mathbf{k}} \pm \mathrm{i}\eta} \tag{3.20}$$

with $\xi_{\mathbf{k}} = \epsilon_{\mathbf{k}} - \mu$.

The spectral function is a δ-distribution:

$$A_{\mathrm{o}}(\mathbf{k};\epsilon) = 2\pi\delta(\epsilon - \xi_{\mathbf{k}})\,. \tag{3.21}$$

In coordinate representation, the form of the Green's function depends on the dimensionality of the system. The result in 2D is

$$G_{\mathrm{o}}^{\pm}(\mathbf{r}-\mathbf{r}';0) = \mp\mathrm{i}\pi\nu J_{\mathrm{o}}(k_{\mathrm{F}}\,|\mathbf{r}-\mathbf{r}'|)\,, \tag{3.22}$$

where ν is the density of states (DOS) at the Fermi energy. $J_{\mathrm{o}}(x) = \frac{1}{\pi}\int_0^{\pi} \mathrm{d}\varphi\, e^{\mathrm{i}x\cos\varphi}$ is the zeroth order Bessel function of the first kind.

A system with disorder can be modeled by introducing a random potential $V(\mathbf{r})$ into the Hamiltonian: $H = H_{\mathrm{o}} + V(\mathbf{r})$ where $V(\mathbf{r}) = \sum_{i=1}^{N_{\mathrm{imp}}} u_i(\mathbf{r})$ (N_{imp}: total number of impurities, u_i: potential of the i-th impurity). Each sample is characterized by a specific impurity configuration. The Green's function for this system can be very complicated as it depends on the position of every single impurity as well as the strength (and form) of its potential. Usually, these details are not available. Furthermore, knowing the Green's function for one particular configuration would not allow one to make predictions for any other sample. That is why it is necessary to calculate averages over different realizations of the disorder.

Ensemble averaging

Instead of choosing one specific disorder potential, a random potential is taken from a certain probability distribution $\mathcal{P}[V(\mathbf{r})]$. For any functional $F[V(\mathbf{r})]$ the impurity average $f_{\mathcal{P}}(\mathbf{r})$ is then defined as

$$f_{\mathcal{P}}(\mathbf{r}) \equiv \langle F[V(\mathbf{r})] \rangle = \int \mathcal{D}[V(\mathbf{r})] \;\; \mathcal{P}[V(\mathbf{r})] F[V(\mathbf{r})] \,, \tag{3.23}$$

where $\mathcal{D}[V(\mathbf{r})]$ is the integration measure.[5]

For example, we could choose the positions (Edwards [48]) or the strengths (Anderson [49]) of the impurities to be random, but in fact, it is not necessary to know the details of the distribution function. It is sufficient to make the usual assumption that the distribution function be Gaussian, thus being characterized by its mean value $\langle V(\mathbf{r}) \rangle$ and the correlation $\langle V(\mathbf{r}) V(\mathbf{r}') \rangle$. Choosing

$$\langle V(\mathbf{r}) \rangle \equiv 0 \,, \tag{3.24}$$

there are two parameters left, namely a potential correlation strength V_{o} and a potential correlation length l_V:

$$\langle V(\mathbf{r}) V(\mathbf{r}') \rangle = {V_{\mathrm{o}}}^2 \, e^{-\frac{|\mathbf{r}-\mathbf{r}'|^2}{{l_V}^2}} \,.$$

If l_V is smaller than any other relevant length scale in the system it can be taken to zero, leading to a δ-correlated white-noise potential:

$$\langle V(\mathbf{r}) V(\mathbf{r}') \rangle = \gamma \delta(\mathbf{r} - \mathbf{r}') \,, \tag{3.25}$$

where $\gamma = {V_{\mathrm{o}}}^2 / (\pi {l_V}^2)$ is kept finite by taking the limit $V_{\mathrm{o}} \to \infty$ at the same time. Now the distribution is characterized by a single parameter, representing the strength of a point-like scatterer.

Still it is not possible to calculate the impurity average exactly. Thus, an expansion of the Green's function is needed. This can best be illustrated in the form of diagrams. Therefore, a brief introduction to diagrammatics follows in the next paragraph.

Diagrammatics

In order to find a diagrammatic representation of the problem, some rules have to be specified. The objects involved are the full Green's functions $G(\mathbf{p}, \mathbf{p}'; \epsilon)$, the unperturbed Green's functions $G_{\mathrm{o}}(\mathbf{p}; \epsilon)$, and the disorder potential $\tilde{V}$ with the corresponding symbols (see *e.g.* [50]):

[5] Usually the integration measure is given by the product $\mathcal{D}[V(\mathbf{r})] = \lim_{N \to \infty} \prod_{i=1}^{N} \mathrm{d}V_i$, where $V_i = V(\mathbf{r}_i)$.

- The full Green's function $G(\mathbf{p}, \mathbf{p}')$ is represented as a thick solid line with an arrow. The two momenta $\mathbf{p}, \mathbf{p}'$ are written at the end of the line with the arrow pointing from the first argument ($\mathbf{p}$) to the second ($\mathbf{p}'$).

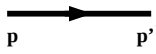

- The unperturbed or 'bare' Green's function is diagonal in momentum, *i.e.* $G_\mathrm{o}(\mathbf{p}, \mathbf{p}') \equiv G_\mathrm{o}(\mathbf{p})\delta(\mathbf{p} - \mathbf{p}')$. It is represented by a thin solid line with an arrow labeled by the momentum $\mathbf{p}$.

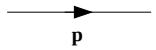

- Impurity scattering is represented by a dashed line with a cross at the end.[6]

The function $G(\mathbf{p}, \mathbf{p}')$ then can be written as a sum of diagrams made out of G_o-lines and impurity vertices as shown in Fig. 3.3, where the internal momenta have to be summed over. This corresponds to an expansion in terms of the disorder potential $\tilde{V}$ that can be written in a symbolic way (omitting all momentum arguments):

$$G = G_\mathrm{o} + G_\mathrm{o} \sum_{n=1}^{\infty} (\tilde{V} G_\mathrm{o})^n \,.$$

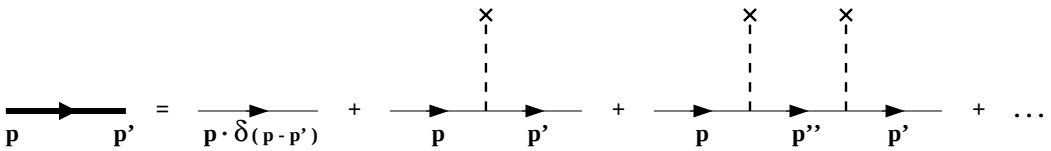

Figure 3.3: Expansion of the full Green's function for one realization of the disorder.

It turns out that it is not sufficient to retain only the leading term in V. Instead, the perturbation series has to be summed up to infinite order, but only considering certain classes of relevant diagrams. This will be discussed in the following for the single-particle Green's function as well as for the correlations of two Green's functions.

[6] Explicitly, this represents $\tilde{V}(\mathbf{p}_\mathrm{in} - \mathbf{p}_\mathrm{out})$ because the scattering process involves a momentum transfer $\mathbf{q} = \mathbf{p}_\mathrm{in} - \mathbf{p}_\mathrm{out}$.

3.3.1 The single-particle Green's function for a disordered system

First we evaluate the single-particle Green's function. After averaging the system is homogeneous. Therefore the impurity averaged Green's function becomes translationally invariant:

$$\langle G(\mathbf{p},\mathbf{p}')\rangle \equiv g(\mathbf{p})\delta(\mathbf{p}-\mathbf{p}')\,.$$

This will be represented diagrammatically by a thick line with one momentum argument.

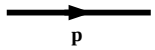

Diagrams with single impurity lines disappear under averaging since $\langle V\rangle = 0$. Then, assuming weak disorder, only diagrams with paired impurity lines have to be summed up (as depicted in Fig. 3.4).

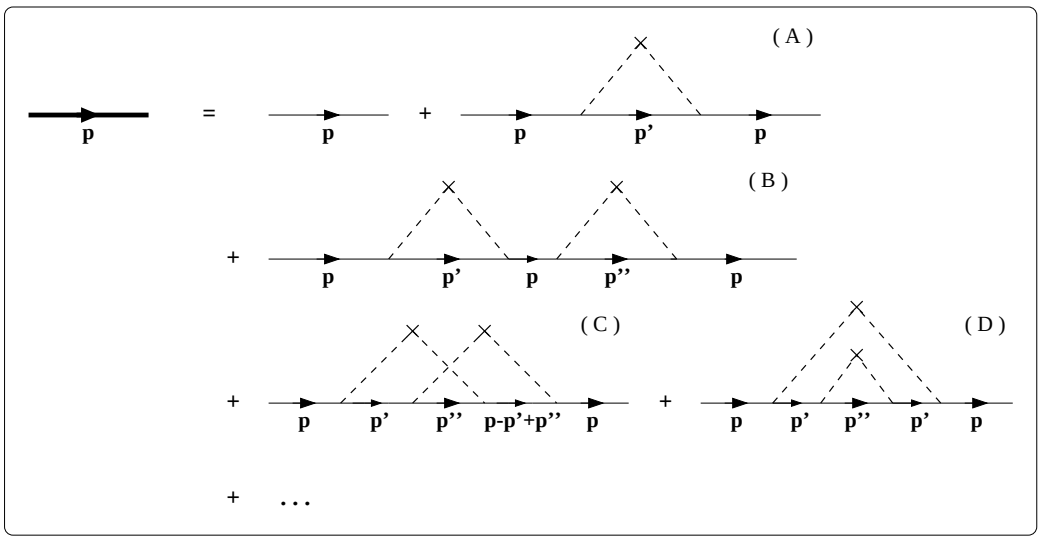

Figure 3.4: Expansion of the full Green's function after impurity averaging.

We now can distinguish *reducible* and *irreducible* diagrams. Diagrams that can be split into two diagrams by cutting one G_o-line are called reducible (*e.g.* diagram B in Fig. 3.4). *I.e.* these reducible diagrams can be built up out of irreducible diagrams. Collecting all irreducible diagrams (without their external G_o-lines) in the so-called *self-energy* Σ, the impurity averaged Green's function g is given by a Dyson equation (see Fig. 3.5):

$$g = G_o + G_o\sum_{n=1}^{\infty}(\Sigma G_o)^n = G_o + G_o\Sigma g \quad\Longleftrightarrow\quad g = \frac{G_o}{1-\Sigma G_o}\,. \tag{3.26}$$

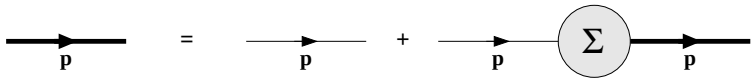

Figure 3.5: Diagrammatic representation of the Dyson equation.

Thus, we are able to sum up the perturbation series to infinite order. But we can not calculate the self-energy, which still consists of an infinite series of diagrams, exactly.

The contribution to the self-energy of diagram A in Fig. 3.4, being the lowest order contribution in V, is given by

$$\Sigma_{\rm o}^{\pm}(\mathbf{p}) = \int (\mathrm{d}q) V(\mathbf{q}) G_{\rm o}^{\pm}(\mathbf{p}-\mathbf{q},\epsilon) V(-\mathbf{q})\,,$$

where the shorthand notation $(\mathrm{d}q) = L^2/(4\pi^2)\,\mathrm{d}^2q$ has been introduced.

Since the potential is δ-correlated in real space, its Fourier transform does not depend on momentum. Therefore Σ is constant in momentum space, too. Hence,

$$\Sigma_{\rm o}^{\pm} = \gamma \int (\mathrm{d}p) G_{\rm o}^{\pm}(\mathbf{p},\epsilon)\,. \tag{3.27}$$

The real part of Σ only leads to a shift in energy and therefore can be absorbed in the ground state energy, while the imaginary part is

$$\begin{aligned} \mathrm{Im}\Sigma_{\rm o}^{\pm} &= \mp\gamma\pi \int (\mathrm{d}p)\delta(\epsilon-\xi_{\mathbf{p}}) \\ &= \mp\gamma\pi L^2\nu \equiv \mp\frac{1}{2\tau}\,, \end{aligned} \tag{3.28}$$

defining the mean free time τ. The associated length scale is the mean free path $l = v_{\rm F}\tau$ ($v_{\rm F}$ Fermi velocity).

In the case of weak disorder $\tau^{-1} \ll \epsilon_{\rm F}$, the self-energy can be seen as an expansion in the small parameter $(k_{\rm F}l)^{-1} \sim (\epsilon_{\rm F}\tau)^{-1}$ where the leading order contribution is given by the expression calculated above. Diagrams with intersecting impurity lines (as diagram C in Fig. 3.4) are suppressed due to the requirement that the momenta of all Green's functions be near the Fermi surface; for such a diagram this is only the case for a limited range of angles while for the relevant diagrams we have a free momentum integration. Diagrams like D in Fig. 3.4 could be included by making Eq. 3.27 self-consistent, *i.e.* replacing $G_{\rm o}$ by the impurity averaged Green's function g, but in fact the corrections are higher order in $(k_{\rm F}l)^{-1}$, too. Therefore the result obtained above (3.28) is sufficient to determine the self-energy Σ in the self-consistent Born approximation (SCBA).

Inserting this into the Dyson equation, we finally get the averaged Green's function

$$\begin{aligned} g^{\pm}(\mathbf{p},\epsilon;\tau) &= \frac{1}{(G_{\mathrm{o}}^{\pm}(\mathbf{p},\epsilon))^{-1}-\Sigma^{\pm}} \\ &= \frac{1}{\epsilon-\xi_{\mathbf{p}}\pm\frac{\mathrm{i}}{2\tau}}\,. \end{aligned} \tag{3.29}$$

We can also have a look at the spectral function $a(\mathbf{p},\epsilon;\tau)$. The δ-distribution of the unperturbed problem is smeared out, giving a Lorentzian of width τ^{-1} instead:

$$a(\mathbf{p},\epsilon;\tau) = \frac{\frac{1}{\tau}}{(\epsilon-\xi_{\mathbf{p}})^2+\frac{1}{4\tau^2}}\,. \tag{3.30}$$

In coordinate representation, disorder leads to a decay of the Green's function on the length scale of the mean free path, *i.e.*

$$g^{\pm}(\mathbf{r}-\mathbf{r}';\tau) = G_{\mathrm{o}}^{\pm}(\mathbf{r}-\mathbf{r}')\cdot e^{-\frac{|\mathbf{r}-\mathbf{r}'|}{2l}}\,. \tag{3.31}$$

Thus, the definition of τ is justified; it represents the typical decay time of a plane-wave state.

3.3.2 Correlations $\langle G^{\pm}G^{\mp}\rangle$

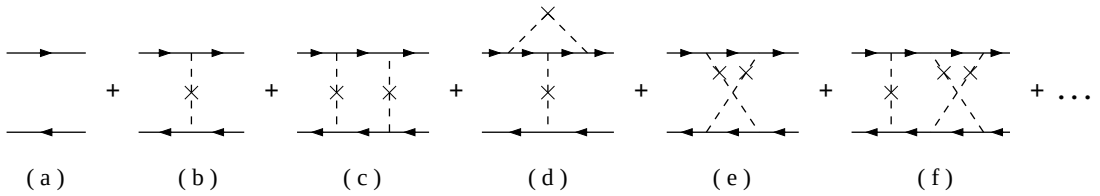

Figure 3.6: Diagrams contributing to $\langle G^{\pm}G^{\mp}\rangle$.

Having found the impurity averaged one-particle Green's function, we now can go on to calculate correlations between two Green's functions. We will see that, depending on their momentum arguments, one of two different contributions is dominant.

The expression to evaluate is

$$\langle G^{+}(\mathbf{p_1},\mathbf{p}_1';\epsilon_1)G^{-}(\mathbf{p_2},\mathbf{p}_2';\epsilon_2)\rangle\,.$$

Again we have to sum up different diagrams with paired impurity lines as shown in Fig. 3.6. The solid lines here represent impurity averaged Green's functions

already. The disconnected part is given by diagram (a) which is just the product of the two Green's functions averaged separately. Hence,

$$\langle G^+G^-\rangle = g^+g^- + \langle G^+G^-\rangle_{\rm c}\,.$$

As before, diagrams with intersecting impurity lines like (d) and (f) only give small contributions due to restrictions on the angular integration. The dominant diagrams are series of *ladder diagrams* (starting with (b), (c), ...) and *maximally crossed diagrams* (starting with (b), (e), ...). The contribution of these connected diagrams can be written as

$$\begin{aligned} & \langle G^+(\mathbf{p_1},\mathbf{p_1'};\epsilon_1)G^-(\mathbf{p_2},\mathbf{p_2'};\epsilon_2)\rangle_{\rm c} \qquad (3.32)\\ = \;& g^+(\mathbf{p_1},\epsilon_1;\tau)g^-(\mathbf{p_2},\epsilon_2;\tau)\Gamma(\mathbf{p_1},\mathbf{p_2},\mathbf{p_1'},\mathbf{p_2'};\epsilon_1,\epsilon_2)g^+(\mathbf{p_1'},\epsilon_1;\tau)g^-(\mathbf{p_2'}\epsilon_2;\tau)\,, \end{aligned}$$

thus defining the reducible vertex function $\Gamma(\mathbf{p_1},\mathbf{p_2},\mathbf{p_1'},\mathbf{p_2'};\epsilon_1,\epsilon_2)$.[7] By overall momentum conservation one gets a δ-distribution $\delta(\mathbf{p_1}-\mathbf{p_2}-\mathbf{p_1'}+\mathbf{p_2'})$, *i.e.* only three momenta are independent. As we will see, Γ does not depend on all the remaining momenta and the two energies, but only on certain combinations of them.

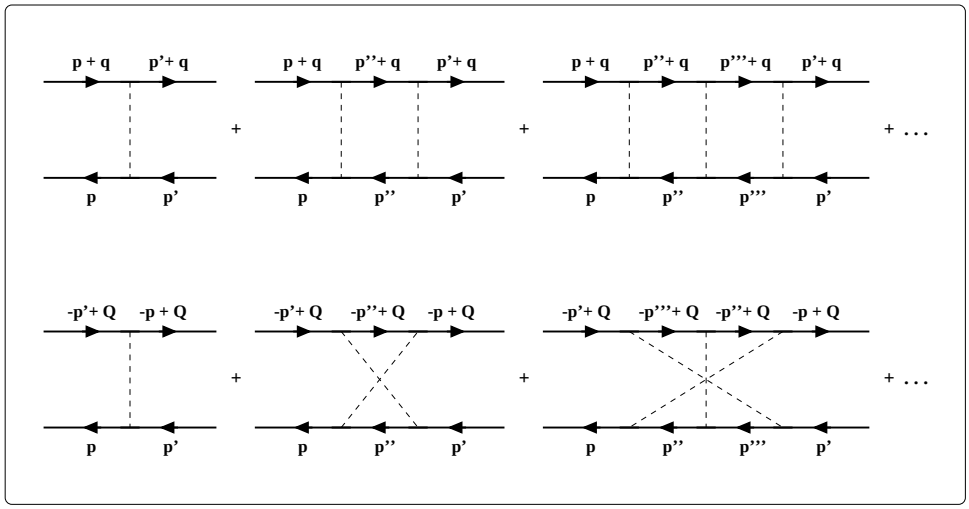

Figure 3.7: Ladder and maximally crossed diagrams.

Ladder diagrams

Let us first treat the summation of the ladder diagrams. Due to momentum conservation at each vertex, the momentum difference $\mathbf{q} \equiv \mathbf{p_1}-\mathbf{p_2}(=\mathbf{p_1'}-\mathbf{p_2'})$

[7] In the case of two-particle functions, a diagram is called reducible if it can be split into two separate diagrams by cutting *two* g-lines. The vertex function Γ contains diagrams with this property (but also irreducible diagrams!).

is constant and $\Gamma_{\rm lad}$ only depends on this difference. Furthermore, the energy dependence is determined by the difference $\omega = \epsilon_1 - \epsilon_2$. Therefore we change variables from $\mathbf{p_1}, \mathbf{p_2}$ to $\mathbf{p}, \mathbf{q}$ and ϵ_1, ϵ_2 to ϵ, ω. Then $\Gamma_{\rm lad}(\mathbf{q}, \omega)$ is given by a Bethe-Salpeter equation, the two-particle analogue of the Dyson equation (see Fig. 3.8):

$$\Gamma_{\rm lad}(\mathbf{q},\omega) = \gamma + \gamma \Big[\underbrace{\int (\mathrm{d}p'') g^+(\mathbf{p}''+\mathbf{q}, \epsilon+\omega;\tau) g^-(\mathbf{p}'',\epsilon;\tau)}_{\equiv \Pi_{\rm lad}(\mathbf{q},\omega)} \Big] \Gamma_{\rm lad}(\mathbf{q},\omega)\,.$$

Therefore we only have to calculate the irreducible vertex function $\Pi_{\rm lad}(\mathbf{q}, \omega)$ in order to get

$$\Gamma_{\rm lad}(\mathbf{q},\omega) = \frac{\gamma}{1 - \gamma\, \Pi_{\rm lad}(\mathbf{q},\omega)}\,. \tag{3.33}$$

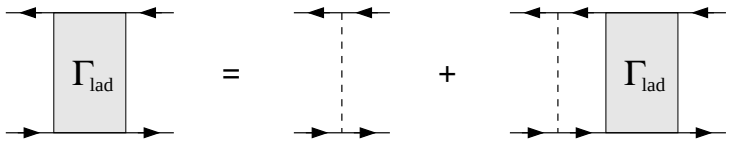

Figure 3.8: Diagrammatic representation of the Bethe-Salpeter equation.

Anticipating the result that $\Gamma_{\rm lad}$ diverges for $q, \omega \to 0$, we can approximate $\Pi_{\rm lad}$ for small q, ω:

$$\Pi_{\rm lad}(\mathbf{q},\omega) \simeq 2\pi L^2 \nu\tau (1 + \mathrm{i}\omega\tau - Dq^2\tau)\,, \tag{3.34}$$

where $D = \frac{1}{2} v_{\rm F}^2 \tau$ is the diffusion constant.

Recalling that $\gamma = (2\pi\nu\tau)^{-1}$, we finally obtain the sum of the ladder diagrams:

$$\Gamma_{\rm lad}(\mathbf{q},\omega) = \frac{1}{2\pi L^2 \nu\tau^2} \frac{1}{Dq^2 - \mathrm{i}\omega}\,. \tag{3.35}$$

This is a diffusion pole. Therefore $\Gamma_{\rm lad}$ is called a *diffuson* and denoted as $\mathrm{D}(\mathbf{q}, \omega)$ in the following. It is the dominant contribution for $\mathbf{p_1} \approx \mathbf{p_2}$.

Maximally crossed diagrams

This class of diagrams has first been considered by Langer and Neal [51]; for a detailed discussion of maximally crossed diagrams (in the context of weak localization) see *e.g.* [9].

A maximally crossed diagram can be converted to a ladder diagram by reversing one G-line (see Fig. 3.9). Since now all the arrows point in the same direction, momentum conservation at the vertices requires the momentum sum $\mathbf{p_1}+\mathbf{p_2'}$ to be constant. The energy dependence is the same as for the ladder diagrams. Then these diagrams can also be summed with a Bethe-Salpeter equation. The result has obviously the same form as the one obtained above for the ladders, but it now involves the momentum sum $\mathbf{Q} = \mathbf{p_1}+\mathbf{p_2'}$ instead of the momentum difference $\mathbf{q} = \mathbf{p_1}-\mathbf{p_2}$, *i.e.*

$$\Gamma_{\rm mc}(\mathbf{Q},\omega) = \frac{1}{2\pi L^2 \nu\tau^2}\frac{1}{DQ^2 - \mathrm{i}\omega}\,. \tag{3.36}$$

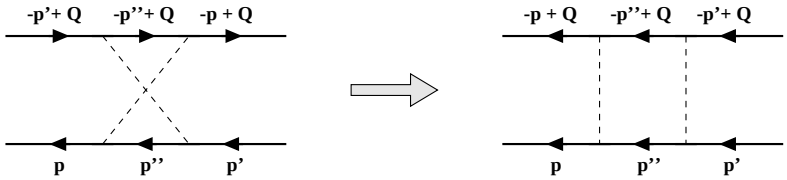

Figure 3.9: The equivalence of maximally crossed and ladder diagrams.

This is called a *Cooperon* and denoted as $\mathrm{C}(\mathbf{Q},\omega)$ in the following. It is the dominant contribution for $\mathbf{p_1} \approx -\mathbf{p_2'}$.

Collecting the results, we get the following expression for the reducible vertex function:

$$\begin{aligned} &\Gamma(\mathbf{p_1},\mathbf{p_2},\mathbf{p_1'},\mathbf{p_2'};\epsilon_1,\epsilon_2) \\ = \;& \delta(\mathbf{p_1}-\mathbf{p_2}-\mathbf{p_1'}+\mathbf{p_2'}) \times \begin{cases} \mathrm{D}(\mathbf{p_1}-\mathbf{p_2},\epsilon_1-\epsilon_2) & \text{for } \mathbf{p_1} \approx \mathbf{p_2}\,, \\ \mathrm{C}(\mathbf{p_1}+\mathbf{p_2'},\epsilon_1-\epsilon_2) & \text{for } \mathbf{p_1} \approx -\mathbf{p_2'}\,, \end{cases} \end{aligned} \tag{3.37}$$

where the functions D and C are given by Eqs. 3.35 and 3.36, respectively.

In both cases there are two 'free' momenta left. One momentum argument has been fixed by momentum conservation while a second momentum argument is restricted to a small relevant range where the contributions are dominant.

The above formulae have been obtained for the correlation $\langle G^+G^-\rangle$. This can be fixed in the notation by writing Γ^{+-}. To get the corresponding results for $\langle G^-G^+\rangle$, one just has to take the complex conjugate of Γ which is equivalent to replacing ω by $-\omega$, *i.e.*

$$\Gamma^{-+}(\omega) = \left(\Gamma^{+-}\right)^*(\omega) = \Gamma^{+-}(-\omega)\,. \tag{3.38}$$

Averages of the form $\langle G^+G^+\rangle$ or $\langle G^-G^-\rangle$ are given by the disconnected parts g^+g^+ and g^-g^-, respectively. Due to the pole structure, the vertex function Π vanishes. Thus, $\Gamma^{++} = \Gamma^{--} = \gamma$, *i.e.* no long-ranged correlations exist.

Now all the methods needed for the evaluation of the tunneling current have been addressed. First, the model of the tunneling Hamiltonian has been introduced and its scope of validity has been discussed. Then the coupling to the magnetic field has been implemented into the formula for the tunneling current. The results have been shown in momentum and coordinate representation. And finally, the one-particle and two-particle Green's functions of the 2DEGs have been evaluated, using a diagrammatic approach.

Chapter 4

Applications

The formalism established in the previous chapter leads to a considerable reduction of the complexity of the problem. Now, all physical properties of the system are contained either in the tunneling matrix elements or in the spectral functions of the different layers. Thus, we have to specify these quantities when studying a particular setup.

The tunneling matrix elements

In the derivation of the tunneling current (Eqs. 3.15 and 3.17), two assumptions about the tunneling matrix elements have already been implemented:

- The energy dependence of the tunneling matrix elements can be neglected as the particle energies involved are close to the Fermi energy.
- Since the tunneling probability decays exponentially with the barrier width, the dominant process is tunneling perpendicular to the barrier. Consequently other processes are neglected, *i.e.* $T_{\mathbf{x}\mathbf{x}'} = T_{\mathbf{x}}\delta(\mathbf{x}-\mathbf{x}')$.

Now the spatial (or momentum) dependence of the tunneling matrix elements has to be established. One can imagine two extreme opposite setups: Either the tunneling matrix elements are constant in space, or tunneling is only allowed at some specific points of the plane. In the latter case the distance between these tunneling centers would determine the behavior.

Unfortunately it is out of the scope of the present work to study both situations. Therefore all the investigations will be restricted to the uniform case

$$T_{\mathbf{x}} \equiv T\,.$$

This implies that momentum is conserved in tunneling: $T_{\mathbf{k}\mathbf{p}} = T\delta(\mathbf{p}-\mathbf{k})$. In general, *i.e.* in arbitrary dimensions, only the momentum parallel to the barrier

is conserved, but in a 2DEG this is equivalent to conservation of total momentum. This specific feature of two-dimensional systems will be important in the following as it leads to sharp features in the I-V- as well as the I-B-characteristics.

The assumption of uniform tunneling requires the distance d between the 2DEGs to be constant with high precision. As the tunneling probability depends exponentially on the barrier width, even small variations would lead to preferential tunneling at the points where the barrier is thinnest. It is difficult to say to what degree this can be realized experimentally because it is not possible to measure directly the homogeneity of the sample. As well as disorder, interface roughness would lead to a smearing of the current characteristics due to momentum non-conserving tunneling processes [52]. Nevertheless, tunneling experiments with 2DEGs (see *e.g.* [22]) are in good agreement with theoretical approaches assuming constant tunneling matrix elements. Therefore $T_{\mathbf{x}} \equiv$ const. should be a reasonable approximation.

Incorporating this into the formulae (3.15) and (3.17), the final expression we will use for the calculation looks as follows:

$$I = 2e\,|T|^2 \sum_{\mathbf{k},\mathbf{k}'} \int (\mathrm{d}\epsilon^{[eV]})\, A_1(\mathbf{K},\mathbf{K}';\epsilon) A_2(\mathbf{k}',\mathbf{k};\epsilon+eV) \tag{4.1}$$

$$= \frac{2e}{L^4}\,|T|^2 \int \mathrm{d}^2x \mathrm{d}^2x' \int (\mathrm{d}\epsilon^{[eV]})\, \mathrm{e}^{-\mathrm{i}e\mathbf{A}(\mathbf{x}-\mathbf{x}')} A_1(\mathbf{x},\mathbf{x}';\epsilon) A_2(\mathbf{x}',\mathbf{x};\epsilon+eV)\,. \tag{4.2}$$

Furthermore, we assume that the disorder potentials of the 2DEGs are uncorrelated. As mentioned in chapter 2, correlations are only important if the impurities, *i.e.* the charged donors, are placed between the 2DEGs. In a usual setup this is not the case. The influence of correlated disorder on the average tunneling current has been investigated by Zheng and MacDonald [23].

In the calculations the momentum representation will be used. Applying the impurity averaging as described in section 3.3.1 to formula (4.1), we get

$$\langle I \rangle = 2e\,|T|^2 \sum_{\mathbf{k}} \int (\mathrm{d}\epsilon^{[eV]})\, a_1(\mathbf{k}-e\mathbf{A},\epsilon;\tau) a_2(\mathbf{k},\epsilon+eV;\tau')\,. \tag{4.3}$$

The averages can be taken separately because the disorder potentials of the two layers are uncorrelated. Then we can also write down immediately the formula for the average of the current squared:

$$\langle I^2 \rangle = 4e^2\,|T|^4 \sum_{\mathbf{k},\mathbf{k}';\mathbf{p},\mathbf{p}'} \int (\mathrm{d}\epsilon^{[eV]})\, (\mathrm{d}\epsilon'^{[eV]}) \tag{4.4}$$
$$\langle A_1(\mathbf{K},\mathbf{K}';\epsilon) A_1(\mathbf{P},\mathbf{P}';\epsilon') \rangle \, \langle A_2(\mathbf{k}',\mathbf{k};\epsilon+eV) A_2(\mathbf{p}',\mathbf{p};\epsilon'+eV) \rangle\,.$$

Since, depending on the chosen setup, different contributions are important, this formula will be kept in its general form for the time being.

The 2DEGs

As discussed in section 3.3, the 2DEGs are characterized by their chemical potential μ and their mean free time τ. The condition that the chemical potentials be matched has already been incorporated in the derivation of the tunneling formula (see section 3.1). However, the mean free time τ can be chosen independently for each layer. Hence, there are three different setups to be studied. As we will see, they show similar results for the average current but not for the current fluctuations.

- For pedagogical reasons we first discuss tunneling between two clean 2DEGs ($\tau \to \infty$) in section 4.1. Even this simple case gives a very intuitive picture of the magnetic field effects on the current. Therefore this section provides a basis for discussing the general features of the I-B-characteristics. Only the average current has to be calculated since $\langle I^2 \rangle = \langle I \rangle^2$, obviously.
- In section 4.2 tunneling from a clean to a disordered 2DEG is studied. First, we discuss the influence of disorder on the average current before coming to the current fluctuations $(\Delta I)^2$. The different contributions are identified and their field dependence is evaluated.
- In section 4.3 tunneling between two disordered 2DEGs is studied. As already mentioned, the impurity potentials on either side of the junction are supposed to be uncorrelated. The structure of this section follows the same lines as the previous one.

The calculations are performed at zero temperature. As the temperature dependence is contained in the Fermi distribution functions n_{F}, the extension to finite temperatures only changes the energy integrations. All the assumptions made in the following stay valid for low temperatures ($k_{\mathrm{B}}T \ll \tau^{-1}$).

4.1 Tunneling between two clean 2DEGs

Let us recall the formula (4.3) for the tunneling current derived in the previous chapter:

$$\langle I \rangle = 2e\,|T|^2 \sum_{\mathbf{k}} \int (\mathrm{d}\epsilon^{[eV]})\, a_1(\mathbf{k} - e\mathbf{A}, \epsilon; \tau) a_2(\mathbf{k}, \epsilon + eV; \tau') \,.$$

To evaluate this formula, we now have to specify the spectral functions. As both layers are clean, the unperturbed spectral functions $A_i^{\mathrm{o}}(\mathbf{k}, \epsilon) = 2\pi\delta(\epsilon - \xi_{\mathbf{k}})$ are inserted in place of the $a_i(\mathbf{k}, \epsilon; \tau)$. Hence,

$$\langle I \rangle = 2e\,|T|^2 \sum_{\mathbf{k}} \int (\mathrm{d}\epsilon^{[eV]})\, 2\pi\delta(\epsilon - \xi_{\mathbf{k}-e\mathbf{A}}) \cdot 2\pi\delta(\epsilon + eV - \xi_{\mathbf{k}}) \,. \qquad (4.5)$$

In the continuum limit the sum over $\mathbf{k}$ is replaced by an integral:

$$\sum_{\mathbf{k}} \longrightarrow L^2 \int \frac{\mathrm{d}^2 k}{4\pi^2} \longrightarrow \frac{L^2 \nu}{2} \int_0^{2\pi} \frac{\mathrm{d}\varphi}{2\pi} \int_0^{\infty} \mathrm{d}\xi_{\mathbf{k}} \,,$$

where L^2 is the area of the plane.

Because of the δ-distribution the integral over $\xi_{\mathbf{k}}$ can be performed easily. For small enough voltages the energy integration is confined to a narrow region around the Fermi energy. Therefore we can neglect the energy dependence of $k = |\mathbf{k}|$ by identifying it with the Fermi momentum k_F. Integration over the Fermi distributions then just gives a factor eV, and we are left with an integral over the angle φ:

$$\begin{aligned} \langle I \rangle(B;V) &= e^2 V \left|T\right|^2 L^2 \nu \int_0^{2\pi} \mathrm{d}\varphi \, \delta(-eV + e v_\mathrm{F} A \cos\varphi - \frac{(eA)^2}{2m}) && (4.6) \\ &= 4e^2 V \left|T\right|^2 L^2 \nu \, \frac{\theta\big((2k_\mathrm{F} - eA)eA - 2meV\big)}{\frac{eA}{m} \cdot \sqrt{4k_\mathrm{F}^2 - (eA + \frac{2m\,eV}{eA})^2}} && (4.7) \end{aligned}$$

with $A = |\mathbf{A}|$.

Introducing a reference current $I_\mathrm{o} = e \left|T\right|^2 L^2 \nu$, the result can be rewritten in terms of dimensionless quantities:

$$\frac{\langle I \rangle}{I_\mathrm{o}}(x, t_\mathrm{F}) = \frac{t_\mathrm{F}}{2x\sqrt{1 - (x + \frac{t_\mathrm{F}}{4x})^2}} \, \theta\big((1-x)x - \frac{t_\mathrm{F}}{4}\big) \,, \qquad (4.8)$$

where $x = eBd/(2k_\mathrm{F}) = B/B_\mathrm{max}$ and $t_\mathrm{F} = eV/\epsilon_\mathrm{F}$. $B_\mathrm{max} = 2k_\mathrm{F}/(ed)$ is the maximum field for which tunneling occurs. Thus, x ranges from 0 to 1 whereas t_F, being the ratio of the applied voltage and the Fermi energy, has to be much smaller than 1 (as discussed in section 3.1).

At zero magnetic field, no tunneling current flows. The current only sets in at $x = \frac{1}{2}(1 - \sqrt{1 - t_\mathrm{F}})$ where it is divergent. With increasing magnetic field it quickly decays, before at $x = \frac{1}{2}(1 + \sqrt{1 - t_\mathrm{F}})$ another divergence occurs. For larger fields the tunneling current is completely suppressed again.

Instead of the current, let us now discuss the tunneling conductance. Without magnetic field the differential conductance $\mathrm{G}(V) = \frac{\partial I}{\partial V}$ is proportional to $\delta(V)$; *i.e.* tunneling is only possible at zero bias. With magnetic field the zero-bias differential conductance $\mathrm{G}(B;0)$ is given as

$$\mathrm{G}(B;0) = 4e^2 \left|T\right|^2 L^2 \nu \frac{\theta(2k_\mathrm{F} - eA)}{\frac{eA}{m} \cdot \sqrt{4k_\mathrm{F}^2 - (eA)^2}} \,. \qquad (4.9)$$

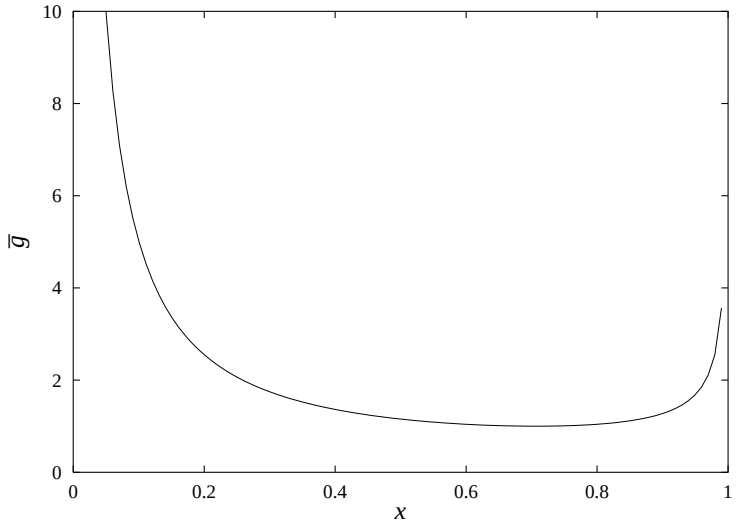

Figure 4.1: Tunneling conductance between two clean 2DEGs as a function of the magnetic field (in dimensionless units).

We can also introduce a dimensionless conductance $\bar{\mathrm{g}} \equiv \mathrm{G}(0) \cdot \epsilon_{\mathrm{F}}(eI_{\mathrm{o}})^{-1}$:

$$\bar{\mathrm{g}}(x) = \frac{\theta(1-x)}{2x\sqrt{1-x^2}}\,. \tag{4.10}$$

The tunneling conductance diverges for $x \to 0$ (or $B \to 0$) as well as for $x \to 1$ (or $B \to B_{\max}$). The region in between is rather flat, reaching its minimal value $\bar{\mathrm{g}} = 1$ at $x = 1/\sqrt{2}$. A plot is shown in Fig. 4.1.

Qualitatively this result can be explained by the relative shift of the Fermi circles of the different layers [22] as represented in Fig. 4.2. Due to momentum conservation, tunneling only takes place at the overlap of the two Fermi surfaces. For $B = 0$ the origins coincide and all $\mathbf{k}$ with $|\mathbf{k}| = k_{\mathrm{F}}$ contribute to the tunneling conductance. With increasing magnetic field, the origins move away from each other. At intermediate fields there are only two points of intersection, resulting in a small tunneling conductance. Reaching $B = B_{\max}$ the circles touch tangentially, causing another rise of the tunneling conductance. For even stronger fields the two Fermi circles are decoupled. Then tunneling is completely suppressed. These sharp features are characteristic for two-dimensional systems where energy and momentum are conserved in tunneling.

As we will see in the next section, the divergences are smeared out in the presence of disorder.

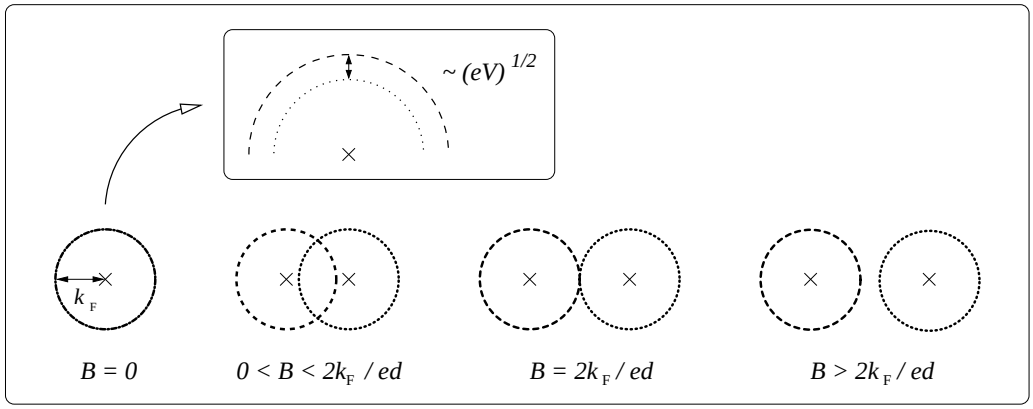

Figure 4.2: Qualitative picture of the I-B-characteristics.

4.2 Tunneling from a clean to a disordered 2DEG

Technical progress made it possible over the last few years to produce very pure samples with mean free paths up to $\sim 10\mu$m. An additional difficulty here is that we need a clean layer close to a disordered layer. In fact it is possible to grow multi-layers with mean free paths differing by more than an order of magnitude (see *e.g.* [16, 53]). Then, in comparison with the more disordered layer, one layer can be considered as clean. In the following, we choose layer 2 to be clean whereas for layer 1 a finite mean free time τ is introduced.

4.2.1 The average tunneling current

Starting from the general formula (4.3),

$$\langle I\rangle = 2e\,|T|^2 \sum_{\mathbf{k}} \int (\mathrm{d}\epsilon^{[eV]}) a_1(\mathbf{k}-e\mathbf{A},\epsilon;\tau) a_2(\mathbf{k},\epsilon+eV;\tau')\,,$$

we now have to insert the unperturbed spectral function $A_2^0(\mathbf{k},\epsilon+eV)$ only for the clean layer 2, whereas for layer 1 the impurity averaged spectral function $a_1(\mathbf{k}-e\mathbf{A},\epsilon;\tau)$ is needed:

$$\langle I\rangle = 2e\,|T|^2 \sum_{\mathbf{k}} \int (\mathrm{d}\epsilon^{[eV]}) \frac{\frac{1}{\tau}}{(\epsilon-\xi_{\mathbf{k}-e\mathbf{A}})^2+\frac{1}{4\tau^2}} \cdot 2\pi\delta(\epsilon+eV-\xi_{\mathbf{k}})\,. \qquad (4.11)$$

Up to the last φ-integral the calculations are exactly the same as in the previous chapter. But since the spectral function for layer 1 is not a δ-distribution

anymore, instead of Eq. 4.6, we get here:

$$\langle I\rangle = e\,|T|^2\,L^2\nu\frac{eV}{\tau}\int_0^{2\pi}\frac{\mathrm{d}\varphi}{2\pi}\frac{1}{(-eV+ev_{\mathrm{F}}A\cos\varphi-\frac{(eA)^2}{2m})^2+\frac{1}{4\tau^2}}\,. \tag{4.12}$$

The remaining integral has been solved analytically, but the exact results are quite lengthy and therefore not very illustrative. The full formula can be found in appendix B.1.1. Here we will restrict ourselves to a discussion of the general features as well as the asymptotic behavior.

In the case of two clean layers, the current has been expressed in terms of the dimensionless variables $x = B/B_{\max}$ for the magnetic field and $t_{\mathrm{F}} = eV/\epsilon_{\mathrm{F}}$ for the applied voltage. Now, the additional parameter $g = k_{\mathrm{F}}l$ as a measure for the strength of disorder is needed. Note that g is the dimensionless conductance in 2D.

Without magnetic field, the integrand of Eq. 4.12 does not depend on φ and we simply get

$$\langle I\rangle = e\,|T|^2\,L^2\nu\frac{eV}{\tau}\frac{1}{(eV)^2+\frac{1}{4\tau^2}} = I_{\mathrm{o}}\,\frac{2t_{\mathrm{F}}g}{1+(t_{\mathrm{F}}g)^2}\,. \tag{4.13}$$

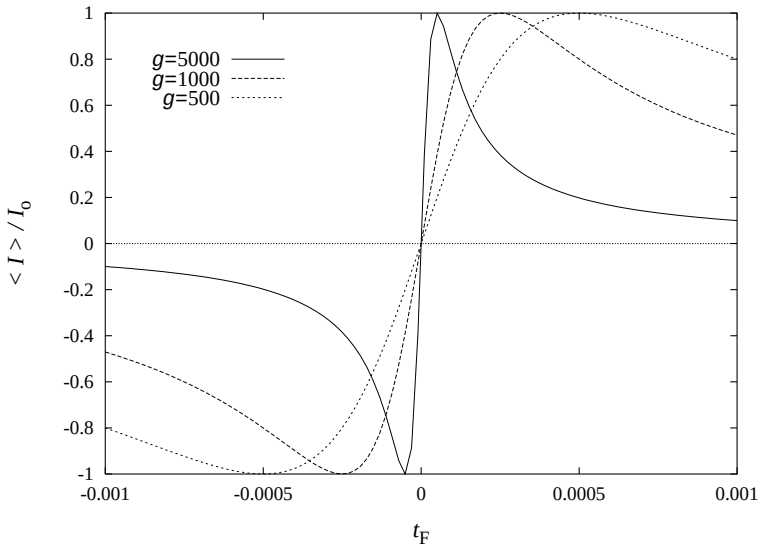

Figure 4.3: I-V-characteristics for different strengths of disorder.

The tunneling current depends only on the product $t_{\mathrm{F}}g = 2eV\tau$. It is maximal for $t_{\mathrm{F}}g = 1$ where it reaches the value $\langle I\rangle = I_{\mathrm{o}}$. A plot is shown in Fig. 4.3. For $t_{\mathrm{F}}g \ll 1$ (corresponding to $eV \ll \tau^{-1}$) the current is linear in V, *i.e.* Ohmic

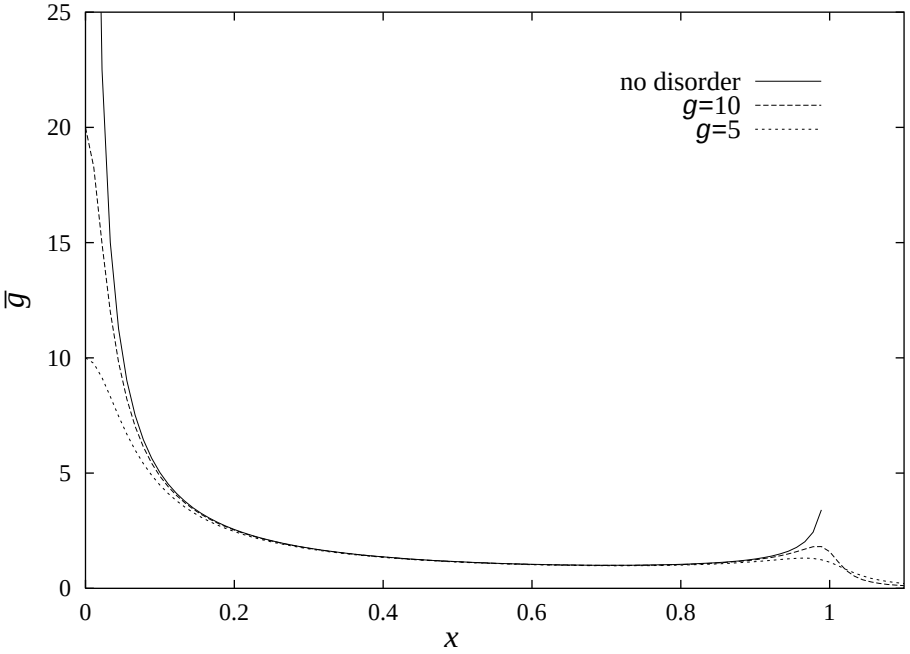

Figure 4.4: Tunneling conductance for different strengths of disorder as a function of the magnetic field.

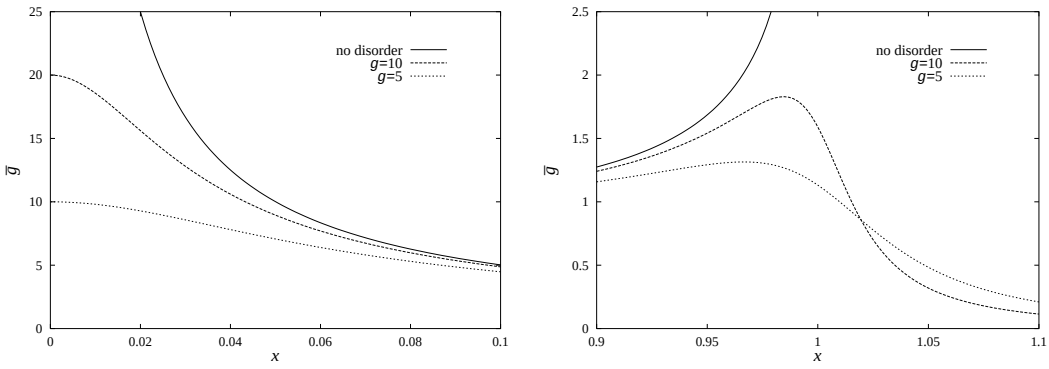

Figure 4.5: Details of Fig. 4.4 for $x \approx 0$ and $x \approx 1$.

behavior is recovered. Concerning the conductance, the δ-peak at $V = 0$ of the clean systems has been broadened, the width of the resonance being τ^{-1}.

In Fig. 4.4 the dimensionless conductance $\bar{\mathrm{g}}(x; g)$ is plotted for different values of g. As we can see the current shows a strong dependence on g only near $x = 0$ and $x = 1$. These regions are shown in more detail in Fig. 4.5. By contrast, disorder has only a very weak effect on $\bar{\mathrm{g}}$ in the flat region in between. The g-dependence of the tunneling conductance for different values of the magnetic

field is shown in Fig. 4.6. At $x=0$ the average conductance $\bar{\mathrm{g}}$ is linear in g

$$\bar{\mathrm{g}}(0;g) = 2g \equiv \bar{\mathrm{g}}_{\mathrm{o}}(g)\,,$$

whereas at $x=1$ the conductance shows only a square-root dependence on g (for $g \gg 1$). Note that the zero-field maximum keeps its position with decreasing g (*i.e.* the term "zero-field maximum" is justified). The high-field maximum is shifted to lower values of x. For large g the shift $\Delta x = 1 - x_{\max}$ is proportional to g^{-1}.

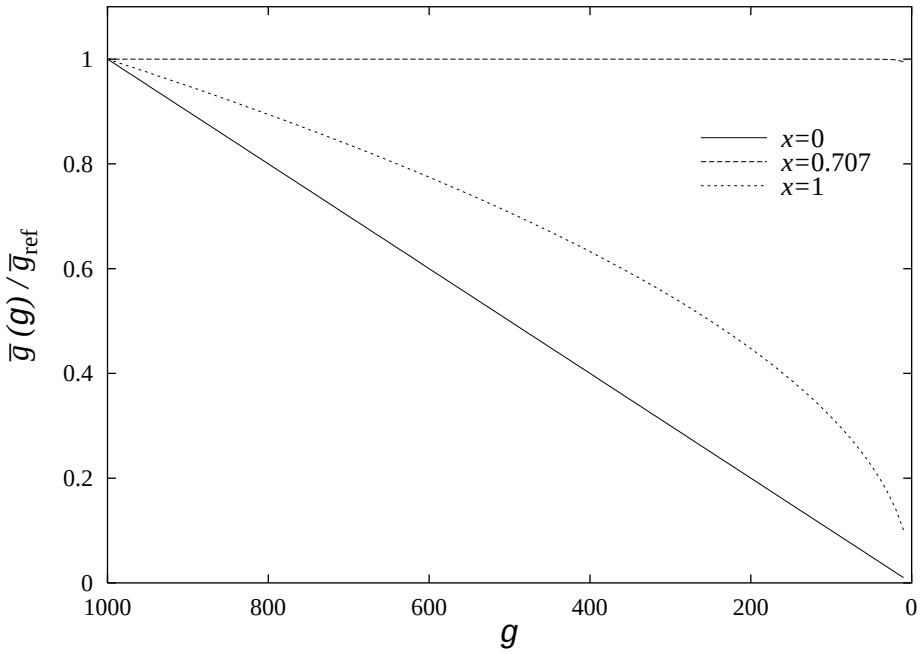

Figure 4.6: Change of the tunneling conductance with increasing disorder for different field strengths (reference conductance $\bar{\mathrm{g}}_{\mathrm{ref}} = \bar{\mathrm{g}}(g=1000)$).

Furthermore, $B = B_{\max}$ is not a sharp cut-off anymore. The $\bar{\mathrm{g}}$-x-curve develops tails which decay like

$$\bar{\mathrm{g}}(x;g) \simeq \frac{1}{8gx^4} \qquad \text{for } x \gg 1\,.$$

In the following let us focus on the results for weak magnetic fields since this is the region where the current fluctuations are most interesting. In that region the dimensionless tunneling conductance can be approximated by

$$\begin{aligned} \frac{\bar{\mathrm{g}}(x;g)}{\bar{\mathrm{g}}_{\mathrm{o}}} &\simeq \frac{1}{\sqrt{1+16g^2x^2}} && \text{for } x \ll 1\,, \\ &\simeq 1 - 8g^2x^2 + O\left((gx)^4\right) && \text{for } x \ll g^{-1}\,. \end{aligned}$$

Note that $gx = \frac{1}{2}eBdl$. Thus, the decay of the tunneling conductance is characterized by the relation between the magnetic length $l_{\rm m} = \sqrt{2}(eBd)^{-1}$ (see section 3.2) and the mean free path l:

$$\frac{\bar{\rm g}(l_{\rm m};l)}{\bar{\rm g}_{\rm o}} \simeq 1 - 4\Big(\frac{l}{l_{\rm m}}\Big)^2 + O\left((l/l_{\rm m})^4\right) . \tag{4.14}$$

Alternatively, a characteristic magnetic field $B_{\rm c}[\langle I\rangle] \equiv B_{\rm c}^{(l)} \equiv \sqrt{2}(edl)^{-1}$ can be defined by the condition that $l_{\rm m}(B_{\rm c}^{(l)}) \doteq l$. The 'range' of the impurity averaged Green's function $g^{\pm}$ is l (see Eq. 3.31). Therefore, the typical area of a current loop is of the order $F = dl$. Since l is a small length scale, $B_{\rm c}^{(l)}$ is large. In order to get a flavor of the sizes of the different quantities in a typical experiment, take for example $d \approx 10$nm. With $l = 100$nm as an upper limit for the mean free path, the lower limit for the characteristic field $B_{\rm c}^{(l)}$ is of the order of 1Tesla.

Keeping this in mind, we will now examine the current fluctuations.

4.2.2 The current fluctuations

The general formula for the current fluctuations is given by Eq. 4.4:

$$\begin{aligned}\langle I^2\rangle &= 4e^2\,|T|^4 \sum_{\mathbf{k},\mathbf{k}';\mathbf{p},\mathbf{p}'} \int (\mathrm{d}\epsilon^{[eV]})\,(\mathrm{d}\epsilon'^{[eV]}) \\ &\quad \times\langle A_1(\mathbf{K},\mathbf{K}';\epsilon)A_1(\mathbf{P},\mathbf{P}';\epsilon')\rangle\,\langle A_2(\mathbf{k}',\mathbf{k};\epsilon{+}eV)A_2(\mathbf{p}',\mathbf{p};\epsilon'{+}eV)\rangle\,.\end{aligned} \tag{4.15}$$

In contrast to the expression for the average current where only the impurity averaged spectral functions a_i appeared, here correlations become important since the formula contains the product of two spectral functions for each layer. In the case of one clean layer, Eq. 4.15 can be simplified considerably by inserting the unperturbed spectral functions $A_2^{\rm o}$, *i.e.*

$$\langle A_2(\mathbf{k}',\mathbf{k};\epsilon{+}eV)A_2(\mathbf{p}',\mathbf{p};\epsilon'{+}eV)\rangle = A_2^{\rm o}(\mathbf{k};\epsilon{+}eV)A_2^{\rm o}(\mathbf{p};\epsilon'{+}eV)\delta(\mathbf{k}{-}\mathbf{k}')\delta(\mathbf{p}{-}\mathbf{p}')\,.$$

Thus, the spectral functions A_1 in layer 1 have to be taken at equal momenta, too, which leads to the following formula with only two momentum sums left:

$$\begin{aligned}\langle I^2\rangle &= 4e^2\,|T|^4 \sum_{\mathbf{k},\mathbf{p}} \int (\mathrm{d}\epsilon^{[eV]})\,(\mathrm{d}\epsilon'^{[eV]}) \\ &\quad \times\langle A_1(\mathbf{K},\mathbf{K};\epsilon)A_1(\mathbf{P},\mathbf{P};\epsilon')\rangle\,A_2^{\rm o}(\mathbf{k};\epsilon{+}eV)A_2^{\rm o}(\mathbf{p};\epsilon'{+}eV)\,.\end{aligned} \tag{4.16}$$

For an intuitive understanding of the situation it is convenient to change to coordinate representation and to write the tunneling current in terms of Green's functions instead of spectral functions. This leads to different combinations of

retarded and advanced Green's functions. But for the moment we just concentrate on one term, writing 'G' without specifying whether it is a retarded or advanced Green's function. Furthermore, the energy arguments (and integrals) are omitted in order to get a more compact notation. This looks as follows:

$$\langle I^2\rangle \sim \int \mathrm{d}^2x\mathrm{d}^2x'\mathrm{d}^2y\mathrm{d}^2y'\, \mathrm{e}^{\mathrm{i}e\mathbf{A}(\mathbf{x}-\mathbf{x}'+\mathbf{y}-\mathbf{y}')}\langle G_1(\mathbf{x},\mathbf{x}')G_1(\mathbf{y},\mathbf{y}')\rangle G_2^{\mathrm{o}}(\mathbf{x}'-\mathbf{x})G_2^{\mathrm{o}}(\mathbf{y}'-\mathbf{y})\,.$$

Now there are three possible situations to distinguish (see Fig. 4.7), characterized by the arrangement of the four coordinates $\mathbf{x},\mathbf{x}',\mathbf{y},\mathbf{y}'$ within the plane:

1. The tunneling sites lie within a distance smaller than the mean free path l from each other pairwise: $|\mathbf{x}-\mathbf{y}'|<l$ and $|\mathbf{x}'-\mathbf{y}|<l$.
2. The complementary combinations of tunneling sites are close to each other, *i.e.* $|\mathbf{x}-\mathbf{y}|<l$ and $|\mathbf{x}'-\mathbf{y}'|<l$.
3. The four coordinates are arbitrary points on the plane which do not fulfill the conditions given in (1.) or (2.).

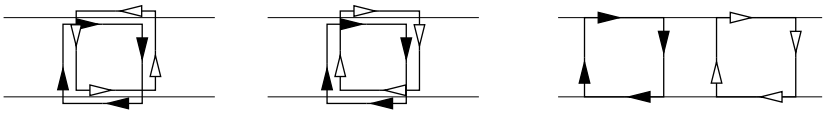

Figure 4.7: Current loops of the different contributions to $\langle I^2\rangle$.

Only in the third case the Green's functions can be averaged separately because they scatter from different impurities and therefore lose coherence. This just leads to the contribution $\langle I\rangle^2$. In contrast, the other cases are more interesting since they include correlations as described in section 3.3.2. In the first case, when the two Green's functions have opposite 'directions', the enclosed magnetic flux is small because the contributions from the two loops almost cancel each other, whereas in the second case the two contributions to the enclosed flux add up, and therefore a strong dependence on the magnetic field is expected.

A very crude picture of the effect can be obtained by identifying the tunneling sites pairwise.

- In the first case ($\mathbf{x}=\mathbf{y}'$ and $\mathbf{x}'=\mathbf{y}$), the magnetic field dependence drops out since the phase factor is just 1.
- By contrast, in the second case ($\mathbf{x}=\mathbf{y}$ and $\mathbf{x}'=\mathbf{y}'$), the phase factor equals $\exp[2\mathrm{i}e\mathbf{A}(\mathbf{x}-\mathbf{x}')]$. Thus, if the correlation function is translationally invariant, this contribution has the form of a Fourier transform with respect to the vector potential.

Although this is an oversimplified picture, we will see that the basic features survive a more careful evaluation. The fact that the field dependent contribution to the current fluctuations can be expressed as a Fourier transform is the reason why tunneling spectroscopy allows one to study local transport properties of the 2DEGs as signaled in the introduction. We will come back later to this important point.

In the following, we discuss the two contributions separately. Therefore, we write the variance $(\Delta I)^2 = \langle I^2\rangle - \langle I\rangle^2$ as a sum

$$(\Delta I)^2 = 4e^2\,|T|^4\left(\mathcal{D}(eV) + \mathcal{C}(2e\mathbf{A}; eV)\right), \tag{4.17}$$

where $\mathcal{D}$ denotes the first contribution being independent of magnetic field and $\mathcal{C}$ stands for the second contribution, as shown in Fig 4.8. The notations $\mathcal{D}$ and $\mathcal{C}$ will become clear in the following.

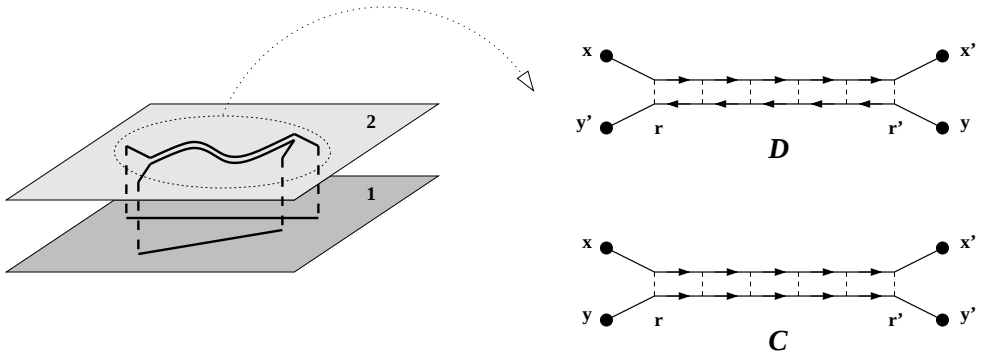

Figure 4.8: The two contributions to $(\Delta I)^2$ for tunneling between a clean and a disordered layer.

While the real space representation is more intuitive, in order to calculate these expressions we go back to momentum representation. Expressing the spectral functions of the disordered layer by Green's functions, Eq. 4.16 reads

$$\begin{aligned}\langle I^2\rangle \;=\; & 4e^2\,|T|^4 \sum_{\mathbf{k},\mathbf{p}} \int (\mathrm{d}\epsilon^{[eV]})\,(\mathrm{d}\epsilon'^{[eV]}) \\ & \times \sum_{\sigma,\sigma'} (-\sigma\cdot\sigma')\langle G_1^{\sigma}(\mathbf{K},\mathbf{K};\epsilon) G_1^{\sigma'}(\mathbf{P},\mathbf{P};\epsilon')\rangle\, A_2^{\mathrm{o}}(\mathbf{k};\epsilon+eV) A_2^{\mathrm{o}}(\mathbf{p};\epsilon'+eV)\,.\end{aligned} \tag{4.18}$$

where $\sigma^{(\prime)} = +, -$.

The method of evaluating the correlations $\langle G_1^{\sigma} G_1^{\sigma'}\rangle$ has been discussed in section 3.3.2. The disconnected part $\langle G_1^{\sigma}\rangle\langle G_1^{\sigma'}\rangle = g_1^{\sigma} g_1^{\sigma'}$ corresponds to the case where tunneling occurs at independent points. As already pointed out this leads

to the averaged current squared $\langle I\rangle^2$, *i.e.* the variance $(\Delta I)^2$ is given by the connected part $\langle G_1^\sigma G_1^{\sigma'}\rangle_{\rm c}$. For $\sigma=\sigma'$ the average $\langle G_1^\sigma G_1^{\sigma'}\rangle$ just equals its disconnected value (cf. section 3.3.2), therefore the only contributions to the variance come from the case $\sigma\neq\sigma'$. Hence,

$$\begin{aligned}(\Delta I)^2 &= 4e^2\,|T|^4 \sum_{\mathbf{k},\mathbf{p}} \int (\mathrm{d}\epsilon^{[eV]})\,(\mathrm{d}\epsilon'^{[eV]}) A_2^{\rm o}(\mathbf{k};\epsilon+eV) A_2^{\rm o}(\mathbf{p};\epsilon'+eV) \qquad (4.19)\\ &\quad\times \sum_{\sigma\neq\sigma'} \Big[g_1^\sigma(\mathbf{K},\epsilon;\tau) g_1^{\sigma'}(\mathbf{P},\epsilon';\tau)\Big]^2 \Gamma^{\sigma\sigma'}(\mathbf{K},\mathbf{P};\mathbf{K},\mathbf{P};\epsilon,\epsilon')\,,\end{aligned}$$

where Eq. 3.32 has been used.

As shown in section 3.3.2 there are two important contributions to the vertex function $\Gamma^{\sigma\sigma'}(\mathbf{K},\mathbf{P};\mathbf{K},\mathbf{P};\epsilon,\epsilon')$. These can be assigned to the different cases, (1.) and (2.), we distinguished in real space representation:

1. For small momentum difference $\mathbf{q}\equiv\mathbf{K}-\mathbf{P}$, the main contribution comes from the ladder diagrams, *i.e.* the diffuson $\mathrm{D}^{\sigma\sigma'}(\mathbf{q},\omega)$. It can be easily seen that the diffuson does not depend on the magnetic field because the vector potential cancels out in the difference ($\mathbf{q}=\mathbf{k}-\mathbf{p}$). This corresponds to the first case, thus justifying the notation $\mathcal{D}(eV)$ introduced above (see also Fig. 4.8 top).

2. If the momentum sum $\tilde{\mathbf{Q}}\equiv\mathbf{K}+\mathbf{P}$ is small, the maximally crossed diagrams give the dominant contribution, namely the Cooperon $\mathrm{C}^{\sigma\sigma'}(\tilde{\mathbf{Q}},\omega)$. Since here the vector potential adds up ($\tilde{\mathbf{Q}}=\mathbf{k}+\mathbf{p}-2e\mathbf{A}$), the Cooperon contribution obviously depends on the magnetic field. This corresponds to the second case, denoted by $\mathcal{C}(2e\mathbf{A};eV)$ (see also Fig. 4.8 bottom).

Now we can write down the different contributions, substituting $\mathbf{q}=\mathbf{k}-\mathbf{p}$ for the diffuson and $\mathbf{Q}=\mathbf{k}+\mathbf{p}$ for the Cooperon, respectively:

$$\begin{aligned}\mathcal{D} &= \sum_{\mathbf{k};\mathbf{q}} \int (\mathrm{d}\epsilon^{[eV]})(\mathrm{d}\epsilon'^{[eV]}) A_2^{\rm o}(\mathbf{k};\epsilon+eV) A_2^{\rm o}(\mathbf{k}-\mathbf{q};\epsilon'+eV) \qquad (4.20)\\ &\quad\times \sum_{\sigma\neq\sigma'} \Big[g_1^\sigma(\mathbf{K},\epsilon;\tau) g_1^{\sigma'}(\mathbf{K}-\mathbf{q},\epsilon';\tau)\Big]^2 \mathrm{D}^{\sigma\sigma'}(\mathbf{q},\omega)\,,\\ \mathcal{C} &= \sum_{\mathbf{k};\mathbf{Q}} \int (\mathrm{d}\epsilon^{[eV]})(\mathrm{d}\epsilon'^{[eV]}) A_2^{\rm o}(\mathbf{k};\epsilon+eV) A_2^{\rm o}(-\mathbf{k}+\mathbf{Q};\epsilon'+eV) \qquad (4.21)\\ &\quad\times \sum_{\sigma\neq\sigma'} \Big[g_1^\sigma(\mathbf{K},\epsilon;\tau) g_1^{\sigma'}(-\mathbf{K}+\mathbf{Q},\epsilon';\tau)\Big]^2 \mathrm{C}^{\sigma\sigma'}(\mathbf{Q}-2e\mathbf{A},\omega)\,.\end{aligned}$$

In the following, the important steps in the evaluation of these expressions will be motivated before discussing the results, while the explicit calculations can be found in appendix B.1.2.

The diffuson contribution

Let us first discuss the diffuson contribution given by Eq. 4.20. Starting with the evaluation of the **k**-summation by replacing it with an integral (continuum limit), the following approximations can be used:

- The absolute value of **k** is set to k_F, its value at the Fermi energy (see section 4.1).
- The small momentum **q** as well as the applied voltage $eV \ll \tau^{-1}$ are neglected in the 'outer' Green's functions g_1 which are smeared out due to disorder.

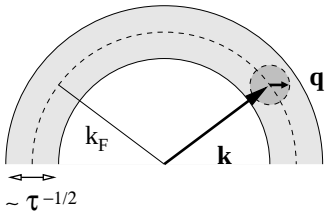

- Furthermore, we restrict ourselves to weak magnetic fields $B \ll B_\mathrm{c}^{(l)}$. Then the effect of the magnetic field on the outer Green's functions is negligible, too. It will become clear when evaluating the Cooperon contribution that this is sufficient because there the magnetic field dependence is much stronger, *i.e.* the Cooperon contribution decays on a field scale $B_\mathrm{c}[(\Delta I)^2] \ll B_\mathrm{c}^{(l)}$.

Thus, each Green's function g_1^σ just contributes a factor $-(\sigma)\mathrm{i}2\tau$. This leads to the formula

$$\mathcal{D} = \frac{8\tau^2}{\pi^2} \int_0^{eV} \mathrm{d}\omega \, (eV - \omega) \sum_{|\mathbf{q}| > \frac{\omega}{v_\mathrm{F}}} \frac{1}{\sqrt{v_\mathrm{F}^2 q^2 - \omega^2}} \frac{2Dq^2}{D^2 q^4 + \omega^2}, \tag{4.22}$$

where one energy integral has been eliminated due to the fact that the integrand only depends on the energy difference ω. The restriction on the **q**-summation comes from the δ-distribution of the second spectral function A_2°. For energies eV larger than the Thouless energy $E_\mathrm{Th} = D/L^2$, the continuum limit can be taken. The condition $eV \ll \tau^{-1}$ can be incorporated at the end of the calculation, or, alternatively, in Eq. 4.22 the energy difference ω can be neglected against $v_\mathrm{F} q$, yielding the same result:

$$\mathcal{D} = \frac{4L^2\tau^2}{\pi^2 v_\mathrm{F}} \int_0^{eV} \mathrm{d}\omega \, (eV - \omega) \frac{1}{\sqrt{2D\omega}}, \tag{4.23}$$

or, after energy integration,

$$\mathcal{D} = \frac{16L^2\tau^2}{3\pi^2 v_\mathrm{F}}\sqrt{\frac{(eV)^3}{2D}}\,. \tag{4.24}$$

In order to discuss this result, we first relate it to the average current, *i.e.*

$$(\Delta I)^2_{\mathcal{D}} \;=\; \langle I(B=0)\rangle^2 \cdot \left(\frac{l}{L}\right)^2 \frac{2}{3(k_\mathrm{F}l)^2\sqrt{eV\tau}}\,. \tag{4.25}$$

Due to the factor $(k_\mathrm{F}l)^{-2} \ll 1$, the current fluctuations are small. On the other hand $(eV\tau)^{-1/2} \gg 1$, *i.e.* for small enough voltages the current fluctuations should be observable. Since they are sub-quadratic in eV, the conductance fluctuations even diverge in the limit $eV \to 0$.

Furthermore, in the thermodynamic limit the current is self-averaging due to the factor $(l/L)^2$ in Eq. 4.25, *i.e.* $(\Delta I)^2/\langle I\rangle^2 \xrightarrow[L\to\infty]{} 0$.

The Cooperon contribution

At zero-field the Cooperon and the diffuson contribution are identical, but this is no longer true in the presence of a magnetic field. We will see that with increasing field the Cooperon will be suppressed while, as already shown, the diffuson is not affected.

We can start following the same lines as for the diffuson. Modified by the additional difficulty coming from the magnetic field, the expression equivalent to Eq. 4.22 looks as follows:

$$\mathcal{C} = \frac{8\tau^2}{\pi^2}\int_0^{eV} \mathrm{d}\omega\,(eV-\omega) \sum_{|\mathbf{Q}|>\frac{\omega}{v_\mathrm{F}}} \frac{1}{\sqrt{v_\mathrm{F}^2Q^2-\omega^2}} \frac{2D(\mathbf{Q}-2e\mathbf{A})^2}{D^2(\mathbf{Q}-2e\mathbf{A})^4+\omega^2}\,. \tag{4.26}$$

Now there are two different possibilities how to proceed:

1. The straightforward way is to search for a solution of the integral. Then we obtain the fluctuations as a function of the magnetic field, *i.e.* $\mathcal{C}(2e\mathbf{A};eV)$.

2. As mentioned earlier, the dependence of the fluctuations on the magnetic field is a means for studying local transport properties, namely the behavior of the Green's functions on different length scales. Thus, we can exploit the fact that the Q-integral is a convolution integral, to calculate the Fourier transform of the fluctuations with respect to the magnetic field, *i.e.* a function $\tilde{\mathcal{C}}(\mathbf{r}_\mathrm{m};eV)$ where $\mathbf{r}_\mathrm{m}$ is the conjugate variable to the vector potential and, therefore, has the dimension of a length.

In the following, both strategies will be discussed, starting with the direct evaluation of the integral.

1. The Cooperon contribution as a function of the magnetic field

In Eq. 4.26, for small voltages, ω can be neglected against $v_{\mathrm{F}}Q$. This is justified for $eV \ll \tau^{-1}$ as mentioned in the case of the diffuson. Then we obtain the following result (for details see appendix B.1.2):

$$\mathcal{C}(2e\mathbf{A}; eV) = \mathcal{D}(eV) \cdot c(2\sqrt{\frac{D}{eV}}eA) \tag{4.27}$$

with

$$c(x) = \frac{4\sqrt{2}}{3\pi}x^3 + \int_0^\pi \frac{\mathrm{d}\varphi}{2\pi}\Big(3\left(\sqrt{x^4\sin^4\varphi+1} - x^2\sin^2\varphi\right)^{\frac{1}{2}} - \left(\sqrt{x^4\sin^4\varphi+1} + x^2\sin^2\varphi\right)^{\frac{3}{2}}\Big).$$

Thus, the Cooperon contribution is given by the diffuson contribution multiplied by a function containing the field dependence. The argument of this function, which gives the scale for the suppression of the Cooperon by the magnetic field, can be expressed by the magnetic length l_{m} defined in section 3.2 and $L_{\mathrm{d}} \equiv \sqrt{D/(eV)}$, the diffusion length for a given time interval $(eV)^{-1}$, *i.e.* x is proportional to the ratio $L_{\mathrm{d}}/l_{\mathrm{m}}$. A plot of the function $c(x)$ (computed numerically) is shown in Fig. 4.9.

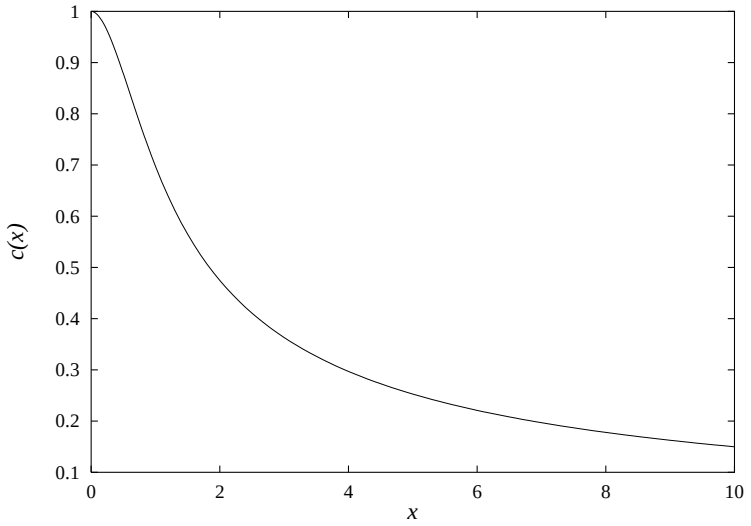

Figure 4.9: Dependence of the Cooperon contribution to $(\Delta I)^2$ on the magnetic field: $c(2\sqrt{D/(eV)}eA)$.

The asymptotic behavior for small and large x is given as

$$\begin{aligned} c(x) &= 1 - \frac{3}{4}x^2 && \text{for } x \ll 1\,, \\ c(x) &\sim x^{-1} && \text{for } x \gg 1\,. \end{aligned}$$

A characteristic magnetic field $B_{\rm c}[(\Delta I)^2] \equiv B_{\rm c}^{(L_{\rm d})} \equiv \sqrt{2}(edL_{\rm d})^{-1}$ can be defined, which now fulfills the equation $l_{\rm m}(B_{\rm c}^{(L_{\rm d})}) = L_{\rm d}$. Comparing this to the characteristic field for the average current, we see that $B_{\rm c}^{(L_{\rm d})} \ll B_{\rm c}^{(l)}$, since typically the diffusion length is much larger than the mean free path. (In fact the diffusion picture is only true for $L_{\rm d} > l$.) While the averaged single-particle Green's functions are short-ranged, the diffuson/Cooperon probes large distances. Thus, the current fluctuations are sensitive to smaller magnetic fields than the average current.

Combining this with the result for the diffuson (Eq. 4.25), we finally get

$$(\Delta I)^2 = \langle I(B=0)\rangle^2 \cdot \left(\frac{l}{L}\right)^2 \frac{2}{3(k_{\rm F}l)^2\sqrt{eV\tau}} \left(1 + c(2\sqrt{\frac{D}{eV}}eA)\right). \qquad (4.28)$$

On small field scales the fluctuations are reduced to half their zero-field value due to the suppression of the Cooperon contribution. Note that for larger magnetic fields $B \sim B_{\rm c}^{(l)}$ the diffuson contribution will be affected by the magnetic field, too, and therefore the fluctuations will be completely suppressed. The prefactors have already been discussed earlier in the context of the diffuson contribution.

Having found an expression for the current fluctuations as a function of the magnetic field, which allows to determine a characteristic field $B_{\rm c}^{(L_{\rm d})}$, we now come to the second possibility of evaluating the Cooperon contribution by studying its Fourier transform.

2. The Fourier transform of the Cooperon contribution

Again we start with Eq. 4.26 which, in the continuum limit, has the following form:

$$\mathcal{C} = \frac{32L^2\nu\tau^4}{\pi} \int_0^{eV} {\rm d}\omega\,(eV-\omega) \cdot \int_{|\mathbf{Q}|>\frac{\omega}{v_{\rm F}}} ({\rm d}Q)\, \frac{1}{\sqrt{v_{\rm F}^2Q^2-\omega^2}} {\rm Re}\left[{\rm C}(\mathbf{Q}-2e{\rm A},\omega)\right]. \qquad (4.29)$$

The Q-integral in Eq. 4.26 is a convolution integral:

$$\int ({\rm d}Q) f_{\rm b}(\mathbf{Q}) {\rm Re}\left[{\rm C}(\mathbf{Q}-2e\mathbf{A})\right] = \left(f_{\rm b} * {\rm Re}[{\rm C}]\right)(2e\mathbf{A})$$

with $f_{\rm b}(\mathbf{Q}) = (v_{\rm F}^2Q^2-\omega^2)^{-1/2}$. This function comes from the clean layer; thus the index 'b' for ballistic.

Then the expression for the Cooperon contribution becomes simpler by Fourier transforming it with respect to the magnetic field, *i.e.* the vector potential:

$$F(\mathbf{r}_\mathrm{m}) = \frac{e^2L^2}{4\pi^2}\int \mathrm{d}^2A\, f(e\mathbf{A})\cdot \mathrm{e}^{\mathrm{i}e\mathbf{A}\mathbf{r}_\mathrm{m}}\,. \tag{4.30}$$

Thus, we introduce a conjugate coordinate $\mathbf{r}_\mathrm{m}$, leading to

$$\tilde{\mathcal{C}}(\mathbf{r}_\mathrm{m};eV) = \frac{32L^2\nu\tau^4}{\pi}\int_0^{eV}\mathrm{d}\omega\,(eV-\omega)F_\mathrm{b}(\mathbf{r}_\mathrm{m};\omega)\cdot F_\mathrm{d}(\mathbf{r}_\mathrm{m};\omega)\,, \tag{4.31}$$

where $F_\mathrm{b}(\mathbf{x})$ and $F_\mathrm{d}(\mathbf{x})$ are the Fourier transforms of $f_\mathrm{b}(\mathbf{k})$ and $\mathrm{Re[C]}(\mathbf{k})$, respectively. The index 'd' stands for diffusive.

The remarkable result is the product structure of $\tilde{\mathcal{C}}(\mathbf{r}_\mathrm{m})$. The correlation functions of the two layers are just multiplied which allows their properties to be analyzed separately.

We find (see appendix B.1.2)

$$F_\mathrm{b}(\mathbf{x}) = \frac{L^2}{2\pi v_\mathrm{F}x}\cos\frac{\omega x}{v_\mathrm{F}} \quad \text{and} \tag{4.32}$$

$$F_\mathrm{d}(\mathbf{x}) = \frac{1}{4\pi^2\nu\tau^2 D}\mathrm{Re}\big[K_\mathrm{o}(\sqrt{\frac{\mathrm{i}\omega}{D}}x)\big] = \frac{1}{4\pi^2\nu\tau^2 D}\mathrm{ker}\big(\sqrt{\frac{\omega}{D}}x\big)\,. \tag{4.33}$$

The functions $\cos(x)/x$ and $\mathrm{ker}(x)$ are plotted in Fig. 4.10. $K_\mathrm{o}(x)$ is the modified Bessel function of zeroth order; $\mathrm{ker}(x)\equiv\mathrm{Re}[K_\mathrm{o}(\sqrt{\mathrm{i}}\,x)]$ is called a Thomson or Kelvin function. For small values of x, the function $\mathrm{ker}(x)$ can be approximated by

$$\mathrm{ker}(x) = -\mathbf{C} - \ln\frac{x}{2} + O(x^2)\,, \tag{4.34}$$

where $\mathbf{C}\approx 0.58...$ is Euler's constant.

In the limit $r_\mathrm{m}\to 0$ the result diverges. This divergence comes from large momenta where the diffusion picture does not apply anymore. Thus, the formula is valid only for $r_\mathrm{m}\gtrsim l$.

It is instructive to compare the arguments of the two functions. In the previous paragraph the diffusion length L_d has been introduced. The analogous definition of a ballistic length within the clean layer is $L_\mathrm{b}\equiv v_\mathrm{F}/(eV)$, for a given time interval $(eV)^{-1}$. In fact, the result only depends on the relative size of the different length scales. To express this, we introduce two parameters $m\equiv r_\mathrm{m}/L_\mathrm{d}$ and $x_\mathrm{db}\equiv L_\mathrm{d}/L_\mathrm{b}$. Rewriting the result in terms of these quantities:

$$\tilde{\mathcal{C}}(m,x_\mathrm{db};eV) = \frac{4L^4\nu^2(eV)^2}{\pi^2\epsilon_\mathrm{F}^2}\int_0^1\mathrm{d}y(1-y)\frac{x_\mathrm{db}}{m}\cos(x_\mathrm{db}my)\mathrm{ker}(m\sqrt{y}) \tag{4.35}$$

with $y=\omega/(eV)$. While $x_\mathrm{db}\ll 1$, typically, there are no restrictions on m.

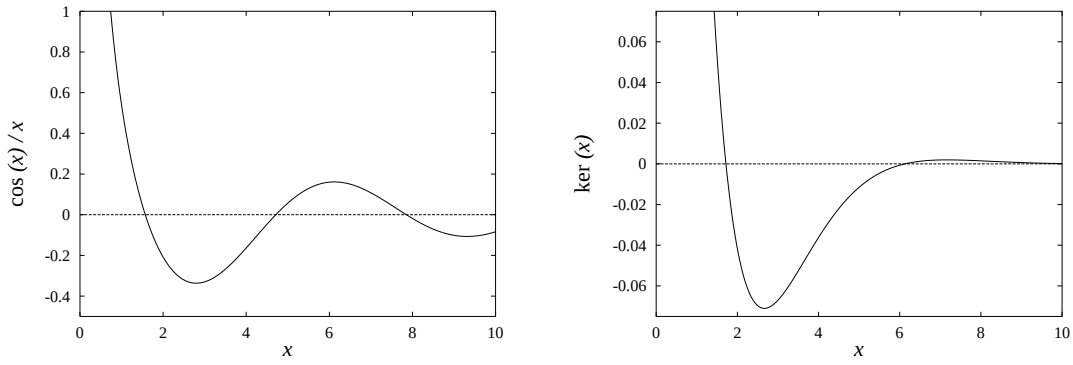

Figure 4.10: The functions $\cos(x)/x$ and $\ker(x)$.

Thus, the function F_{d} varies on much shorter length scales r_{m} than F_{b}, *i.e.* the behavior of the Cooperon contribution is governed by the disordered layer. The range of the Cooperon within the disordered layer sets a limit to the distance between the tunneling sites and therefore determines the area typically enclosed by the current loops. The ratio of the arguments of the two functions $s = x_{\mathrm{d}}/x_{\mathrm{b}}$ is proportional to $(\omega\tau)^{-1/2} \gg 1$. In Fig. 4.11 the product $F_{\mathrm{b}}(x) \cdot F_{\mathrm{d}}(sx)$ is plotted for different values of s.

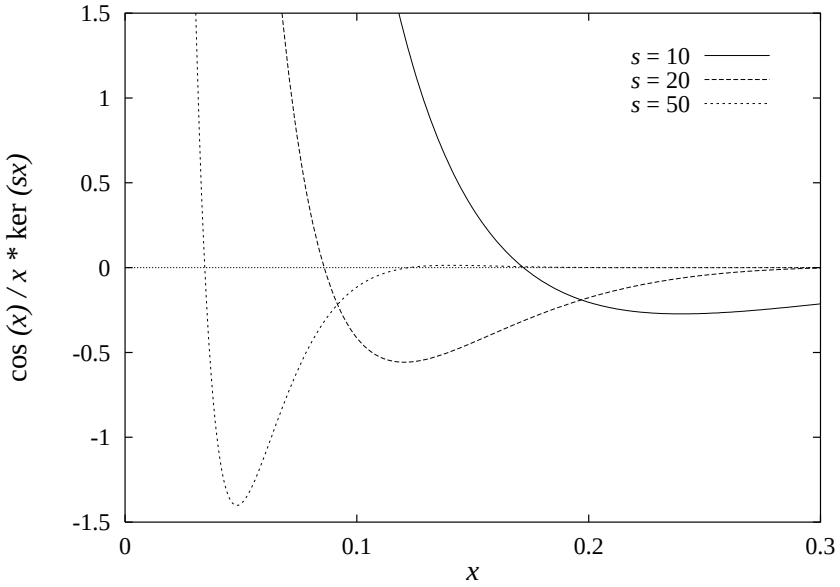

Figure 4.11: $(\cos(x)/x) \cdot \ker(sx)$ for $s = 10, 20, 50$.

Alternatively we can discuss the contribution to the conductance fluctuations, *i.e.* to their Fourier transform:

$$\widetilde{(\Delta\bar{\mathrm{g}})^2_{\mathcal{C}}} \sim \frac{\tilde{\mathcal{C}}}{(eV)^2} = \frac{4L^4\nu^2}{\pi^2\epsilon_{\mathrm{F}}^2}\int\limits_0^1 \mathrm{d}y(1-y)\frac{x_{\mathrm{db}}}{m}\cos(x_{\mathrm{db}}my)\mathrm{ker}(m\sqrt{y})\,. \tag{4.36}$$

A plot of $\widetilde{(\Delta\bar{\mathrm{g}})^2_{\mathcal{C}}}$ against m and against x_{db} is shown in Fig. 4.12. For $x_{\mathrm{db}}m \ll 1$, $\widetilde{(\Delta\bar{\mathrm{g}})^2_{\mathcal{C}}}$ is linear in x_{db}. In the limit $m \sim \sqrt{eV} \to 0$ the result diverges. This has already been pointed out when discussing $\mathcal{C}(2e\mathbf{A}; eV)$.

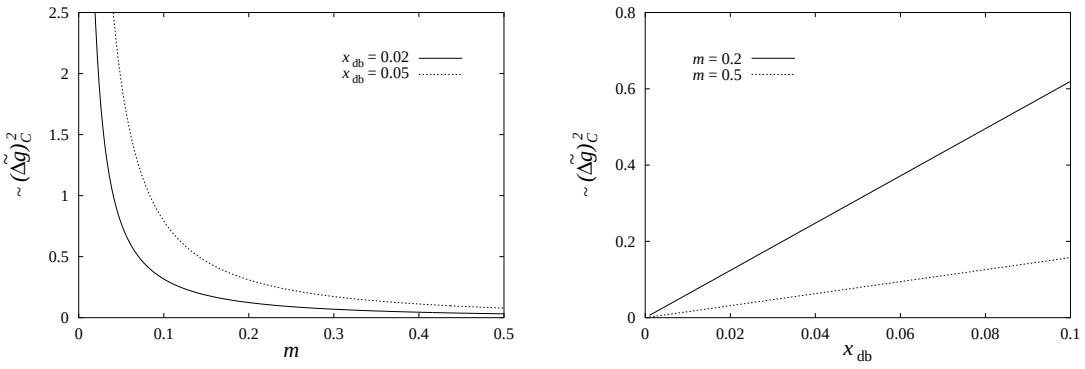

Figure 4.12: $\widetilde{(\Delta\bar{\mathrm{g}})^2_{\mathcal{C}}}$ as a function of m (left plot) and x_{db} (right plot).

Before discussing the case of two disordered layer, let us summarize the results. The overall shape of the I-B-characteristics can be understood by the relative shift of the Fermi circles of the two layers. At small magnetic field, the field dependence of the average current $\langle I\rangle$ is characterized by the field scale $B_{\mathrm{c}}^{(l)} \sim l^{-1}$, where the mean free path l is the typical range of the impurity averaged Green's function. The current fluctuations $(\Delta I)^2$ comprise two contributions, namely the diffuson and the Cooperon contribution, but only the latter is sensitive to the magnetic field. The Cooperon shows structure on a much smaller field scale than the average current, the characteristic field $B_{\mathrm{c}}^{(L_{\mathrm{d}})} \sim L_{\mathrm{d}}^{-1}$ being determined by the diffusion length $L_{\mathrm{d}} \gg l$. The behavior of the average current as well as of the fluctuations is governed by the disordered layer. Furthermore, the Cooperon contribution can be expressed as the Fourier transform of the correlation functions of the 2DEGs. Thus, the field dependence of the current fluctuations yields information about the spatial correlations in the layers.

4.3 Tunneling between two disordered 2DEGs

A setup with two disordered 2DEGs is clearly easier to realize experimentally than the one discussed in the previous section. We will start with mean free times τ_1, τ_2 chosen separately for the two layers, but the special case of $\tau_1 = \tau_2$ will be discussed, too. However, we still assume that the two layers have different disorder potentials, *i.e.* interlayer correlations do not play a role (cf. p. 32).

4.3.1 The average tunneling current

We start again with the tunneling current formula (4.3):

$$\langle I \rangle = 2e\,|T|^2 \sum_{\mathbf{k}} \int (\mathrm{d}\epsilon^{[eV]}) a_1(\mathbf{k} - e\mathbf{A}, \epsilon; \tau_1) a_2(\mathbf{k}, \epsilon + eV; \tau_2)\,,$$

where now the impurity averaged spectral functions have to be taken for both layers.

Although the formula looks more complicated, the result is similar to what was found in section 4.2.1. The only difference is that τ has to be replaced by a combination of the individual mean free times:

$$\bar{\tau} \equiv \frac{\tau_1 \tau_2}{\tau_1 + \tau_2}\,. \tag{4.37}$$

For the calculation see appendix B.2.1.

This means that the scattering rates τ_i^{-1} of the two layers are additive. In the limit $\tau_2 \to \infty$ one recovers the earlier result ($\bar{\tau} = \tau_1$). On the other hand, in the special case $\tau_1 = \tau_2 \equiv \tau$, the combined mean free time is $\bar{\tau} = \tau/2$. We see that, in comparison with the previous case of only one disordered 2DEG, the average tunneling current is further suppressed, but there is no significant change in the I-B-characteristics. The relevant length scale for the field dependence is simply given by the combined mean free path $\bar{l}$. Thus, the characteristic field may be defined in the same way, too.

However, the current fluctuations are qualitatively different as will be shown in the following.

4.3.2 The current fluctuations

As discussed before, the current fluctuations in tunneling from a clean to a disordered 2DEG have two different contributions, only one of them being influenced by the magnetic field. By contrast, in the case of two disordered 2DEGs, there are in principle five terms contributing to the current fluctuations because now

correlations are possible within both layers. The different contributions can be distinguished by the number of diffusons and/or Cooperons they involve. This motivates the notation introduced in the following list:

- 1 diffuson (in layer 1 or 2) $\rightarrow \mathcal{D}_1$,
- 1 Cooperon (in layer 1 or 2) $\rightarrow \mathcal{C}_1$,
- a diffuson in one layer and a Cooperon in the other layer $\rightarrow X_{\mathcal{DC}}$,
- 2 diffusons $\rightarrow \mathcal{D}_2$, and
- 2 Cooperons $\rightarrow \mathcal{C}_2$.

The corresponding diagrammatic representation is shown in Fig. 4.13 (in the same order).

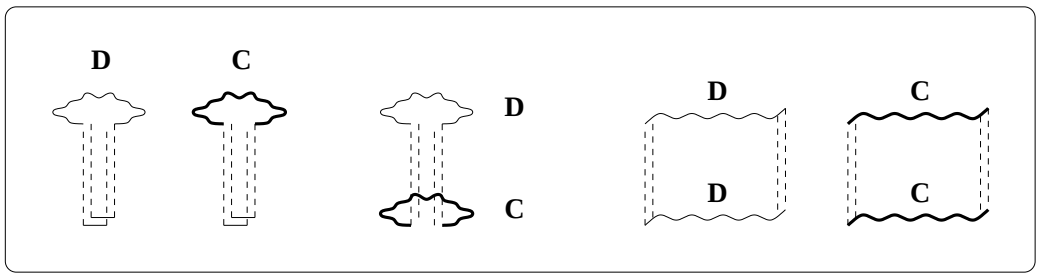

Figure 4.13: The different contributions to the current fluctuations for the case of two disordered layers.

Clearly the diffuson contributions $\mathcal{D}_1$ and $\mathcal{D}_2$ do not depend on the magnetic field, but likewise the 1-Cooperon contribution $\mathcal{C}_1$ and the 1-diffuson-1-Cooperon contribution $X_{\mathcal{DC}}$ are field independent because all the tunneling sites have to be nearby (within the mean free path l). Furthermore, it will be shown that for the same reason the terms containing only one diffuson and/or Cooperon are negligibly small against the ones involving two diffusons or Cooperons.

We can rewrite the current fluctuations again as a sum of the different contributions which will be evaluated separately:

$$(\Delta I)^2 = 4e^2 \left|T\right|^4 \left(\mathcal{D}_1(eV) + \mathcal{C}_1(eV) + X_{\mathcal{DC}}(eV) + \mathcal{D}_2(eV) + \mathcal{C}_2(2e\mathbf{A}; eV)\right). \tag{4.38}$$

To do so we start from the general formula (4.4):

$$\begin{aligned} \langle I^2 \rangle &= 4e^2 \left|T\right|^4 \sum_{\mathbf{k},\mathbf{k}';\mathbf{p},\mathbf{p}'} \int (\mathrm{d}\epsilon^{[eV]}) \, (\mathrm{d}\epsilon'^{[eV]}) \\ &\quad \times \langle A_1(\mathbf{K}, \mathbf{K}'; \epsilon) A_1(\mathbf{P}, \mathbf{P}'; \epsilon') \rangle \, \langle A_2(\mathbf{k}', \mathbf{k}; \epsilon + eV) A_2(\mathbf{p}', \mathbf{p}; \epsilon' + eV) \rangle \, . \end{aligned} \tag{4.39}$$

First we distinguish between the connected and disconnected parts of this expression. Taking the disconnected part of both correlators we obtain again $\langle I\rangle^2$. The cross terms give the 1-diffuson and 1-Cooperon contributions

$$\mathcal{D}_1+\mathcal{C}_1 \sim a_2(\mathbf{k})a_2(\mathbf{p})\langle A_1(\mathbf{K},\mathbf{K})A_1(\mathbf{P},\mathbf{P})\rangle_{\rm c} + a_1(\mathbf{K})a_1(\mathbf{P})\langle A_2(\mathbf{k},\mathbf{k})A_2(\mathbf{p},\mathbf{p})\rangle_{\rm c}\,. \tag{4.40}$$

These correspond to the contributions found earlier in the case of tunneling from a clean to a disordered 2DEG. However, they are now 'short-ranged' due to the impurity averaged spectral functions a_i (cf. Fig. 4.13). The remaining contributions which did not exist in the previous case contain both connected parts:

$$X_{\mathcal{DC}}+\mathcal{D}_2+\mathcal{C}_2 \sim \langle A_1(\mathbf{K},\mathbf{K}')A_1(\mathbf{P},\mathbf{P}')\rangle_{\rm c}\langle A_2(\mathbf{k}',\mathbf{k})A_2(\mathbf{p}',\mathbf{p})\rangle_{\rm c}\,. \tag{4.41}$$

To further separate these contributions we have to look at the relations between the different momenta. In (4.40) there are only two momentum arguments $\mathbf{k}$ and $\mathbf{p}$. If the momentum difference is small, the ladder diagrams, *i.e.* the diffuson, are important, whereas, if the momentum sum is small, the maximally crossed diagrams, *i.e.* the Cooperon, dominate. This is equivalent to the case discussed in section 4.2.2. In (4.41) there are four momentum arguments, but only three of them are independent, due to overall momentum conservation: $\mathbf{k}-\mathbf{p}=\mathbf{k}'-\mathbf{p}'$. The 2-diffuson contribution requires $\mathbf{q}=\mathbf{k}-\mathbf{p}$ to be small while the 2-Cooperon contribution is obtained for small $\mathbf{Q}=\mathbf{k}+\mathbf{p}'$. In both cases this is one supplementary condition. Therefore two free momentum integrations are left. The two diffusons (Cooperons) have equal momenta $\mathbf{q}$ ($\mathbf{Q}$). For the 1-diffuson-1-Cooperon contribution, finally, both these conditions have to be fulfilled, *i.e.* there is only one free momentum integration (but the diffuson and the Cooperon may have different (small) momenta $\mathbf{q}$ and $\mathbf{Q}$). Due to these constraints the contribution $X_{\mathcal{DC}}$ is suppressed by a factor $(k_{\rm F}l)^{-1}$ and therefore negligible.

Introducing the notation $Y=\int(\mathrm{d}\epsilon^{[eV]})\,(\mathrm{d}\epsilon'^{[eV]})Y^{\omega}$ (for $Y=\mathcal{D}_1,\mathcal{C}_1,\mathcal{D}_2,\mathcal{C}_2$), the relevant contributions are given by the following expressions[1]:

$$\begin{aligned}\mathcal{D}_1{}^{\omega} &= \sum_{\mathbf{q}}\int(\mathrm{d}k)\,\Big\{a_2(\mathbf{k};\epsilon+eV)a_2(\mathbf{k}-\mathbf{q};\epsilon'+eV) \\ &\quad\times\sum_{\sigma\neq\sigma'}\Big[g_1^{\sigma}(\mathbf{K},\epsilon)g_1^{\sigma'}(\mathbf{K}-\mathbf{q},\epsilon')\Big]^2\,\mathrm{D}^{\sigma\sigma'}(\mathbf{q},\omega;\tau_1) \;+\; (1\leftrightarrow 2)\Big\}\,,\end{aligned} \tag{4.42}$$

$$\begin{aligned}\mathcal{C}_1{}^{\omega} &= \sum_{\mathbf{Q}}\int(\mathrm{d}k)\,\Big\{a_2(\mathbf{k};\epsilon+eV)a_2(-\mathbf{k}+\mathbf{Q};\epsilon'+eV) \\ &\quad\times\sum_{\sigma\neq\sigma'}\Big[g_1^{\sigma}(\mathbf{K},\epsilon)g_1^{\sigma'}(-\mathbf{K}+\mathbf{Q},\epsilon')\Big]^2\,\mathrm{C}^{\sigma\sigma'}(\mathbf{Q}-2e\mathbf{A},\omega;\tau_1) \;+\; (1\leftrightarrow 2)\Big\}\,,\end{aligned} \tag{4.43}$$

[1] In Eqs. 4.42 and 4.43 the full expressions are written down only for a diffuson/Cooperon in layer 1. The acronym $(1\leftrightarrow 2)$ denotes that a similar term is obtained for layer 2.

$$\mathcal{D}_2^{\ \omega} = \sum_{\mathbf{q}} \sum_{\sigma_i \neq \sigma_i'} \mathrm{D}^{\sigma_1\sigma_1'}(\mathbf{q},\omega;\tau_1)\mathrm{D}^{\sigma_2\sigma_2'}(\mathbf{q},\omega;\tau_2) \tag{4.44}$$
$$\times\Big[\int(\mathrm{d}k)\, g_1^{\sigma_1}(\mathbf{K},\epsilon)g_1^{\sigma_1'}(\mathbf{K}-\mathbf{q},\epsilon')g_2^{\sigma_2}(\mathbf{k},\epsilon+eV)g_2^{\sigma_2'}(\mathbf{k}-\mathbf{q},\epsilon'+eV)\Big]^2\,,$$

$$\mathcal{C}_2^{\ \omega} = \sum_{\mathbf{Q}} \sum_{\sigma_i \neq \sigma_i'} \mathrm{C}^{\sigma_1\sigma_1'}(\mathbf{Q}-2e\mathbf{A},\omega;\tau_1)\mathrm{C}^{\sigma_2\sigma_2'}(\mathbf{Q},\omega;\tau_2) \tag{4.45}$$
$$\times\Big[\int(\mathrm{d}k)\, g_1^{\sigma_1}(\mathbf{K},\epsilon)g_1^{\sigma_1'}(-\mathbf{K}+\mathbf{Q},\epsilon')g_2^{\sigma_2}(\mathbf{k},\epsilon+eV)g_2^{\sigma_2'}(-\mathbf{k}+\mathbf{Q},\epsilon'+eV)\Big]^2\,.$$

These contributions will be discussed now.

The 1-diffuson and 1-Cooperon contributions

The formulae (4.42) and (4.43) corresponding to the 1-diffuson and 1-Cooperon contributions look similar to the expressions for only one disordered 2DEG in section 4.2.2. However, they differ, because now the small momentum $\mathbf{q}$ ($\mathbf{Q}$) can be neglected not only in the outer Green's functions, but also in the spectral functions of the other layer, which are smeared out due to the disorder in that layer. This means we have a 'free' diffuson (Cooperon):

$$\int(\mathrm{d}q)\,\mathrm{D}(\mathbf{q},\omega) = \tilde{\mathrm{D}}(0,\omega)\,, \tag{4.46}$$

where $\tilde{\mathrm{D}}(\mathbf{x},\omega)$ is the Fourier transform of $\mathrm{D}(\mathbf{q},\omega)$.

In the case of the Cooperon this implies that the magnetic field dependence vanishes[2], *i.e.*

$$\int(\mathrm{d}Q)\,\mathrm{C}(\mathbf{Q}-2e\mathbf{A},\omega) = \int(\mathrm{d}Q')\,\mathrm{C}(\mathbf{Q}',\omega) = \tilde{\mathrm{C}}(0,\omega) = \tilde{\mathrm{D}}(0,\omega)\,. \tag{4.47}$$

Therefore the diffuson and the Cooperon contributions yield the same result. The calculation is presented in appendix B.2.2. Collecting all these contributions, we finally get

$$(\Delta I)_1{}^2 = 4e^2\,|T|^4\,\frac{2L^2\bar{\tau}^2}{\pi^3}(\tau_1+\tau_2+\bar{\tau})\sum_{i=1,2}\int_0^{eV}\mathrm{d}\omega\,(eV-\omega)\frac{1}{D_i}\ln(1+\frac{1}{(\omega\tau_i)^2})\,. \tag{4.48}$$

[2]Note that this is only valid for not too small energies when the continuum limit can be taken. In a summation the field dependence of the zero-mode $\mathbf{Q}=0$ would be left.

For the special case $\tau_1 = \tau_2 \equiv \tau$, this takes the form

$$(\Delta I)_1{}^2 = 4e^2 |T|^4 \frac{5L^2\tau^3}{2\pi^3 D} \int_0^{eV} \mathrm{d}\omega\,(eV-\omega) \ln(1+\frac{1}{(\omega\tau)^2}) \tag{4.49}$$

$$= \langle I(B=0)\rangle^2 \cdot \left(\frac{l}{L}\right)^2 \frac{5}{\pi(k_\mathrm{F}l)^2} \int_0^1 \mathrm{d}y\,(1-y) \ln(1+\frac{1}{(eV\tau y)^2})\,. \tag{4.50}$$

Again the current fluctuations are suppressed by a factor $(k_\mathrm{F}l)^{-2}$. The integral is finite and its solution is given in appendix B.2.2. Only in the limit $eV \to 0$ the conductance fluctuations $\sim (\Delta I)^2/(eV)^2$ diverge. This behavior has already been observed in section 4.2.2 for tunneling between a clean and a disordered 2DEG. There it also has been pointed out that the tunneling current is self-averaging.

We will see in the following that these are not the dominant contributions to the current fluctuations, however. More important are the 2-diffuson and 2-Cooperon contributions which will be discussed in the subsequent paragraphs.

The 2-diffuson contribution

Due to energy and momentum conservation in tunneling, the two diffusons involved have equal energies and momenta. But in contrast to the previous cases, now, the two tunneling processes can take place at different momenta. With the same approximations discussed earlier, Eq. 4.44 reads

$$\mathcal{D}_2^\omega = 4\sum_{\mathbf{q}} \mathrm{Re}\left[\mathrm{D}(\mathbf{q},\omega;\tau_1)\right] \mathrm{Re}\left[\mathrm{D}(\mathbf{q},\omega;\tau_2)\right] \left\{\int (\mathrm{d}k)\, g_1^+(\mathbf{k}) g_1^-(\mathbf{k}) g_2^+(\mathbf{k}) g_2^-(\mathbf{k})\right\}^2. \tag{4.51}$$

The evaluation is straightforward (see appendix B.2.2), leading to the result

$$(\Delta I)^2_{\mathcal{D}_2} = 4e^2 |T|^4 \frac{L^2\bar{\tau}^2}{\pi^2(D_1+D_2)} \int_0^{eV} \mathrm{d}\omega\,(eV-\omega)\,\frac{1}{\omega}\,. \tag{4.52}$$

For the special case $\tau_1 = \tau_2 \equiv \tau$, Eq. 4.52 reduces to

$$(\Delta I)^2_{\mathcal{D}_2} = 4e^2 |T|^4 \frac{L^2\tau^2}{8\pi^2 D} \int_0^{eV} \mathrm{d}\omega\,(eV-\omega)\,\frac{1}{\omega}\,. \tag{4.53}$$

Comparing this result with the 1-diffuson contribution, we get

$$\mathcal{D}_1^\omega/\mathcal{D}_2^\omega \sim (\omega\tau)\cdot\ln(1+\frac{1}{(\omega\tau)^2}) \ll 1\,. \tag{4.54}$$

Therefore, the 1-diffuson and 1-Cooperon contributions are negligible. Then, as in the case of tunneling from a clean to a disordered 2DEG, there are only two dominant contributions to the current fluctuations.

Furthermore, we see that in this case even the current fluctuations are divergent. The integral in Eq. 4.53 diverges at the lower limit, *i.e.* for $\omega \to 0$. Thus, a cut-off has to be introduced. A natural limit for the validity of the diffusion picture is the Thouless energy $E_{\rm Th}$. Hence,

$$(\Delta I)^2_{\mathcal{D}_2} = \langle I(B=0)\rangle^2 \cdot \left(\frac{l}{L}\right)^2 \frac{1}{4(k_{\rm F}l)^2 eV\tau}\Big(\ln\frac{eV}{E_{\rm Th}} - 1\Big)\,. \tag{4.55}$$

Below that limit, the replacement of the $\mathbf{q}$-summation by an integral is no longer correct. In order to continue to lower energies, the so-called 'zero-modes' ($\mathbf{q}=0$) become important. Then, in many cases, the diagrammatic approach can be extended down to the level spacing Δ. However, this requires a separate consideration.

As before, the fluctuations are suppressed by a factor $(k_{\rm F}l)^{-2}$. Moreover, the current is self-averaging in the thermodynamic limit.

The 2-Cooperon contribution

The 2-Cooperon contribution is the only term being influenced by the magnetic field. The expression for this contribution (Eq. 4.45) can be transformed into a form similar to Eq. 4.51:

$$\begin{aligned}\mathcal{C}_2^{\,\omega} &= 4\sum_{\mathbf{Q}} \mathrm{Re}\left[\mathrm{C}(\mathbf{Q}-2e\mathbf{A},\omega;\tau_1)\right]\mathrm{Re}\left[\mathrm{C}(\mathbf{Q},\omega;\tau_2)\right] \\ &\quad\times\Big\{\int(\mathrm{d}k)\, g_1^+(\mathbf{k})\, g_1^-(\mathbf{k})\, g_2^+(\mathbf{k})\, g_2^-(\mathbf{k})\Big\}^2\,.\end{aligned} \tag{4.56}$$

Again for $B = 0$, the result of the Cooperon contribution is identical with the result of the diffuson contribution. With magnetic field the Q-integral is a convolution integral (cf. section 4.2.2):

$$\int(\mathrm{d}Q)\,\mathrm{Re}[\mathrm{C}(\mathbf{Q}-2e\mathbf{A},\omega;\tau_1)]\,\mathrm{Re}[\mathrm{C}(\mathbf{Q},\omega;\tau_2)] = (\mathrm{Re}[\mathrm{C}^{\tau_1}]*\mathrm{Re}[\mathrm{C}^{\tau_2}])(2e\mathbf{A})\,. \tag{4.57}$$

The Fourier transforms $F_{\mathrm{d}i}$ of $\mathrm{Re}[\mathrm{C}^{\tau_i}]$ are given by Eq. 4.33, *i.e.*

$$F_{\mathrm{d}i}(\mathbf{x}) = \frac{1}{4\pi^2\nu\tau_i^2 D_i}\ker\Big(\sqrt{\frac{\omega}{D_i}}x\Big)\,. \tag{4.58}$$

Thus, the 2-Cooperon contribution as a function of the spatial variable $\mathbf{r}_\mathrm{m}$ takes the following form:

$$\tilde{\mathcal{C}}_2(\mathbf{r}_\mathrm{m};eV) = \frac{2L^4\bar{\tau}^2}{\pi^4 D_1 D_2}(eV)^2 \int_0^1 \mathrm{d}y\,(1-y)\mathrm{ker}\big(\frac{r_\mathrm{m}}{L_\mathrm{d1}}\sqrt{y}\big)\mathrm{ker}\big(\frac{r_\mathrm{m}}{L_\mathrm{d2}}\sqrt{y}\big)\,, \tag{4.59}$$

where $L_{\mathrm{d}i} = \sqrt{D_i/(eV)}$ is the diffusion length in layer i.

The two length scales L_d1 and L_d2 are typically of the same order of magnitude. Again the result can be expressed by the ratios of the different length scales. Therefore, the parameters $m_1 \equiv r_\mathrm{m}/L_\mathrm{d1}$ and $m_2 \equiv r_\mathrm{m}/L_\mathrm{d2}$ are introduced. In terms of these dimensionless variables, the 2-Cooperon contribution is given by the following expression:

$$\tilde{\mathcal{C}}_2(m_1,m_2;eV) = \frac{2L^4\nu^2(eV)^2}{\pi^2\epsilon_\mathrm{F}^2}\cdot\left(\frac{m_1 m_2}{m_1^2+m_2^2}\right)^2 \int_0^1 \mathrm{d}y\,(1-y)\mathrm{ker}\big(m_1\sqrt{y}\big)\mathrm{ker}\big(m_2\sqrt{y}\big)\,. \tag{4.60}$$

A plot of $\tilde{\mathcal{C}}_2(m_1,m_2)$ is shown in Fig. 4.14 and 4.15. In the special case of equal mean free times $\tau_1 = \tau_2 \equiv \tau$, the result takes the form

$$\tilde{\mathcal{C}}_2(m;eV) = \frac{L^4\nu^2(eV)^2}{2\pi^2\epsilon_\mathrm{F}^2}\int_0^1 \mathrm{d}y\,(1-y)\left(\mathrm{ker}(m\sqrt{y})\right)^2\,. \tag{4.61}$$

This function is plotted in Fig. 4.16. For $r_\mathrm{m} \to 0$ the result diverges. As mentioned before, this is due to the fact that in this case our approximations fail. The smallest distance that can be resolved is the mean free path l. At fixed r_m, the conductance fluctuations $\sim \tilde{\mathcal{C}}_2/(eV)^2$ diverge in the limit $eV \to 0$.

In conclusion, the average current shows qualitatively the same behavior as in the previous case, while different results have been obtained for the fluctuations. The dominant contributions to the fluctuations have been identified and it has been shown that they are much larger than for tunneling from a clean to a disordered 2DEG. This will be discussed in more detail in the following section.

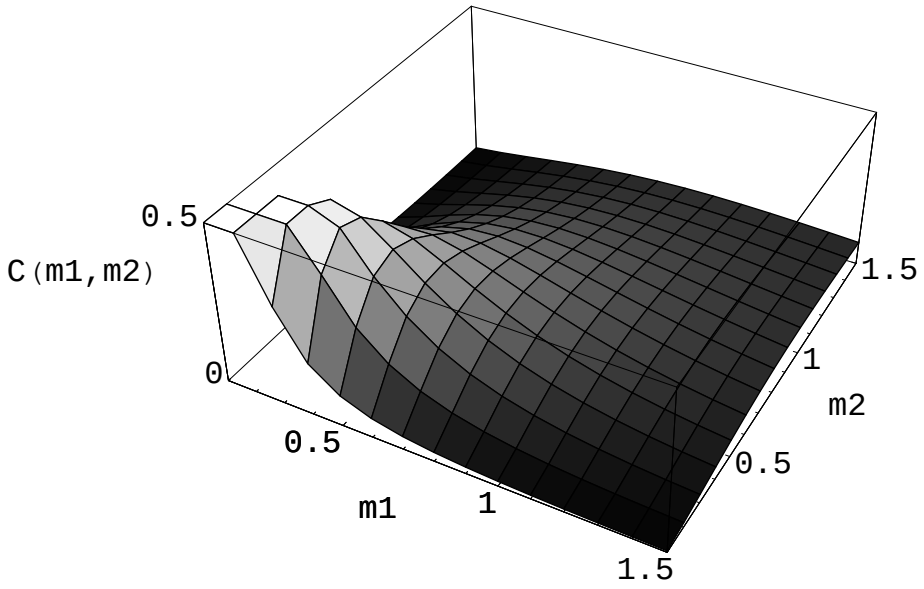

Figure 4.14: The dependence of the 2-Cooperon contribution on the ratios of r_{m} and the two diffusion lengths.

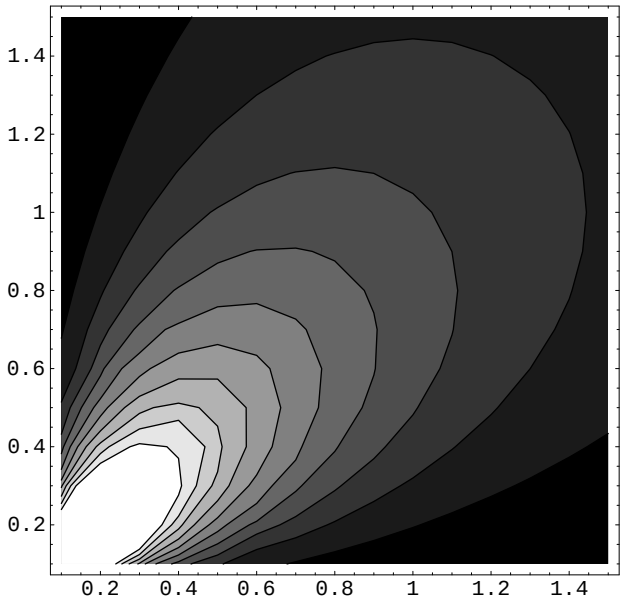

Figure 4.15: Contour plot corresponding to Fig. 4.14.

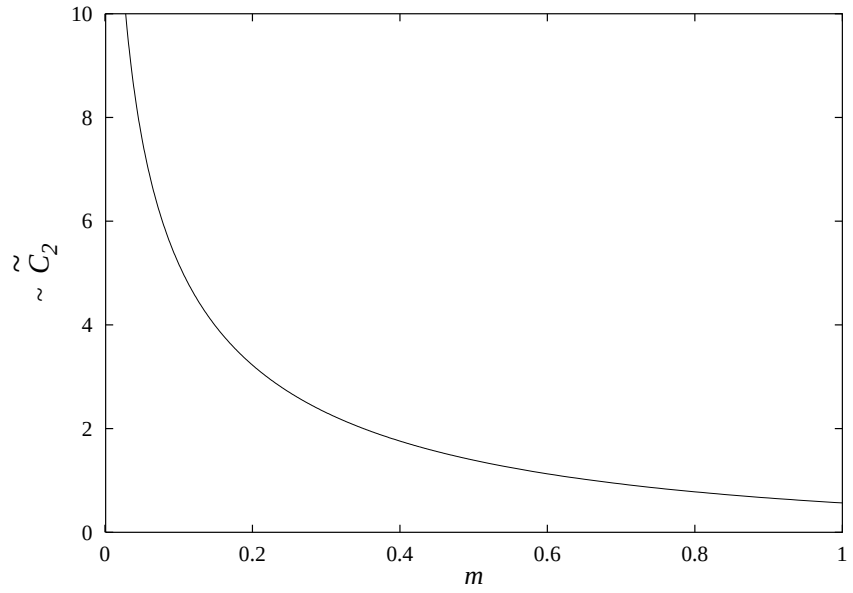

Figure 4.16: The 2-Cooperon contribution $\tilde{\mathcal{C}}_2(r_\mathrm{m}/L_\mathrm{d})$ for $\tau_1 = \tau_2$.

4.4 Comparison of the results

In the discussion of the results we will focus on two aspects, namely the magnitude of the tunneling current and its field dependence. In both cases the average current as well as the fluctuations will be considered.

Magnitude of the tunneling current at zero magnetic field

Concerning the averaged quantities, it is more convenient to discuss the conductance instead of the current. In the clean limit the average conductance diverges at zero magnetic field. This divergence is smeared out in the presence of disorder, leading to a finite peak height proportional to $\bar{\tau} = \tau_1\tau_2/(\tau_1 + \tau_2)$. Note that the scattering rates τ_i^{-1} of the 2DEGs are additive. If only one 2DEG is disordered, $\bar{\tau}$ equals the mean free time of that layer, whereas if the disorder has the same strength in both layers, $\bar{\tau}$ is just half of the individual mean free times. However, the qualitative behavior of the average current is the same for both cases.

In contrast, a qualitative difference has been found for the fluctuations. On a technical level, we first notice that there are more distinguishable contributions to $(\Delta I)^2$ when both layers are disordered. However, we have shown that, as in the case of one clean and one disordered 2DEG, there are only two *dominant* contributions, namely a diffuson and a Cooperon contribution. But these are not the corresponding diagrams in an expansion. That means, for tunneling from a

clean to a disordered 2DEG, the fluctuations are composed of contributions of the form $\langle G_1 G_1 \rangle_c G_2^o G_2^o$, containing one correlator and two single-particle Green's functions. The corresponding expressions in the case of two disordered 2DEGs are obtained by replacing the unperturbed Green's functions G_2^o with the impurity averaged Green's functions g_2. But, since the impurity averaged single-particle Green's functions are short-ranged, these terms are now suppressed. Thus, they are negligible against contributions of the form $\langle G_1 G_1 \rangle_c \langle G_2 G_2 \rangle_c$, containing two correlators. There is no analogue to these terms if only one layer is disordered. This is shown schematically in Fig. 4.17.

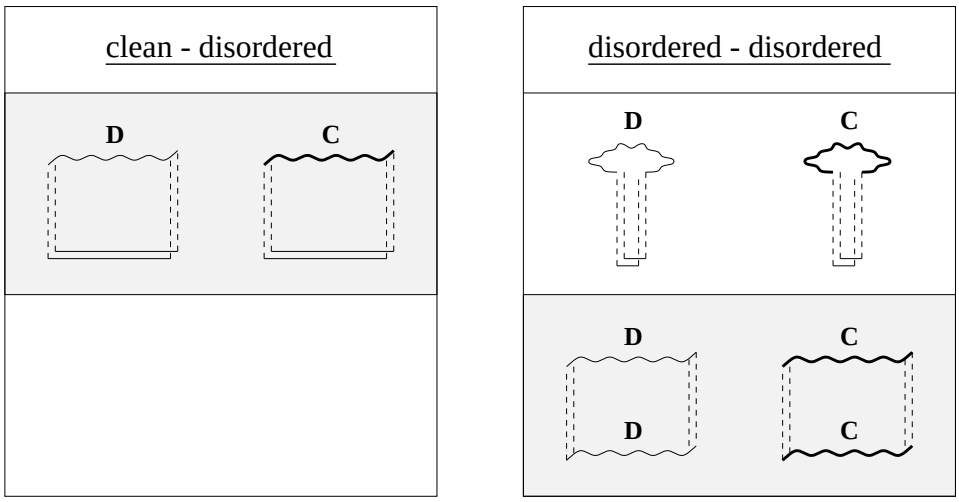

Figure 4.17: Diagrams contributing to the current fluctuations. Corresponding diagrams are drawn at the same level while the dominant diagrams are highlighted by a shaded box.

Comparing now the dominant contributions, one can get a rough estimate by counting powers of $\mathbf{q}$. The *slow* diffusive processes are characterized by the time scale $(Dq^2)^{-1}$ while the *fast* ballistic propagation within the clean layer is characterized by the time scale $(v_F q)^{-1}$. In the case of tunneling from a clean to a disordered layer, the integrand is proportional to q^{-3}, being composed of a fast (q^{-1}) and a slow (q^{-2}) process. By contrast, for tunneling between two disordered 2DEGs, the integrand is proportional to q^{-4} because it now contains two slow processes. In this case the available phase space is larger, *i.e.* more processes contribute to the fluctuations. The momentum integration compensates for two powers of q. Then, with $\omega \sim q^2$, the energy integral yields a finite result in the former case while for tunneling between two disordered 2DEGs a logarithmic divergence is left. Therefore, in the latter case one has to introduce a lower cut-off as discussed on p. 56. To go below that limit, a separate consideration of zero-modes would be necessary.

Field dependence of the tunneling current

We have seen that the suppression of the tunneling current due to the in-plane magnetic field is characterized by different length scales of the system. The relevant length scale for the average current is the mean free path l, *i.e.* the 'range' of the impurity averaged single-particle Green's function. If both 2DEGs are disordered, the scattering rates of the individual layers are additive which leads to a combined mean free path $\bar{l} \equiv l_1 l_2/(l_1+l_2)$. Since the mean free path is a small length scale, the corresponding characteristic field scale $B_{\rm c}^{(l)}$ is large.

The fluctuations are composed of two (dominant) contributions. At $B=0$ both terms, *i.e.* the diffuson and the Cooperon contribution, yield the same result, but they evolve differently when a weak in-plane magnetic field is applied. While the diffuson contribution is insensitive to the magnetic field, at least on the small field scales considered here, the Cooperon contribution is suppressed with increasing field. If only one 2DEG is disordered, this layer governs the field dependence. Thus, in the presence of a magnetic field the relevant length scale is the range of the Cooperon given by the diffusion length $L_{\rm d} = \sqrt{D/(eV)}$ for a given time interval $(eV)^{-1}$. The diffusion length being typically much larger than the mean free path, the fluctuations vary on a field scale $B_{\rm c}^{(L_{\rm d})} \ll B_{\rm c}^{(l)}$. This implies that one can study the current fluctuations over a region where the average current can still be regarded as constant. If both 2DEGs are disordered, one associates a diffusion length $L_{{\rm d}i}$ to each layer. The interplay of these two length scales can be studied best by analyzing the Fourier spectrum of the Cooperon contribution.

	clean - disordered	disordered - disordered
$\langle I \rangle$	l	$\bar{l} = l_1 l_2/(l_1+l_2)$
$(\Delta I)^2$	$L_{\rm d}$ (and $L_{\rm b}$)	$L_{\rm d1}$, $L_{\rm d2}$

Table 4.1: Relevant length scales for the field dependence of the average current and the current fluctuations.

The field dependent contribution to the current fluctuations has been shown to be a Fourier transform (with respect to the magnetic field) of the product of the correlation functions of the 2DEGs, *i.e.*

$$\tilde{\mathcal{C}}^{\omega}(\mathbf{r}_{\rm m}) \sim F^{(1)}(\mathbf{r}_{\rm m},\omega) \cdot F^{(2)}(\mathbf{r}_{\rm m},\omega)\,, \tag{4.62}$$

where $F^{(i)}$ is the two-particle correlation function within layer i.

For a disordered layer, the function $F_{\mathrm{d}}^{(i)}$ (d='diffusive') is given by the Fourier transform of the real part of the Cooperon, and the relevant length scale is the diffusion length L_{d}. By contrast, for a clean layer, $F_{\mathrm{b}}^{(i)}$ (b='ballistic') is the Fourier transform of the 'ballistic Cooperon', the relevant length scale being the ballistic length $L_{\mathrm{b}} = v_{\mathrm{F}}/(eV)$.

Thus, for tunneling from a clean to a disordered layer we have two length scales of different orders of magnitude: $L_{\mathrm{d}} \ll L_{\mathrm{b}}$. Hence, the behavior of $\tilde{\mathcal{C}}^{\omega}(\mathbf{r}_{\mathrm{m}})$ is dominated by F_{d} which has structure on the diffusive scale while F_{b} only varies on the much larger ballistic length scale. If both layers are disordered, however, the relevant length scales are of the same order of magnitude. Then $\tilde{\mathcal{C}}^{\omega}(\mathbf{r}_{\mathrm{m}})$ is equally influenced by both layers. Due to the product structure of $\tilde{\mathcal{C}}^{\omega}(\mathbf{r}_{\mathrm{m}})$, the contributions $F^{(i)}$ of the different layers can be analyzed independently as explained in the previous sections (cf. also Figs. 4.14 and 4.15).

Chapter 5

Summary

In the present work the tunneling current and conductance between two parallel two-dimensional electron gases (2DEGs) have been investigated theoretically. The main focus has been directed on the aspect of using the dependence of the tunneling current on a weak, in-plane magnetic field for 'tunneling spectroscopy'.

The tunneling current is described by an overlap integral of the spectral functions of the two layers. The interesting feature of the chosen setup is the possibility to control this overlap sensitively by tuning external parameters like the magnetic field. Thus, the analysis of the tunneling current allows one to extract far reaching information about the properties of the spectral functions or the corresponding Green's functions which characterize the microscopic physics of the system. Concerning the impurity averaged current, this has been extensively studied, both experimentally [22] and theoretically [23]. However, the additional information contained in the current fluctuations has not been exploited so far. While the average current probes the short-ranged impurity averaged Green's functions, the current fluctuations are governed by the long-ranged correlations. We have shown that the dependence of the current fluctuations on an in-plane magnetic field allows these correlations to be probed.

Chapter 4 is the central part of this work. As a basis for investigations on the current fluctuations, the average current is discussed. We concentrate on the case of uniform tunneling rates and uncorrelated disorder potentials. The overall shape of the I-B-characteristics finds a very intuitive explanation by the shift of the Fermi circles of the 2DEGs [22]. Tunneling only takes place at the overlap of the two circles because energy and momentum are conserved. In a clean system the conductance diverges at $B = 0$ as well as at $B = B_{\max}$ where the two circles decouple. These divergences are smeared out in the presence of disorder [23]. The characteristic magnetic field scale over which the average current is suppressed is determined by the mean free path l, namely $B_{\mathrm{c}}[\langle I \rangle] = \sqrt{2}(edl)^{-1}$. This reflects the fact that the 'range' of the impurity averaged Green's functions is given by

the mean free path. As this is a small length scale, the characteristic field for the average current is large. By contrast, the Green's function of a specific sample is long-ranged. As a result, the current fluctuations are much more sensitive to the magnetic field.

Two different setups have been studied, namely tunneling from a clean to a disordered 2DEG and tunneling between two disordered 2DEGs. In the case of tunneling between a clean and a disordered 2DEG, there are only two contributions to the current fluctuations $(\Delta I)^2$, namely the diffuson and the Cooperon contribution. The diffuson contribution is insensitive to the magnetic field whereas the Cooperon contribution is quickly suppressed with increasing field, the characteristic field scale $B_{\rm c}[(\Delta I)^2] = \sqrt{2}(ed\sqrt{D/eV})^{-1}$ being related to the diffusion length $L_{\rm d} = \sqrt{D/eV}$ for a given time interval $(eV)^{-1}$. The behavior is governed by the disordered 2DEG which sets the limit for the typical distance between the tunneling sites. Since the diffusion length is much larger than the mean free path, the field dependence of the current fluctuations can be studied in a regime where the average current $\langle I\rangle$ is almost constant. Due to the fact that only the Cooperon contribution depends on the magnetic field, the fluctuations cannot be completely suppressed on these field scales, but only be reduced to about half their zero-field value. (Note that on larger field scales $B \gtrsim B_{\rm c}[\langle I\rangle]$ the diffuson contribution will be influenced by the magnetic field, too.)

In the case of tunneling between two disordered 2DEGs, there are in principle five contributions to the current fluctuations, but it has been shown that the dominant processes are the 2-diffuson and 2-Cooperon contributions. However, these are not the same terms accounting for the fluctuations in a setup with only one disordered layer. Thus, the result is qualitatively different. A divergence at small energies is observed. Therefore, a cut-off at the Thouless energy has been introduced. Beyond that limit, the chosen perturbative approach is not reliable and a separate consideration of 'zero-modes' is necessary. The field dependence is now equally influenced by both layers, the relevant scales being the diffusion lengths $L_{\rm d1}$ and $L_{\rm d2}$ which are of the same order of magnitude typically.

In order to study the interplay of the different length scales, the Fourier spectrum, *i.e.* the dependence of the tunneling current on the conjugate length $r_{\rm m}$ which can be identified with the distance of the tunneling sites, has been considered. We have shown that the Fourier transform of the field dependent contribution to $(\Delta I)^2$ is given by the product of the correlation functions of the individual layers. This product structure allows the spatial correlations of the two layers to be investigated separately. Thus, the current fluctuations yield information about local transport properties of the 2DEGs. Assuming that the characteristics of one of the layers are known, this setup can be used as a spectroscope for the other layer.

Outlook

The appearance of singularities at low energies suggests that the phenomenon is non-perturbative. The study of this kind of effects requires also non-perturbative methods. Thus, we are planning to continue the investigations with field theoretical methods, *i.e.* a non-linear σ-model. Another aspect which has been left out so far are interlayer Coulomb interactions. The attraction of the tunneled electron and the hole it leaves behind leads to a correlation of the propagators within the different layers which influences the tunneling current. Therefore, this setup is suitable to study the interplay of disorder and Coulomb interactions. Furthermore, the assumption of spatially uniform tunneling has to be reconsidered. It has been found that by rotating the in-plane magnetic field, the spatial structure of tunneling may be investigated. A 2π-scan of the field yields information about the correlator of the tunneling amplitudes. Thus, a more realistic description of tunneling between 2DEGs which allows for these different aspects should be possible.

Appendix A

Green's functions

Consider a system of electrons described by a Hamiltonian H. At zero temperature the electron Green's function is defined as

$$G(\lambda, \lambda'; t - t') = -\mathrm{i} \left\langle \, | \mathrm{T}\, c_\lambda(t) c^\dagger_{\lambda'}(t') | \, \right\rangle , \tag{A.1}$$

where T is the time ordering operator,

$$\mathrm{T} c_\lambda(t) c^\dagger_{\lambda'}(t') = \begin{cases} c_\lambda(t) c^\dagger_{\lambda'}(t') & \text{for } t > t' \ , \\ -c^\dagger_{\lambda'}(t') c_\lambda(t) & \text{for } t < t' \ . \end{cases}$$

$| \, \rangle$ denotes the ground state with respect to H. $c^\dagger_\lambda, c_\lambda$ is a complete set of Fermi creation and annihilation operators, with λ being some quantum numbers depending on the problem of interest. (In the following we will adopt the usual choice $\lambda = (\mathbf{p})$, assuming spin degeneracy.) Eq. A.1 is defined in the Heisenberg representation, *i.e.*

$$c^{(\dagger)}_\lambda(t) = \mathrm{e}^{\mathrm{i}Ht} c^{(\dagger)}_\lambda \mathrm{e}^{-\mathrm{i}Ht}$$

while $| \, \rangle$ is time-independent.

At finite temperatures the so-called Matsubara formalism is used. The Matsubara Green's function is defined as

$$\mathcal{G}(\mathbf{p}, \mathbf{p}'; \tau - \tau') = - \left\langle \mathrm{T}_\tau \, c_{\mathbf{p}}(\tau) c^\dagger_{\mathbf{p}'}(\tau') \right\rangle .$$

The τ-ordering operator T_τ arranges the operators by increasing τ from right to left. The bracket $\langle ... \rangle$ denotes the thermodynamic average $\mathrm{Tr}(\mathrm{e}^{-\beta(H - \mu N - \Omega)} ...)$ with β inverse temperature, μ chemical potential, and N number of particles; the thermodynamic potential Ω is a normalization factor: $\mathrm{e}^{-\beta\Omega} = \mathrm{Tr}(\mathrm{e}^{-\beta(H - \mu N)})$. The τ-dependence of the operators is given by

$$c^{(\dagger)}_\lambda(\tau) = \mathrm{e}^{(H - \mu N)\tau} c^{(\dagger)}_\lambda \mathrm{e}^{-(H - \mu N)\tau} \ .$$

Since $\mathcal{G}$ is a function of $\Delta\tau$ only, we can also write

$$\mathcal{G}(\mathbf{p},\mathbf{p}';\tau) = -\left\langle \mathrm{T}_\tau\, c_{\mathbf{p}}(\tau) c^\dagger_{\mathbf{p}'}(0)\right\rangle . \tag{A.2}$$

$\mathcal{G}$ can be expanded in a Fourier series:

$$\begin{aligned} \mathcal{G}(\mathbf{p},\mathbf{p}';\mathrm{i}\omega_n) &= \int_0^\beta \mathrm{d}\tau\, \mathrm{e}^{\mathrm{i}\omega_n\tau}\mathcal{G}(\mathbf{p},\mathbf{p}';\tau) \\ \mathcal{G}(\mathbf{p},\mathbf{p}';\tau) &= \frac{1}{\beta}\sum_n \mathrm{e}^{-\mathrm{i}\omega_n\tau}\mathcal{G}(\mathbf{p},\mathbf{p}';\mathrm{i}\omega_n) \end{aligned} \tag{A.3}$$

with the fermion frequencies $\omega_n = (2n+1)\pi/\beta$.

Finally, we come to the retarded $(+)$ and advanced $(-)$ Green's functions which are the quantities of physical interest. They can be obtained from the Matsubara Green's function by analytic continuation, *i.e.*

$$G^\pm(\mathbf{p},\mathbf{p}';\epsilon) = \underset{\mathrm{i}\omega_n\to\epsilon\pm\mathrm{i}\delta}{\text{change}}\ \mathcal{G}(\mathbf{p},\mathbf{p}';\mathrm{i}\omega_n) . \tag{A.4}$$

The advanced function G^- is the complex conjugate of the retarded function G^+. Thus we can define the spectral function $A(\mathbf{p},\mathbf{p}';\epsilon)$:

$$A(\mathbf{p},\mathbf{p}';\epsilon) = \mathrm{i}[G^+(\mathbf{p},\mathbf{p}';\epsilon) - G^-(\mathbf{p},\mathbf{p}';\epsilon)] = -2\,\mathrm{Im}\,G^+(\mathbf{p},\mathbf{p}';\epsilon) . \tag{A.5}$$

For a more detailed review see *e.g.* [44]. The explicit Green's functions needed in this work are presented in section 3.3.

Appendix B

Details of calculations and results of chapter 4

B.1 Tunneling from a clean to a disordered 2DEG

B.1.1 Complete formula for the average current

In section 4.2.1 we derived the average current for tunneling between a clean and a disordered 2DEG.

The remaining integral in Eq. 4.12 has the form $J = \int_0^{2\pi} d\varphi \frac{1}{(\cos\varphi - b)^2 + c^2}$, giving the result

$$J = \sqrt{2}\,\pi \frac{1}{\sqrt{C + \sqrt{DE}}} \left(\frac{1}{\sqrt{D}} + \frac{1}{\sqrt{E}} \right) ,$$

where $C = c^2 + b^2 - 1$,
$D = c^2 + (b-1)^2$, and
$E = c^2 + (b+1)^2$.

This finally leads to the following expression for the average tunneling current:

$$\frac{\langle I \rangle}{I_o} = \frac{eV}{\sqrt{2}\tau} \left(\frac{1}{\sqrt{\frac{1}{4\tau^2} + (eAv_F + \frac{(eA)^2}{2m} + eV)^2}} + \frac{1}{\sqrt{\frac{1}{4\tau^2} + (eAv_F - \frac{(eA)^2}{2m} - eV)^2}} \right) \tag{B.1}$$

$$\times \left(\sqrt{\frac{1}{4\tau^2} + (eAv_F + \frac{(eA)^2}{2m} + eV)^2} \sqrt{\frac{1}{4\tau^2} + (eAv_F - \frac{(eA)^2}{2m} - eV)^2} + \frac{1}{4\tau^2} + (\frac{(eA)^2}{2m} + eV)^2 - (eA)^2 v_F^2 \right)^{-\frac{1}{2}}$$

$$= 4\sqrt{2}\, t_F g \left(\frac{1}{\sqrt{1 + 16g^2(x(1+x) + t_F)^2}} + \frac{1}{\sqrt{1 + 16g^2(x(1-x) - t_F)^2}} \right) \tag{B.2}$$

$$\times \left(\sqrt{1+16g^2(x(1+x)+t_F)^2} \sqrt{1+16g^2(x(1-x)-t_F)^2} + 1 + 16g^2(x^2 + t_F)^2 - 16g^2x^2 \right)^{-\frac{1}{2}} .$$

Then the result for the zero-bias dimensionless conductance is

$$\begin{aligned}\bar{\mathrm{g}} &= \sqrt{2}g\,(\frac{1}{\sqrt{1+16g^2x^2(1+x)^2}}+\frac{1}{\sqrt{1+16g^2x^2(1-x)^2}}) \\ &\times\left(\sqrt{1+16g^2x^2(1+x)^2}\sqrt{1+16g^2x^2(1-x)^2}+1-16g^2x^2(1-x^2)\right)^{-\frac{1}{2}}\,.\end{aligned} \tag{B.3}$$

The asymptotic behavior of this formula for small magnetic fields is discussed in section 4.2.1.

B.1.2 The fluctuations

The diffuson

Starting from Eq. 4.20,

$$\begin{aligned}\mathcal{D} &= \sum_{\mathbf{k};\mathbf{q}}\int(\mathrm{d}\epsilon^{[eV]})(\mathrm{d}\epsilon'^{[eV]})A_2^{\mathrm{o}}(\mathbf{k};\epsilon+eV)A_2^{\mathrm{o}}(\mathbf{k}-\mathbf{q};\epsilon'+eV) \\ &\times\sum_{\sigma\neq\sigma'}\left[g_1^{\sigma}(\mathbf{K},\epsilon;\tau)g_1^{\sigma'}(\mathbf{K}-\mathbf{q},\epsilon';\tau)\right]^2\mathrm{D}^{\sigma\sigma'}(\mathbf{q},\omega)\,,\end{aligned}$$

first, the k-integral (continuum limit) is evaluated. With the spectral functions A_2^{o} being δ-distributions, this can easily be done, using the approximation $\xi_{\mathbf{k}-\Delta\mathbf{k}}\approx\xi_{\mathbf{k}}-v_{\mathrm{F}}\Delta k\cos\varphi$, *i.e.*

$$\begin{aligned}\mathcal{D} &= \pi L^2\nu\sum_{\mathbf{q}}\int(\mathrm{d}\epsilon^{[eV]})(\mathrm{d}\epsilon'^{[eV]})\int_o^{2\pi}\mathrm{d}\varphi\,\delta(-v_{\mathrm{F}}q\cos\varphi+\omega) \\ &\times\sum_{\sigma\neq\sigma'}\frac{1}{\left(-eV+ev_{\mathrm{F}}A\cos\varphi+(\sigma)\frac{\mathrm{i}}{2\tau}\right)^2}\frac{1}{\left(-eV+v_{\mathrm{F}}|e\mathbf{A}+\mathbf{q}|\cos\varphi+(\sigma')\frac{\mathrm{i}}{2\tau}\right)^2}\mathrm{D}^{\sigma\sigma'}(\mathbf{q},\omega)\,.\end{aligned} \tag{B.4}$$

For $eV\ll\tau^{-1}$, $B\ll B_{\mathrm{c}}^{(l)}$ which is the most interesting region, the terms coming from the outer Green's functions just contribute a factor $-(\sigma)\mathrm{i}2\tau$ each. This leads to the following expression

$$\mathcal{D}=16\pi L^2\nu\tau^4\sum_{\mathbf{q}}\int(\mathrm{d}\epsilon^{[eV]})(\mathrm{d}\epsilon'^{[eV]})\,2\mathrm{Re}\left[\mathrm{D}(\mathbf{q},\omega)\right]\int_0^{2\pi}\mathrm{d}\varphi\,\delta(\omega-v_{\mathrm{F}}q\cos\varphi)\,. \tag{B.5}$$

Integrating out the angles with the help of the δ-distribution which causes a restriction of the $\mathbf{q}$-summation, and eliminating one energy integral, we get Eq. 4.22:

$$\mathcal{D}=\frac{8\tau^2}{\pi^2}\int_0^{eV}\mathrm{d}\omega\,(eV-\omega)\sum_{|\mathbf{q}|>\frac{\omega}{v_{\mathrm{F}}}}\frac{1}{\sqrt{v_{\mathrm{F}}^2q^2-\omega^2}}\frac{2Dq^2}{D^2q^4+\omega^2}\,. \tag{B.6}$$

In the continuum limit, the q-integral can be solved by means of the substitution $x = \sqrt{q^2 - (\omega/v_\mathrm{F})^2}$. Thus,

$$\int\limits_{q>\frac{\omega}{v_\mathrm{F}}} (\mathrm{d}q) \frac{1}{\sqrt{v_\mathrm{F}^2 q^2 - \omega^2}} \frac{2Dq^2}{D^2 q^4 + \omega^2} = \frac{L^2}{2\sqrt{2D\omega}} \frac{\sqrt{\sqrt{D^2\omega^2 + v_\mathrm{F}^4} + D\omega}}{\sqrt{D^2\omega^2 + v_\mathrm{F}^4}} \qquad \text{(B.7)}$$

$$\simeq \frac{L^2}{2v_\mathrm{F}\sqrt{2D\omega}} \qquad \text{for } \omega \ll \tau^{-1}\,.$$

Inserting this into Eq. B.6 leads to the result (4.23).

The Cooperon

Following the same lines as for the diffuson, we obtain Eq. 4.26:

$$\mathcal{C} = \frac{8\tau^2}{\pi^2} \int\limits_0^{eV} \mathrm{d}\omega\,(eV - \omega) \sum_{|\mathbf{Q}|>\frac{\omega}{v_\mathrm{F}}} \frac{1}{\sqrt{v_\mathrm{F}^2 Q^2 - \omega^2}} \frac{2D(\mathbf{Q} - 2e\mathbf{A})^2}{D^2(\mathbf{Q} - 2e\mathbf{A})^4 + \omega^2}\,. \qquad \text{(B.8)}$$

As explained in section 4.2.2, starting from there, two strategies may be applied.

1. $\underline{\mathcal{C}(2e\mathbf{A}; eV)}$

To evaluate the Q-integral, we have to neglect ω against $v_\mathrm{F}Q$. In the case of the diffuson contribution it has been pointed out that this approximation is valid for $eV \ll \tau^{-1}$. With the substitution $Q' = Q - 2eA\cos\varphi$, this leads to

$$\mathcal{C}(2e\mathbf{A}; eV) = \frac{8L^2\tau^2}{\pi^3 v_\mathrm{F} D} \int\limits_0^{2\pi} \frac{\mathrm{d}\varphi}{2\pi} \int\limits_0^{eV} \mathrm{d}\omega\,(eV - \omega) \int \mathrm{d}Q' \frac{(Q'^2 + 4(eA)^2\sin^2\varphi)}{(Q'^2 + 4(eA)^2\sin^2\varphi)^2 + (\frac{\omega}{D})^2}$$

$$= \frac{4L^2\tau^2}{\sqrt{2}\pi^2 v_\mathrm{F} D} \int\limits_0^{2\pi} \frac{\mathrm{d}\varphi}{2\pi} \int\limits_0^{eV} \mathrm{d}\omega\,(eV - \omega) \frac{\sqrt{\sqrt{16(eA)^4\sin^4\varphi + (\frac{\omega}{D})^2} + 4(eA)^2\sin^2\varphi}}{\sqrt{16(eA)^4\sin^4\varphi + (\frac{\omega}{D})^2}}\,.$$

In the next step the energy integration can be carried out, using the substitution $u = \sqrt{16D^2(eA)^4\sin^4\varphi + \omega^2}$, which leads to the result (4.27).

2. $\underline{\mathcal{C}(\mathbf{r}_\mathrm{m}; eV)}$

Since the Q-integral in Eq. B.8 is a convolution integral, the Fourier transform of the Cooperon contribution has a simpler form:

$$\tilde{\mathcal{C}}(\mathbf{r}_\mathrm{m}; eV) = \frac{32L^2\nu\tau^4}{\pi} \int\limits_0^{eV} \mathrm{d}\omega\,(eV - \omega) F_\mathrm{b}(\mathbf{r}_\mathrm{m}; \omega) \cdot F_\mathrm{d}(\mathbf{r}_\mathrm{m}; \omega)\,, \qquad \text{(B.9)}$$

where $F_\mathrm{b}(\mathbf{r}_\mathrm{m}; \omega) = \mathrm{FT}\left\{(v_\mathrm{F}^2 Q^2 - \omega^2)^{-1/2}\right\}$, and $F_\mathrm{d}(\mathbf{r}_\mathrm{m}; \omega) = \mathrm{FT}\left\{\mathrm{Re}\left[\mathrm{C}(\mathbf{Q}, \omega)\right]\right\}$.

These Fourier transforms are calculated as follows:

- in the ballistic case (see Gradshteyn [54], 6.554 (3.)),

$$\begin{aligned}
\mathrm{FT}\left\{(v_\mathrm{F}^2Q^2-\omega^2)^{-1/2}\right\} &= \frac{L^2}{4\pi^2}\int_0^{2\pi}\mathrm{d}\varphi\int_{\omega/v_\mathrm{F}}^{\infty}Q\mathrm{d}Q\,\frac{1}{\sqrt{v_\mathrm{F}^2Q^2-\omega^2}}\,e^{iQr\cos\varphi}\\
&= \frac{L^2\omega}{2\pi v_\mathrm{F}^2}\int_1^{\infty}\mathrm{d}q\,\frac{q}{\sqrt{q^2-1}}\,J_o(\frac{\omega r}{v_\mathrm{F}}q)\\
&= \frac{L^2}{2\pi v_\mathrm{F}r}\cos\frac{\omega r}{v_\mathrm{F}} \qquad \xrightarrow[\omega\to 0]{} \qquad \frac{L^2}{2\pi v_\mathrm{F}r}\,,
\end{aligned}$$

- and in the diffusive case (see Gradshteyn [54], 6.536),

$$\begin{aligned}
\mathrm{FT}\left\{\mathrm{Re}\left[\mathrm{C}(\mathbf{Q},\omega)\right]\right\} &= \frac{1}{8\pi^3\nu\tau^2}\int_0^{2\pi}\mathrm{d}\varphi\int_0^{\infty}Q\mathrm{d}Q\,\frac{DQ^2}{D^2Q^4+\omega^2}\,e^{iQr\cos\varphi}\\
&= \frac{1}{4\pi^2\nu\tau^2D}\int_0^{\infty}\mathrm{d}Q\,\frac{Q^3}{Q^4+(\frac{\omega}{D})^2}J_o(rQ)\\
&= \frac{1}{4\pi^2\nu\tau^2D}\mathrm{Re}\big[K_\mathrm{o}(\sqrt{\frac{\mathrm{i}\omega}{D}}r)\big] = \frac{1}{4\pi^2\nu\tau^2D}\mathrm{ker}\big(\sqrt{\frac{\omega}{D}}r\big)\,.
\end{aligned}$$

Inserting these functions into the expression for $\tilde{\mathcal{C}}$ (Eq. B.9), the final result is

$$\tilde{\mathcal{C}}(\mathbf{r}_\mathrm{m};eV) = \frac{4L^4\tau^2}{\pi^4Dv_\mathrm{F}}\int_0^{eV}\mathrm{d}\omega\,(eV-\omega)\,\frac{1}{r_\mathrm{m}}\cos\frac{\omega r_\mathrm{m}}{v_\mathrm{F}}\mathrm{ker}\big(\sqrt{\frac{\omega}{D}}r_\mathrm{m}\big)\,. \tag{B.10}$$

Rewriting this in terms of the ballistic and diffusion lengths, L_b and L_d, respectively, yields

$$\tilde{\mathcal{C}}(\mathbf{r}_\mathrm{m};eV) = \frac{4L^4\tau^2(eV)^2}{\pi^4D^2}\int_0^{1}\mathrm{d}y(1-y)\frac{L_\mathrm{d}^2}{L_\mathrm{b}r_\mathrm{m}}\cos\big(\frac{r_\mathrm{m}}{L_\mathrm{b}}y\big)\mathrm{ker}\big(\frac{r_\mathrm{m}}{L_\mathrm{d}}\sqrt{y}\big) \tag{B.11}$$

with $y=\omega/(eV)$.

B.2 Tunneling between two disordered 2DEGs

B.2.1 Evaluation of the average current

Again the starting point is Eq. 4.3:

$$\langle I\rangle = 2e\,|T|^2 \sum_{\mathbf{k}} \int (\mathrm{d}\epsilon^{[eV]}) a_1(\mathbf{k}-e\mathbf{A},\epsilon;\tau_1) a_2(\mathbf{k},\epsilon+eV;\tau_2)\,.$$

Without the δ-distribution from the clean layer, the energy integral has to be evaluated by contour integration. Splitting the spectral functions into Green's functions ($a_i = \mathrm{i}(g_i^+ - g_i^-)$), we get four terms, but only the cross terms $g_1^+ g_2^-$ ($g_1^- g_2^+$) contribute to the integral, *i.e.*

$$\langle I\rangle = 2e\,|T|^2 \sum_{\mathbf{k}} \int (\mathrm{d}\epsilon^{[eV]}) \left[g_1^+(\mathbf{k}-e\mathbf{A},\epsilon) g_2^-(\mathbf{k},\epsilon+eV) + g_1^+(\mathbf{k}-e\mathbf{A},\epsilon) g_2^-(\mathbf{k},\epsilon+eV)\right]\,. \tag{B.12}$$

As the Green's functions are strongly peaked around the Fermi circle, the identification $|\,\mathbf{k}\,| = k_F$ is a good approximation. Then the integral over the real axis can be closed at infinity and the result of the integration over the complex half-plane is given by the Cauchy formula. Thus,

$$\langle I\rangle = 2e^2 V\,|T|^2\, L^2 \nu \frac{\tau_1+\tau_2}{\tau_1\tau_2} \int_0^{2\pi} \frac{\mathrm{d}\varphi}{2\pi} \frac{1}{(eAv_F\cos\varphi - \frac{(eA)^2}{2m})^2 + \frac{(\tau_1+\tau_2)^2}{4\tau_1^2\tau_2^2}}\,.$$

For the final result see Eq. B.1 or B.2 with τ replaced by $\bar{\tau} \equiv \tau_1\tau_2/(\tau_1+\tau_2)$.

B.2.2 The fluctuations

$\mathcal{D}_1$ and $\mathcal{C}_1$

The calculation is presented for a diffuson in layer 1: $\mathcal{D}_1^\omega(1)$. As indicated in section 4.3.2, the Cooperon contribution gives the same result. The contribution for a diffuson (Cooperon) in layer 2 can easily be obtained by exchanging τ_1 and τ_2 (as well as D_1 and D_2, of course).

Neglecting the energy differences as well as the field dependence of the outer Green's functions, too (see section 4.2.2), Eq. 4.42 takes the form

$$\mathcal{D}_1^\omega(1) = \int (\mathrm{d}k)[g_1^+(\mathbf{k}) g_1^-(\mathbf{k}) a_2(\mathbf{k})]^2 \cdot \int (\mathrm{d}q) 2\mathrm{Re}\left[\mathrm{D}(\mathbf{q},\omega;\tau_1)\right]\,. \tag{B.13}$$

The two integrals can be evaluated separately. For the k-integral we use the relation $a_i = g_i^+ g_i^- / \tau_i$. Hence,

$$\begin{aligned}\int (\mathrm{d}k)[g_1^+(\mathbf{k})g_1^-(\mathbf{k})a_2(\mathbf{k})]^2 &= \frac{L^2\nu}{2\tau_2^2}\int \mathrm{d}\xi_{\mathbf{k}}[g_1^+(\mathbf{k})g_1^-(\mathbf{k})g_2^+(\mathbf{k})g_2^-(\mathbf{k})]^2 \\ &= \frac{\mathrm{i}\pi L^2\nu}{\tau_2^2}\left[\frac{\partial}{\partial\xi_{\mathbf{k}}}(g_1^- g_2^+ g_2^-)^2|_{\xi_{\mathbf{k}}=\epsilon+\frac{\mathrm{i}}{2\tau_1}} + \ (1\leftrightarrow 2)\ \right] \\ &= 16\pi L^2\nu\frac{\tau_1^4\tau_2^2}{(\tau_1+\tau_2)^3}(\tau_1^2+3\tau_1\tau_2+\tau_2^2)\,.\end{aligned}$$

The q-integral has to be cut off at $q_{\max}^2 = (D_1\tau_1)^{-1} \sim l_1^{-2}$, giving

$$\begin{aligned}\int (\mathrm{d}q)\,2\mathrm{Re}[\mathrm{D}(\mathbf{q},\omega;\tau_1)] &= \frac{1}{4\pi^2\nu\tau_1^2}\int \mathrm{d}(q^2)\frac{D_1 q^2}{D_1^2 q^4+\omega^2} \\ &= \frac{1}{8\pi^2\nu D_1\tau_1^2}\ln(1+\frac{1}{(\omega\tau_1)^2})\,. \qquad \text{(B.14)}\end{aligned}$$

Combining this:

$$\mathcal{D}_1{}^{\omega}(1) = \frac{2L^2}{\pi D_1}\frac{\tau_1^2\tau_2^2}{(\tau_1+\tau_2)^3}(\tau_1^2+3\tau_1\tau_2+\tau_2^2)\ln(1+\frac{1}{(\omega\tau_1)^2})\,.$$

Collecting all the contributions, after energy integration, this leads to the result (for $\tau_1 = \tau_2 \equiv \tau$)

$$\begin{aligned}(\Delta I)_1{}^2 &= \langle I(B{=}0)\rangle^2\cdot\left(\frac{l}{L}\right)^2\frac{5}{2\pi(k_{\mathrm{F}}l)^2} \qquad \text{(B.15)} \\ &\quad\times\left(\frac{4}{eV\tau}\arctan(eV\tau)+\ln(1+\frac{1}{(eV\tau)^2})-\frac{1}{(eV\tau)^2}\ln(1+(eV\tau)^2)\right) \\ &\approx -\langle I(B{=}0)\rangle^2\cdot\left(\frac{l}{L}\right)^2\frac{5}{\pi(k_{\mathrm{F}}l)^2}\ln(eV\tau)\,. \qquad \text{(B.16)}\end{aligned}$$

The 2-diffuson contribution: $\mathcal{D}_2$

To get this contribution, Eq. 4.51 has to be evaluated, *i.e.*

$$\mathcal{D}_2^{\omega} = 4\sum_{\mathbf{q}}\mathrm{Re}\left[\mathrm{D}(\mathbf{q},\omega;\tau_1)\right]\mathrm{Re}\left[\mathrm{D}(\mathbf{q},\omega;\tau_2)\right]\cdot\left\{\int(\mathrm{d}k)\,g_1^+(\mathbf{k})g_1^-(\mathbf{k})g_2^+(\mathbf{k})g_2^-(\mathbf{k})\right\}^2. \qquad \text{(B.17)}$$

The k-integral gives

$$\int(\mathrm{d}k)g_1^+(\mathbf{k})g_1^-(\mathbf{k})g_2^+(\mathbf{k})g_2^-(\mathbf{k}) = 4\pi\nu L^2\frac{\tau_1^2\tau_2^2}{\tau_1+\tau_2}\,.$$

From the q-integral, *i.e.* the diffusons, we get

$$\begin{aligned}
&\int(\mathrm{d}q)\,2\mathrm{Re}[\mathrm{D}(\mathbf{q},\omega;\tau_1)]\,2\mathrm{Re}[\mathrm{D}(\mathbf{q},\omega;\tau_2)] \\
= \;& \frac{1}{4\pi^3\nu^2L^2\tau_1^2\tau_2^2}\int \mathrm{d}(q^2)\frac{D_1q^2}{D_1^2q^4+\omega^2}\frac{D_2q^2}{D_2^2q^4+\omega^2} \\
= \;& \frac{1}{8\pi^2\nu^2L^2(D_1+D_2)\tau_1^2\tau_2^2\omega}\,.
\end{aligned}$$

This leads to the result (4.52).

The 2-Cooperon contribution: $\mathcal{C}_2$

Similar to the case in section 4.2.2, the Cooperon contribution can be written as a convolution integral, *i.e.*

$$\mathcal{C}_2(2e\mathbf{A};eV) = 32L^4\nu^2(\tau_1\tau_2\bar{\tau})^2\int_0^{eV}\mathrm{d}\omega\,(eV-\omega)\,(\mathrm{Re}[\mathrm{C}^{\tau_1}]*\mathrm{Re}[\mathrm{C}^{\tau_2}])(2e\mathbf{A})\,. \quad \text{(B.18)}$$

Then its Fourier transform has the following form:

$$\tilde{\mathcal{C}}_2(\mathbf{r}_\mathrm{m};eV) = 32L^4\nu^2(\tau_1\tau_2\bar{\tau})^2\int_0^{eV}\mathrm{d}\omega\,(eV-\omega)\,F_{\mathrm{d}1}(\mathbf{r}_\mathrm{m};\omega)\cdot F_{\mathrm{d}2}(\mathbf{r}_\mathrm{m};\omega)\,, \quad \text{(B.19)}$$

where $F_{\mathrm{d}i} = \mathrm{FT}\,\{\mathrm{Re}[\mathrm{C}^{\tau_i}]\}$. These functions are given by Eq. 4.58, leading to the result

$$\tilde{\mathcal{C}}_2(\mathbf{r}_\mathrm{m};eV) = \frac{2L^4\bar{\tau}^2}{\pi^4D_1D_2}\int_0^{eV}\mathrm{d}\omega\,(eV-\omega)\,\mathrm{ker}\Big(\sqrt{\frac{\omega}{D_1}}r_\mathrm{m}\Big)\mathrm{ker}\Big(\sqrt{\frac{\omega}{D_2}}r_\mathrm{m}\Big)\,. \quad \text{(B.20)}$$

For further discussion see section 4.3.2.

Bibliography

[1] L. Esaki, Phys. Rev. **109**, 603 (1958).

[2] M. Cohen, L. Falicov, and J. Phillips, Phys. Rev. Lett. **8**, 316 (1962).

[3] L. Chang, L. Esaki, and R. Tsu, Appl. Phys. Lett. **24**, 593 (1974).

[4] C. Beenakker and H. van Houten, in *Solid state physics*, edited by H. Ehrenreich and D. Turnbull (Academic Press, Inc., San Diego, 1991).

[5] J. Smoliner, E. Gornik, and G. Weimann, Appl. Phys. Lett. **52**, 2136 (1988).

[6] N. van Kampen, *Stochastic processes in physics and chemistry* (North-Holland, Amsterdam, 1981).

[7] Y. Imry, in *Directions in condensed matter physics*, edited by G. Grinstein and G. Mazenko (World Scientific, Singapore, 1986).

[8] *Quantum chaos: between order and disorder*, edited by G. Casati and B. Chirikov (Cambridge University Press, Cambridge, 1995).

[9] G. Bergmann, Phys. Rep. **107**, 2 (1984).

[10] S. Washburn and R. Webb, Rep. Prog Phys. **55**, 1311 (1992).

[11] U. Aharonov and D. Bohm, Phys. Rev. **115**, 485 (1959).

[12] H. Stoermer *et al.*, J. Vac. Sci. and Technol. **16**, 1517 (1979).

[13] K. von Klitzing, G. Dorda, and M. Pepper, Phys. Rev. Lett. **45**, 494 (1980).

[14] A. Palevski *et al.*, Phys. Rev. Lett. **65**, 1929 (1990).

[15] G. Boebinger, A. Passner, L. Pfeiffer, and K. West, Phys. Rev. B **43**, 12673 (1991).

[16] A. Kurobe *et al.*, Phys. Rev. B **50**, 4889 (1994).

[17] Y. Berk *et al.*, Phys. Rev. B **51**, 2604 (1995).

[18] J. Eisenstein, L. Pfeiffer, and K. West, Appl. Phys. Lett. **57**, 2324 (1990).

[19] W. Demmerle *et al.*, Phys. Rev. B **44**, 3090 (1991).

[20] J. Simmons *et al.*, Phys. Rev. B **47**, 15741 (1993).

[21] K. Brown *et al.*, Appl. Phys. Lett. **64**, 1827 (1994).

[22] J. Eisenstein, T. Gramila, L. Pfeiffer, and K. West, Phys. Rev. B **44**, 6511 (1991).

[23] L. Zheng and A. MacDonald, Phys. Rev. B **47**, 10619 (1993).

[24] S. Murphy, J. Eisenstein, L. Pfeiffer, and K. West, Phys. Rev. B **52**, 14825 (1995).

[25] T. Jungwirth and A. MacDonald, Phys. Rev. B **53**, 7403 (1996).

[26] A. Altland, C. Barnes, F. Hekking, and A. Schofield, unpublished.

[27] M. Kelly, *Low-dimensional semiconductors: Materials, physics, technology, devices* (Clarendon Press, Oxford, 1995).

[28] G. Weimann and W. Schlapp, Appl. Phys. Lett. **46**, 411 (1985).

[29] J. Smoliner *et al.*, Phys. Rev. Lett. **63**, 2116 (1989).

[30] A. Zaslavsky *et al.*, Phys. Rev. B **42**, 1374 (1990).

[31] N. Turner *et al.*, cond-mat/9503040.

[32] L. Zheng and S. Das Sarma, Phys. Rev. B **53**, 9964 (1996).

[33] L. Levitov, private communications.

[34] Y. Berk *et al.*, Phys. Rev. B **50**, 15420 (1995).

[35] J. Simmons, S. Lyo, N. Harff, and J. Klem, Phys. Rev. Lett. **73**, 2256 (1994).

[36] S. Stoddart *et al.*, Physica B **256-258**, 413 (1998).

[37] M. Pogrebinskii, Sov. Phys. Semicond. **11**, 372 (1977).

[38] P. Price, Physica B **117**, 750 (1983).

[39] T. Gramila *et al.*, Phys. Rev. Lett. **66**, 1216 (1991).

[40] A.-P. Jauho and H. Smith, Phys. Rev. B **47**, 4420 (1993).

[41] L. Zheng and A. MacDonald, Phys. Rev. B **48**, 8203 (1993).

[42] A. Kamenev and Y. Oreg, Phys. Rev. B **52**, 7516 (1995).

[43] I. Gornyi, A. Yashenkin, and D. Khveshchenko, cond-mat/9901098.

[44] G. Mahan, *Many-Particle Physics* (Plenum Press, New York and London, 1981).

[45] D. Rogovin and D. Scalapino, Ann. Phys. **86**, 1 (1974).

[46] B. Josephson, Phys. Lett. **1**, 251 (1962).

[47] J. Schrieffer, D. Scalapino, and J. Wilkins, Phys. Rev. Lett. **10**, 336 (1963).

[48] S. Edwards, Phil. Mag. **3**, 1020 (1958).

[49] P. Anderson, Phys. Rev. **109**, 1492 (1958).

[50] A. Abrikosov, L. Gorkov, and I. Dzyaloshinskii, *Methods of quantum field theory in statistical physics* (Prentice-Hall, Inc., Englewood Cliffs, N.J., 1963).

[51] J. Langer and T. Neal, Phys. Rev. Lett. **16**, 984 (1966).

[52] S. Levitov and A. Shytov, cond-mat/9507058.

[53] S. Lyo and J. Simmons, J. Phys. Cond. Matt. **5**, L299 (1993).

[54] I. Gradshteyn and I. Ryzhik, *Table of integrals, series, and products* (Academic Press, New York and London, 1965).

Danksagung

In diesem ganzen Jahr haben viele Leute in irgendeiner Weise zum Gelingen meiner Arbeit beigetragen. Ich danke all denjenigen, die mich unterstützt haben, insbesondere

- Dr. Martin Janßen und Prof. Alexander Altland für den Themenvorschlag sowie die gute Betreuung, hilfreiche Diskussionen und viele Anregungen,
- Prof. János Hajdu dafür, daß er mir die Arbeit in seiner Gruppe ermöglicht hat,
- meinen „Mitbewohnern“ in Zimmer 126, Rainer Merkt und Frank Pfeiffer, für die angenehme Arbeitsatmosphäre,
- Christian Dziurzik, Dagmar Klasen, Rainer Merkt, meiner Mutter, Olaf Petersen, Bert Reinold, Ludger Santen, Prof. Terry Sloan und Ute Zimmermann dafür, daß sie meine Arbeit (oder Teile davon) Korrektur gelesen haben,
- und meinen Eltern, die das alles überhaupt erst möglich gemacht haben, und die mich immer in allem unterstützt haben.